NASA TECHNICAL NOTE

NASA TN D-4809

NASA TN D-4809

FLOW-FIELD PROPERTIES NEAR AN ARROW-WING—BODY MODEL AT MACH NUMBERS OF 1.60, 2.36, AND 2.96

by Robert L. Weirich and Walter A. Vahl

Langley Research Center
Langley Station, Hampton, Va.

NATIONAL AERONAUTICS AND SPACE ADMINISTRATION • WASHINGTON, D. C. • OCTOBER 1968

FLOW-FIELD PROPERTIES NEAR AN ARROW-WING—BODY MODEL AT MACH NUMBERS OF 1.60, 2.36, AND 2.96

By Robert L. Weirich and Walter A. Vahl

Langley Research Center
Langley Station, Hampton, Va.

NATIONAL AERONAUTICS AND SPACE ADMINISTRATION

For sale by the Clearinghouse for Federal Scientific and Technical Information
Springfield, Virginia 22151 – CFSTI price $3.00

FLOW-FIELD PROPERTIES NEAR AN ARROW-WING—BODY MODEL AT MACH NUMBERS OF 1.60, 2.36, AND 2.96

By Robert L. Weirich and Walter A. Vahl
Langley Research Center

SUMMARY

A wind-tunnel investigation was conducted at supersonic Mach numbers to determine the flow-field properties near an arrow-wing—body model at several stations which were considered to be potential locations for engine air inlets. The tests were conducted at Mach numbers of 1.60, 2.36, and 2.96 at a Reynolds number of 9.84×10^6 based on a 1-meter length. The model angle-of-attack range was 0° to 9° and the model angles of sideslip were 0°, 5°, and -5°. The local flow parameters – Mach number, upwash and sidewash angles, and ratio of local to free-stream total pressure – were measured by pressure-instrumented 15° half-angle conical probes. These local flow characteristics are presented as contour plots for the locations which were surveyed.

The results of this investigation indicate that several locations are potentially suitable as inlet locations. Below the wing-body, the Mach numbers are less than the free-stream value and the flow is reasonably uniform except in the region of the wing-body juncture. Locations below the fuselage and below the wing appear suitable for inlets. Above the plane of the wing, the Mach number is generally greater than the free-stream value. However, near the fuselage the flow is uniform except at high angles of attack, and this region appears suitable as an inlet location. Above the wing, away from the fuselage, the flow is characterized by large gradients in the local flow parameters. These regions are not suitable for inlets. Increasing the free-stream Mach number tends to reduce the angle of attack at which flow nonuniformities first occur. Sidewash conditions either above or below the plane of the wing are not mitigated by wing-body shielding. Finally, no significant fluctuations of the local pitot pressure exist except in regions of vortices.

INTRODUCTION

At supersonic cruise speeds, overall engine-airframe performance is very sensitive to the engine air-inlet performance. For a given inlet, the pressure recovery, which is affected by local Mach number and flow angle, directly influences the engine airflow, thrust, and specific fuel consumption. In addition, the internal flow distortion may have

a direct influence on the operation of the engine components and thereby cause such problems as compressor stall and hot spots. Obviously, since the inlet performance reflects the characteristics of the local flow field, it is beneficial to locate the inlet in a region where the flow is relatively uniform and varies little with changes in airplane attitude. These requirements on the inlet location can pose a difficult problem for the designer, who must also consider such factors as weight, balance, number of engines, structural requirements, exhaust-jet impingement, ground-debris ingestion, pressure drag (airplane area distribution), and nacelle interference.

In this context, an inlet location above the fuselage may prove advantageous. The wing and fuselage provide some shielding from the free stream. However, the local Mach number above the fuselage may be large compared with the free-stream value and could adversely affect inlet performance. Also, the flow may separate above the body and thus allow disturbances to enter the inlet.

Relatively little information is presently available on the flow characteristics above the plane of the wing of a vehicle designed for supersonic cruise flight. Some data (ref. 1) indicate that locations above the fuselage may be satisfactory. Reference 2, on the other hand, indicates otherwise.

The purpose of this investigation was to determine characteristics of the flow field near an arrow-wing—body model which is typical of supersonic-cruise aircraft designs. The flow field above the plane of the wing was surveyed at Mach numbers of 1.60, 2.36, and 2.96 to obtain measurements of the local Mach number, flow angles, and total-pressure ratio. The model angle of attack was varied from 0° to 9° at angles of sideslip of 0°, 5°, and -5°. Limited data were also obtained below the plane of the wing. Surveys of the fluctuations of local pitot pressure were conducted at the rear of the model. The results are presented as contour plots for the locations which were surveyed.

SYMBOLS

M_l local Mach number

M_∞ free-stream Mach number

$p_{t,i}$ total pressure inside inlet, newtons/meter^2

$p_{t,l}$ local total pressure, newtons/meter^2

$p_{t,\infty}$ free-stream total pressure, newtons/meter^2

x	distance along model longitudinal axis, centimeters
α_l	local flow angle in vertical plane relative to model longitudinal axis, positive with flow upward, degrees
α_m	model angle of attack, degrees
β_l	local flow angle in horizontal plane relative to model longitudinal axis, positive with flow toward the vertical center plane of the model, degrees
β_m	model angle of sideslip, degrees
ΔM	incremental change in Mach number from free-stream value
Δp_p	incremental change in pitot pressure, newtons/meter^2
ϕ	circumferential angle of survey rake about model, measured clockwise from vertical plane looking upstream with 0^o at top of model, degrees

APPARATUS

Wind Tunnel

The tests were conducted in the low and high Mach number test sections of the Langley Unitary Plan wind tunnel, which is a variable pressure, continuous-flow tunnel. The test section is approximately 1.22 meters square and 2.13 meters long. The tunnel is equipped with a central support system which permits remote control of the angle of attack and angle of sideslip of a sting-mounted model.

Model

The model about which the flow was surveyed is illustrated in figure 1. It is a wing-body combination which is described in detail in reference 3 (model 3). The arrow wing is warped and cambered to achieve a design lift coefficient of 0.063 at $M_\infty = 2.6$. The wing has a leading-edge sweep of 76^o and an aspect ratio of 1.71.

The model body is designed to fulfill essentially the volume and space requirements of a supersonic-cruise vehicle. The wing and body are oriented so that the body volume is equally distributed above and below the mean camber surface of the wing. The model of reference 3 was modified by adding a cylindrical extension rearward from the point of maximum diameter. With this extension, the total length also approximates that of a

supersonic-cruise vehicle. The rear portion of the basic body of reference 3 is shown in figure 1 by dashed lines.

Instrumentation

The local flow-field parameters, M_l, α_l, β_l, and $\frac{p_{t,l}}{p_{t,\infty}}$, were measured by means of eight 15° half-angle conical probes which were mounted on two rakes. A sketch of a rake is presented in figure 2. The conical probes each contained a pitot-pressure orifice and four static-pressure orifices spaced at 90° intervals around the cone. The pressures obtained were used with a previous calibration (ref. 4) to determine the local flow parameters.

As indicated in figure 3, the two rakes were mounted so that they rotated concentrically about the sting center line. The rakes were inclined with respect to each other at an angle of 57° and were positioned circumferentially and longitudinally by remotely controlled electric motors. The probes were spaced 2.54 cm apart, but they were interdigitated so that the measurements were actually made at 1.27-cm radial increments. The closest probe was 4.75 cm from the sting center line.

The pitot pressures were measured by 103 421-N/m^2 (15-psi) differential transducers which were referenced to atmospheric pressure. The static pressures were measured simultaneously by 13 790-, and 34 474-, and 51 711-N/m^2 (2.0-, 5.0-, and 7.5-psi) absolute-pressure transducers. These three gages were necessary to provide sufficient accuracy over the large range of static pressures which were measured during the investigation. Of the three values thus obtained, the most accurate with respect to gage range was automatically selected for use by the data-processing equipment. The pressures were allowed to achieve a stable value before they were recorded.

The pressure data obtained with the cone probes were recorded digitally on magnetic tape and were reduced to local flow parameters (Mach number, flow angles, and pressure ratio) by preprogramed automatic data-processing equipment which, as was mentioned, used the calibration which appears in reference 4. The method of data reduction was similar to the one described in reference 4.

A separate rake, illustrated in figure 4, was used to indicate the pitot-pressure fluctuations in the flow field. The fluctuating pressures were measured by 27 579-N/m^2 (4-psi) differential transducers which were referenced to the local pitot pressure. These transducers were capable of accurately sensing pressure fluctuations up to about 750 cps (750 hertz). Reference pressure fluctuations above 1 cps were filtered out. The pressure fluctuations of the dynamic survey were recorded as traces on photographic oscillograph paper.

TESTS AND ACCURACY

The wind-tunnel tests were conducted at Mach numbers of 1.60, 2.36, and 2.96 at a Reynolds number of 9.84×10^6 based on a 1-meter length. The tunnel stagnation temperature was 325° K at $M_\infty = 1.60$ and 339° K at $M_\infty = 2.36$ and $M_\infty = 2.96$. The angle-of-attack range was from 0° to 9° at angles of sideslip of 0°, 5°, and -5°. At $x = 97.49$ cm, data were obtained only for 0° sideslip.

Data were obtained at three longitudinal stations as indicated in figure 5. Each symbol represents a survey-probe location at which data were taken for this report. Surveys were conducted above and below the plane of the wing at the forward station. At the center and rear stations, surveys were conducted primarily above the plane of the wing. The body cross-sectional shapes and the rake angles at which data were obtained are also shown in figure 5. The shaded circular areas represent the approximate capture area of a typical inlet.

Boundary-layer transition was accomplished through 0.16-cm-wide strips of number 60 carborundum grit. These strips were located 2.46 cm aft of the body nose and 0.16 cm (measured perpendicularly) behind the wing leading edge.

The fluctuations of the pitot pressure at the farthest aft station were measured at Mach numbers of 1.60 and 2.96. Data were taken for angles of attack from 0° to 9° and angles of sideslip of 0°, 5°, and -5°. Since these surveys were intended to provide data on the fluctuations near disturbances, the rake positions shown in figure 5 were not always used. Rather, the oscillograph was monitored during a preliminary circumferential traverse, and data were taken primarily in areas of apparent disturbances.

The absolute level of accuracy is difficult to establish because of the combined effect of many possible sources of error. A number of precautions were taken, however, to reduce both the magnitude and the probability of significant errors. The more important of these are described herein. The free-stream conditions are considered accurate within the following limits:

α_m, deg	± 0.1
β_m, deg	± 0.1
M_∞	± 0.015
$p_{t,\infty}$, N/m^2	± 436.0

The test-section flow angularity had been measured and was taken into account when model angle of attack was set. In order to account for deflections due to load, the model angle of attack was set with a cathetometer while the tunnel was running. The pressure instrumentation was calibrated both before and after the tests with the same equipment that was used to record the data. By taking into consideration these precautions and the

known calibration accuracies and repeatability, the accuracy of the computed results can be estimated as follows:

M_∞	α_l, deg	β_l, deg	M_l	$\frac{p_{t,l}}{p_{t,\infty}}$, %
1.6	±0.25	±0.25	±0.02	±2
2.36	±.25	±.25	±.03	±3
2.96	±.25	±.25	±.04	±4

PRESENTATION OF BASIC RESULTS

The results of this investigation consist of values of local flow parameters which were computed from the measured pressure data. This information is presented as contour plots of local Mach number, local flow angles, and ratio of local to free-stream total pressure in figures 6 to 14. An index of the location of the specific results follows:

Figure	Station	M_∞	α_m, deg	β_m, deg
6	80.21	1.60	0 to 9	0, 5, -5
7	80.21	2.36	0 to 9	0, 5, -5
8	80.21	2.96	0 to 9	0, 5, -5
9	97.49	1.60	0 to 9	0
10	97.49	2.36	0 to 9	0
11	97.49	2.96	0 to 9	0
12	115.14	1.60	0 to 9	0, 5, -5
13	115.14	2.36	0 to 9	0, 5, -5
14	115.14	2.96	0 to 9	0, 5, -5

DISCUSSION OF RESULTS

Selected portions of the data which appear generally characteristic of the phenomena are discussed in detail. Several comments concerning the method of presentation of these and the general results are pertinent. First, the contours are used to show gradients. Thus, closely spaced contours do not necessarily indicate extensive data. Where necessary for clarity, dashed data lines were extended into the region between the body and the probes. These lines do not necessarily indicate the edge of the boundary layer. The increment that each contour represents is consistent in each plot. However, between plots, the size of the increment was increased for purposes of clarity when the gradients were large. In regions where no significant gradients occurred, the (constant) value of the local property is indicated by the last preceding contour line. Finally, the

words "No data" are used to indicate the few regions within the surveyed areas where the results were not considered reliable.

General Characteristics

The general characteristics of the flow field near this wing-body are illustrated by the data in figure 15. These data for the three longitudinal stations correspond to a free-stream Mach number of 2.36 and model angles of attack and sideslip of 6° and 0°, respectively. The data appear to illustrate features which are typical of most of the data in the report.

The flow field above the plane of the wing is characterized by local Mach numbers which are generally greater than the free-stream value. Above the fuselage near the vertical center plane, the flow direction is downward with respect to free stream. Above the wing, strong gradients are apparent in the flow properties. These gradients are generated by the wing-leading-edge circulation at the forward station and by the trailing-edge vortex at the two following stations. The strong gradients in this region would make it undesirable as an inlet location because they might subject the inlet to large asymmetric flow conditions. In addition, the internal flow distortions which result from the external flow gradients usually severely degrade inlet and engine performance. Finally, the local total pressure is low in this region.

Relatively close to the body center line, the flow is conical in nature. That is, as distance from the fuselage center line increases, the upwash angle tends toward the free-stream value and the sidewash angle increases. At the forward station, the gradients near the top of the fuselage are mild. At $x = 97.49$ cm, the downwash above the fuselage center line is somewhat greater than at the preceding station. However, the gradients are still mild, and the pressure contours show no significant accumulation of low-energy air above the fuselage.

Near $x = 97.49$ cm, the wing-trailing-edge shock passes over the body. The existence of this wave is indicated by both the data in figure 15 and the schlieren photograph of figure 16 (for $M_{\infty} = 1.60$). Behind the shock wave, the local Mach number is reduced and the flow demonstrates less downwash. Some reduction in local total pressure must occur, though from the data it appears to be very small. Some accumulation of low-energy air at the rear station is indicated by the total-pressure contours in figure 15(c). This accumulation is probably due to the combination of upwash around the body and any effects of interaction between the wing shock and boundary layer. Thus, although the boundary layer appears to remain thin while shielded by the wing area, it thickens rapidly behind the trailing-edge shock wave.

Positions above the fuselage along the center line, then, appear to offer some possibilities as inlet locations. The Mach number is generally greater than the free-stream value, but neither the local flow angles nor the flow gradients are severe. Low total pressures at $x = 115.14$ cm, however, indicate that the inlet should not be too far aft.

As would be expected, the flow field below the plane of the wing at the forward station is also conical. The local Mach number and local upwash angle increase toward the free-stream values as distance from the body is increased. (See figs. 15(a) and 15(b).) The local sidewash angle increases in magnitude with increasing distance from the body center line toward the wing tip. The wing-body juncture has a noticeable influence on the sidewash, as indicated by the gradients near the juncture. This region is of appreciable size and appears to be the only area where significant total-pressure losses occur. The exact cause of the disturbance is unknown.

Below the plane of the wing, two locations are potentially suitable for inlets. These regions are (1) below the fuselage near the center line and (2) about halfway out to the wing tip. They are characterized by local Mach numbers which are below the free-stream value and by local flow angles and gradients which are relatively small.

Effects of Angle of Attack

Typical effects of angle of attack on the local flow field at three stations are illustrated in figure 17. The data are presented for zero angle of sideslip and a free-stream Mach number of 2.36. Below the plane of the wing, the local Mach numbers decrease with increasing angle of attack, and the flow field remains conical up to the highest angle of the tests. With increasing angle of attack, sidewash increases in magnitude, as would be expected, and the magnitude of the downwash decreases. The strength of the disturbance near the wing-body juncture increases with angle of attack. In general, the larger variation in flow angle is in the sidewash direction. Below the wing, the change in sidewash angle is significant. The flow near the vertical center plane is least affected by angle of attack.

Above the fuselage at $x = 80.21$ cm, increasing the model angle of attack increases the local Mach number and downwash. The extent of the disturbance field generated by the wing leading edge also increases with angle of attack, and at $\alpha_m = 9^o$ it begins to influence the flow near the fuselage center line. These same general comments apply at $x = 97.49$ cm. At this station, however, the influence of the wing-generated disturbances appears to be more pronounced than at $x = 80.21$ cm. As would be expected, the wing-trailing-edge shock becomes stronger with increasing angle of attack, as evidenced by the more pronounced change in local flow angles and Mach number at $x = 97.49$

and $x = 115.14$ cm. At $x = 115.14$ cm, boundary-layer accumulation above the fuselage is evident from the total-pressure contours at all positive angles of attack.

In considering the flow above the fuselage along the vertical center plane, it is of interest to note the sensitivity of local Mach number to model angle of attack. But since the local flow is deflected by an amount which is often different from the model angle of attack (depending on body slopes, wing pressure gradients, etc.), perhaps a more general indication of sensitivity is the change in local Mach number with local-flow vertical deflection from the free stream. In figure 18, typical data are presented which illustrate the effect of flow deflection angle on local Mach number. Data from probe locations along the vertical center plane above the fuselage are presented for three longitudinal stations. The free-stream Mach number is 1.60 and the model angle of sideslip is 0°. A least-squares fit to the data and the Prandtl-Meyer expansion curve are also presented. At $x = 80.21$ cm and 97.49 cm, the data indicate that the local Mach number increases with flow deflection angle at less than one-half the rate that is predicted by the Prandtl-Meyer relation. The effect of the wing shock wave (at $x = 115.14$ cm) is to return the local flow to essentially the free-stream Mach number.

Above the plane of the wing, increasing the angle of attack would be expected to have two primary effects on the flow in terms of performance of an inlet located near the vertical center plane. The first of these is the tendency for the local Mach number to increase as the angle of attack increases. Also, particularly at the stations behind the wing-trailing-edge shock, increasing the angle of attack tends to increase the accumulation of low-energy air above the fuselage. Inlet performance is sensitive to both of these phenomena.

Effects of Free-Stream Mach Number

The effects of free-stream Mach number on the local flow conditions are illustrated in figure 19 for an angle of attack of 6° and an angle of sideslip of 0°. The flows have generally similar characteristics except for changes in the magnitude of the local Mach number. Above the plane of the wing, the wing-trailing-edge shock passes over the upper surface of the fuselage at somewhat different locations, depending on the Mach number. The effect of free-stream Mach number on the change in local Mach number with flow deflection is illustrated in figure 20. At all three free-stream Mach numbers, the local Mach number increases with flow deflection at a rate which is less than one-half the Prandtl-Meyer result. Increasing the Mach number does, however, tend to aggravate any flow disturbances. (See fig. 19.) Also, below the plane of the wing, the size of the disturbance near the wing-body juncture appears to increase with Mach number. Therefore, in terms of inlet locations, the primary effects of increasing the

free-stream Mach number are an increase in local Mach number and an increase in the size and strength of flow disturbances.

Effects of Sideslip

The effects of sideslip are illustrated in figures 21 and 22 for a free-stream Mach number of 2.36 and angles of attack of 0° and 6°. Both above and below the wing plane, very little shielding is evident. Below the wing, the local Mach numbers at a given angle of attack remain approximately unchanged with sideslip. The sidewash angles, however, vary significantly with model angle of attack and become appreciably greater than the model angle of sideslip for $\beta_m = -5^{\circ}$. At zero angle of attack and sideslip angle of -5°, for example, the largest value of β_l is approximately -6°, while at a 6° angle of attack and sideslip angle of -5°, the sidewash reaches -10° (below the wing). The effect of the wing-body juncture on the flow below it is pronounced at zero angle of attack for $\beta_m = -5^{\circ}$, but this effect decreases with increasing angle of attack.

Above the wing, the effects of sideslip are more dramatic. Sharp gradients in the flow properties appear and extend close to the vertical center plane. The sidewash angles are large near the vertical center plane, and increasing the angle of attack aggravates the situation. At the forward station, extensive boundary-layer thickening is evident at 6° angle of attack. At the rear station, vortices (either from the wing or from the body) are apparent slightly off the center plane. Generally, the variations of sidewash with angle of attack appear to induce flow conditions which are detrimental to inlet operation at all potential inlet locations.

Pitot-Pressure Fluctuations

Typical results of the survey of the pitot-pressure fluctuations at $x = 115.14$ cm are presented in figure 23 for a Mach number of 1.60. From their location, the fluctuations appear to be related to the circulatory flow near the wing. The flow in other regions appears to be steady. Since inlets are not normally located in regions where extensive circulatory flow exists, flow unsteadiness should not be a problem.

Inlet Placement

Typical variations of estimated inlet pressure recovery with model angle of attack for several possible locations are presented in figure 24. These curves were obtained from the flow-field data of the present investigation combined with the axisymmetric, mixed-compression inlet characteristics of reference 5. Information in reference 1 was used to account for the effect of flow-angle variation across the inlet face. In the calculations, it was assumed that the inlet was alined with the local flow at a model

angle of attack of 6^{o}, to simulate cruise conditions. All the possible locations which are presented provide better inlet pressure-recovery variation with angle of attack than would be demonstrated by the inlet in the free stream.

CONCLUDING REMARKS

A wind-tunnel investigation was performed to determine the flow-field properties near an arrow-wing—body model at supersonic speeds. The results indicate that several locations are potentially suitable as inlet locations. Below the wing-body, the Mach numbers are less than the free-stream value and the flow is reasonably uniform except in the region of the wing-body juncture. Locations below the fuselage and below the wing appear suitable for inlets. Above the plane of the wing, the Mach number is generally greater than the free-stream value. However, near the fuselage the flow is uniform except at high angles of attack, and this region appears suitable as an inlet location. Above the wing, away from the fuselage, the flow is characterized by large gradients in the local flow parameters. These regions are not suitable for inlets. Increasing the free-stream Mach number tends to reduce the angle of attack at which flow nonuniformities first occur. Sidewash conditions either above or below the plane of the wing are not mitigated by wing-body shielding. Finally, no significant fluctuations of the local pitot pressure exist except in regions of vortices.

Langley Research Center,
National Aeronautics and Space Administration,
Langley Station, Hampton, Va., May 20, 1968,
720-03-00-02-23.

REFERENCES

1. Reinhart, W. A.; and Tjonneland, E.: Inlet Flow Field Studies for the Supersonic Transport. [Preprint] 650198, Soc. Automotive Eng., Apr. 1965.

2. Griffiths, R. T.: Tests on an Engine Installation for a Slender Gothic Wing at M = 1.82. Tech. Note No. Aero 2982, Brit. R.A.E., Aug. 1964.

3. McLean, F. Edward; and Fuller, Dennis E.: Effects of Thickness on Supersonic Performance of a Wing-Body Configuration Employing a Warped Highly Swept Arrow Wing. NASA TN D-3034, 1965.

4. Vahl, Walter A.; and Weirich, Robert L.: Calibration of 30^{o} Included-Angle Cone for Determining Local Flow Conditions in Mach Number Range of 1.51 to 3.51. NASA TN D-4679, 1968.

5. Stitt, Leonard E.; and Salmi, Reino J.: Performance of a Mach 3.0 External-Internal-Compression Axisymmetric Inlet at Mach Numbers From 2.0 to 3.5. NASA TM X-145, 1960.

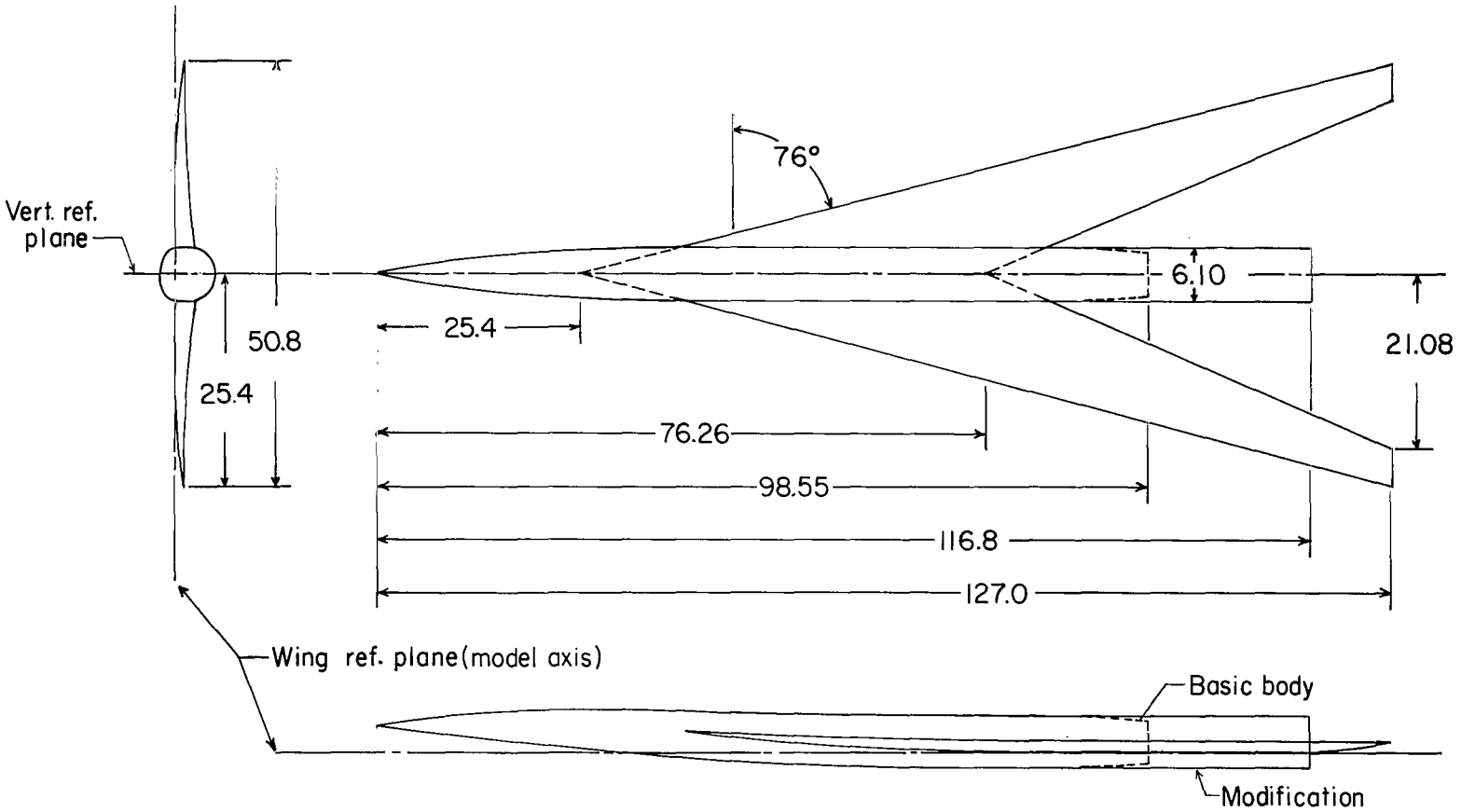

Figure 1. - Three-view sketch of model about which flow survey was made. All dimensions are in centimeters unless otherwise indicated.

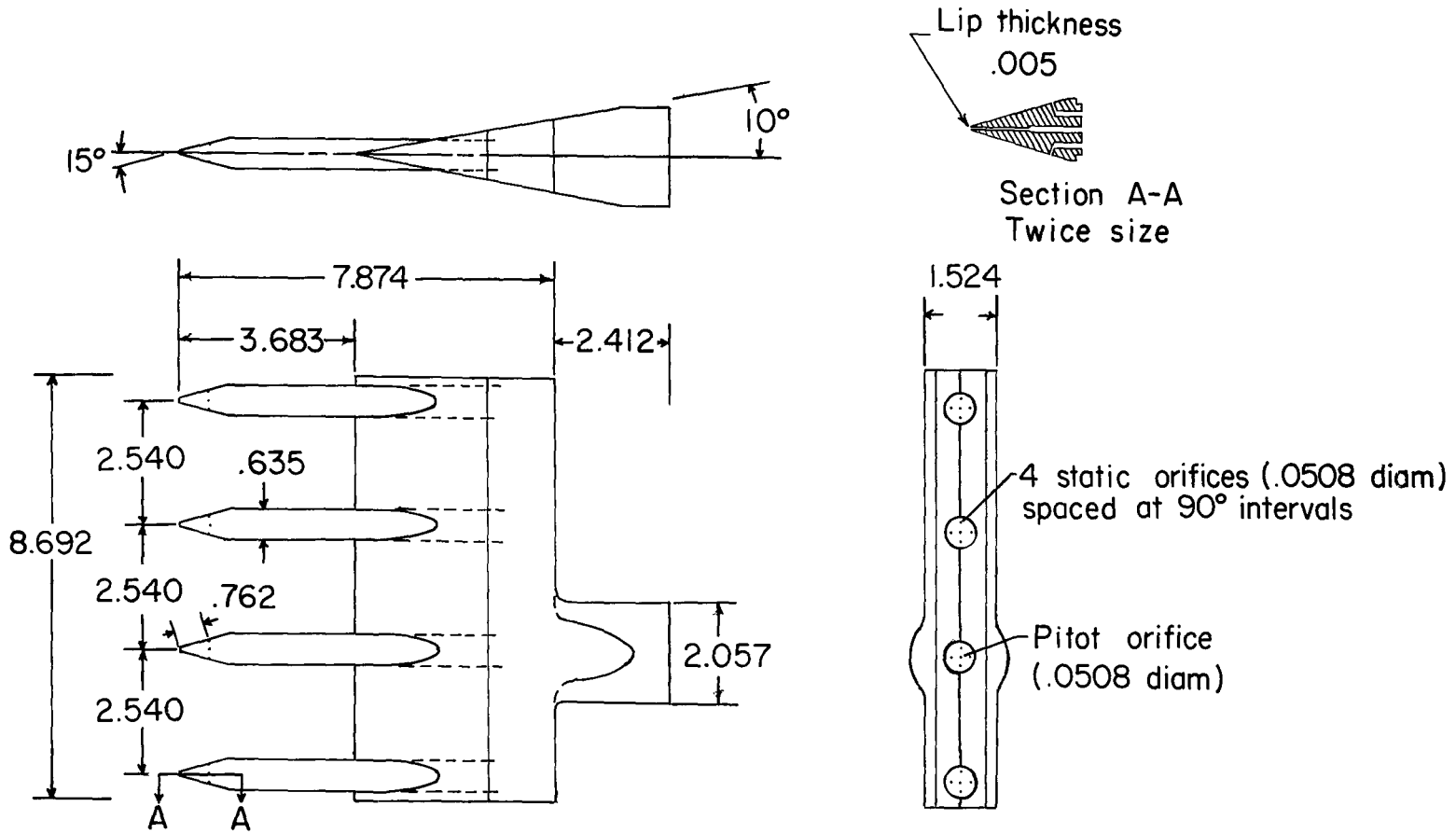

Figure 2.- Three-view sketch of flow-survey rake. All dimensions are in centimeters unless otherwise indicated.

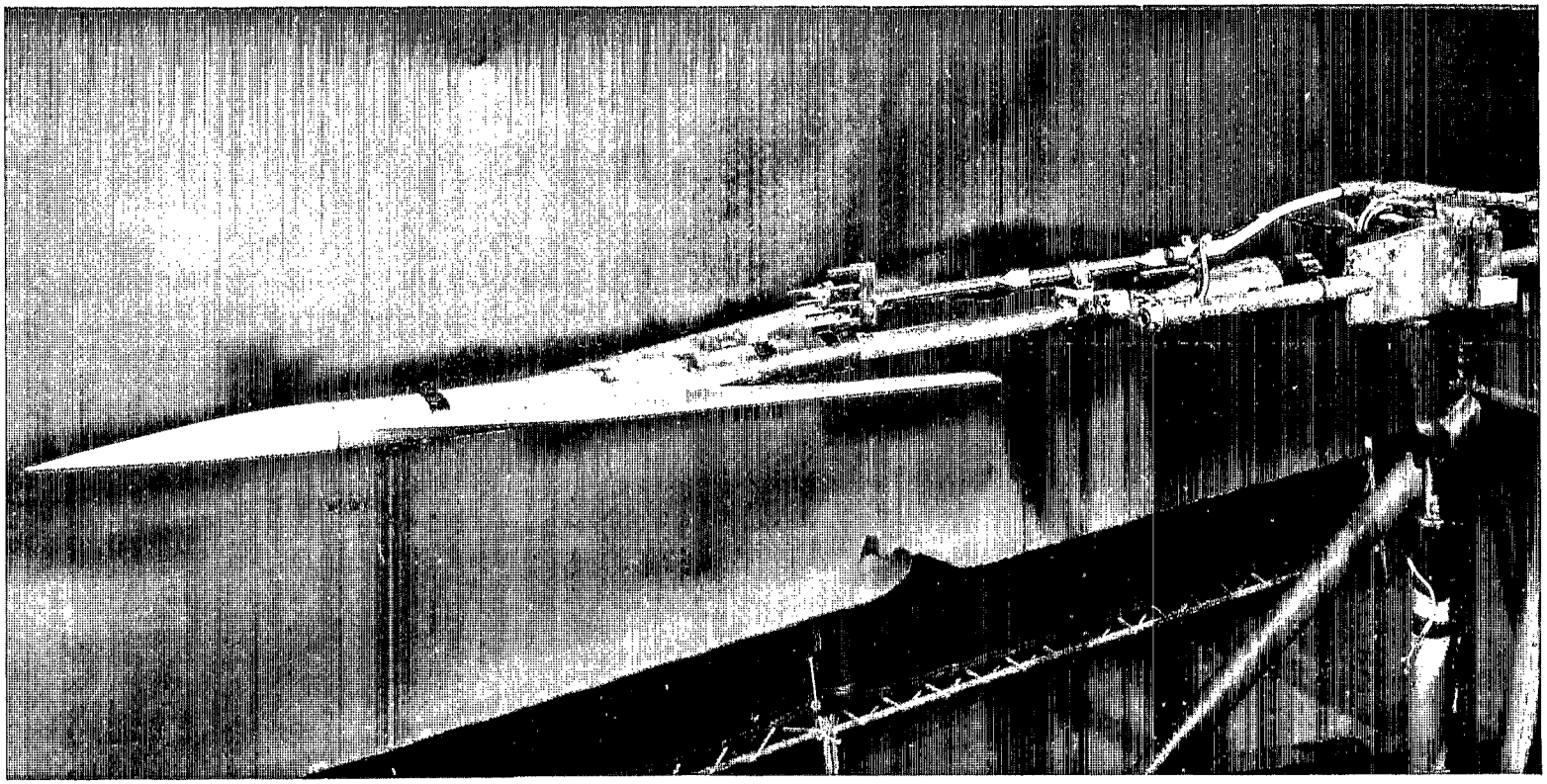

Figure 3.- Model, sting, and rake assembly used in flow-field survey. L-64-2123

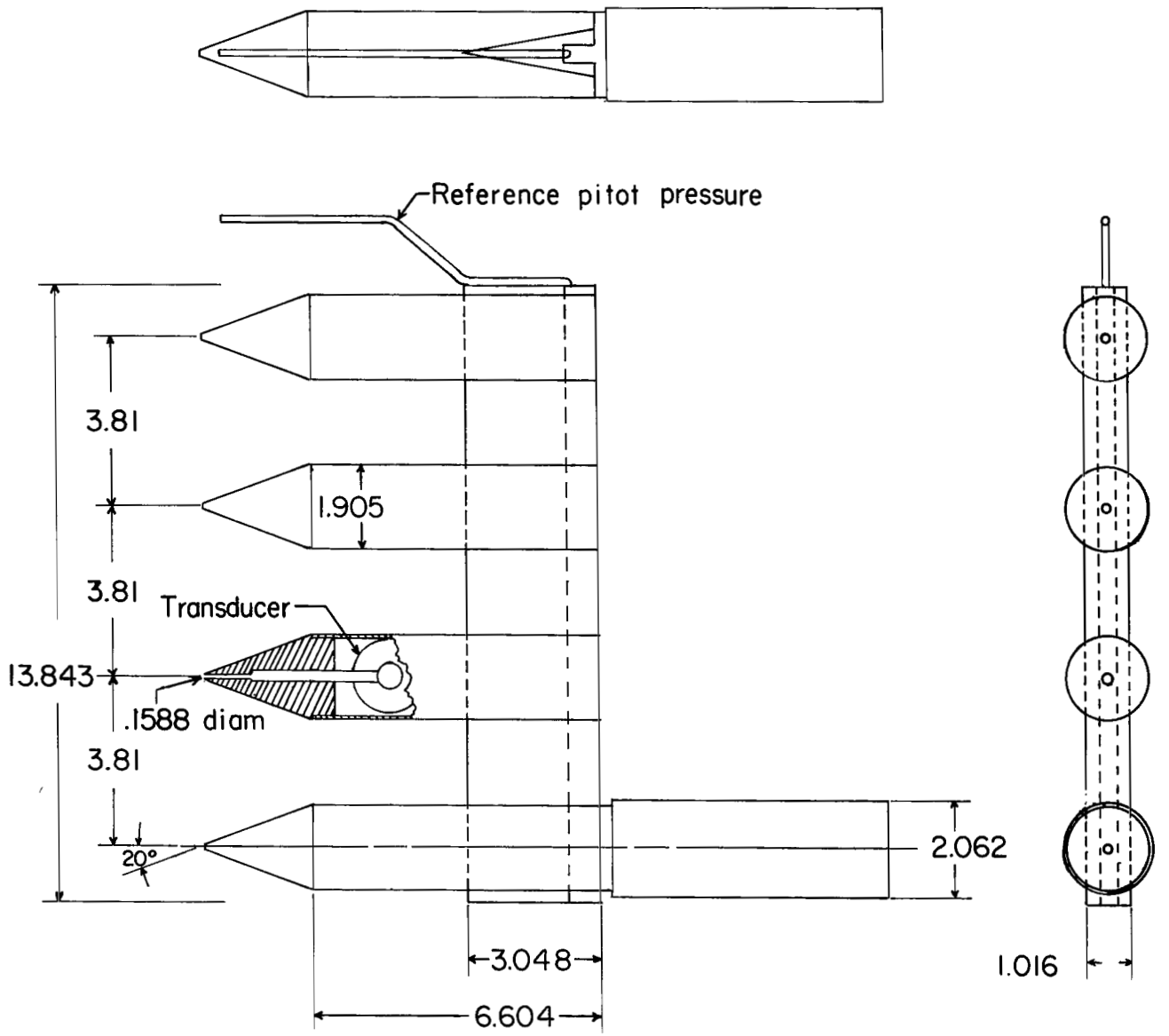

Figure 4.- Three-view sketch of rake used to measure fluctuations of local pitot pressure. All dimensions are in centimeters unless otherwise indicated.

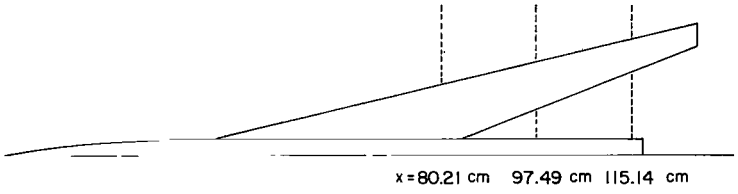

(a) Station locations.

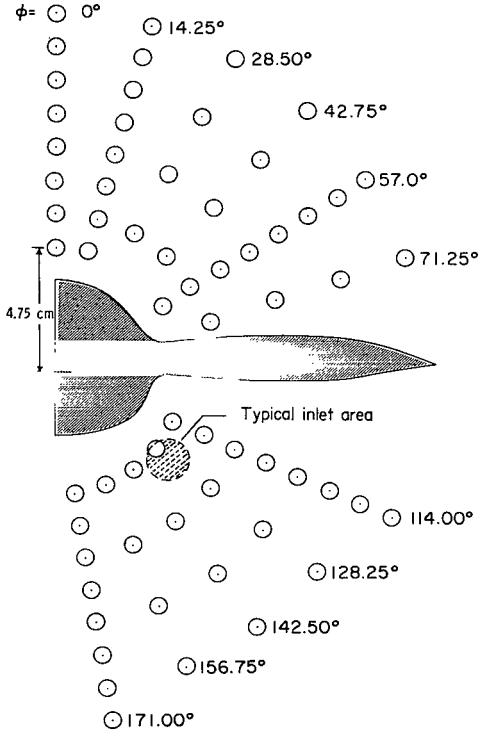

(b) Details at x = 80.21 cm.

Figure 5.- Description of stations at which flow surveys were conducted.

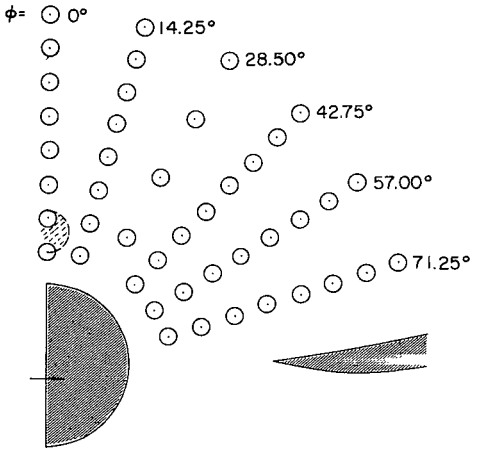

(c) Details at x = 97.49 cm.

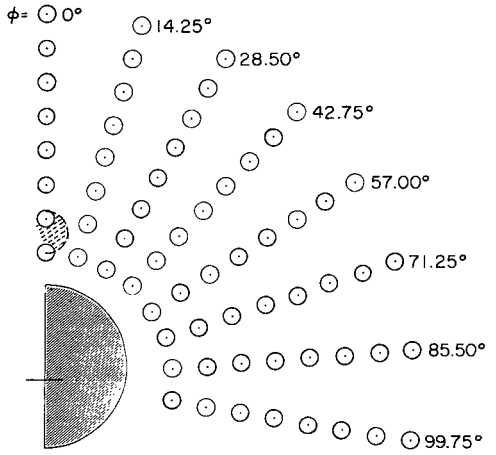

(d) Details at x = 115.14 cm.

Figure 5.- Concluded.

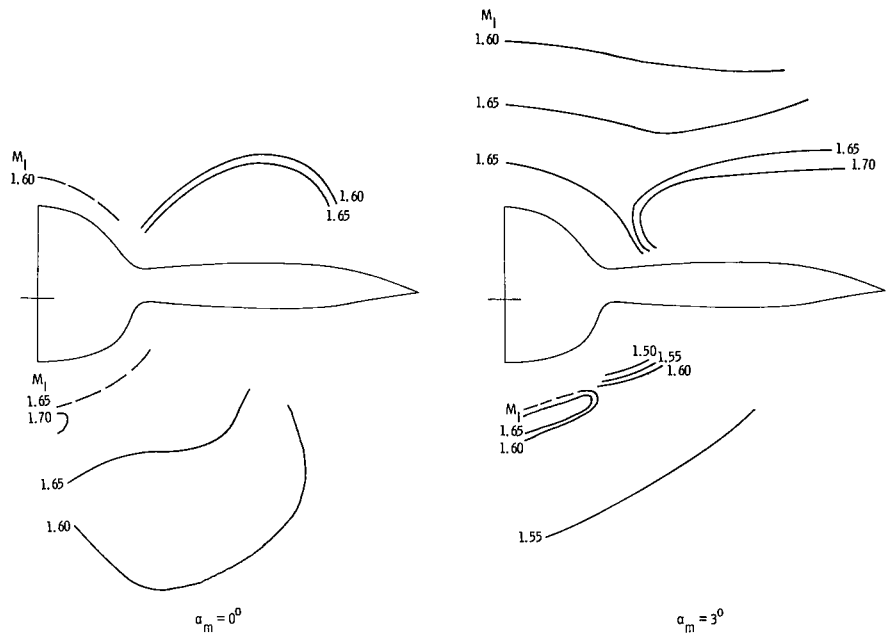

(a) Local Mach number. $\beta_m = 0^o$.

Figure 6.- Local flow parameters at $x = 80.21$ cm. $M_\infty = 1.60$.

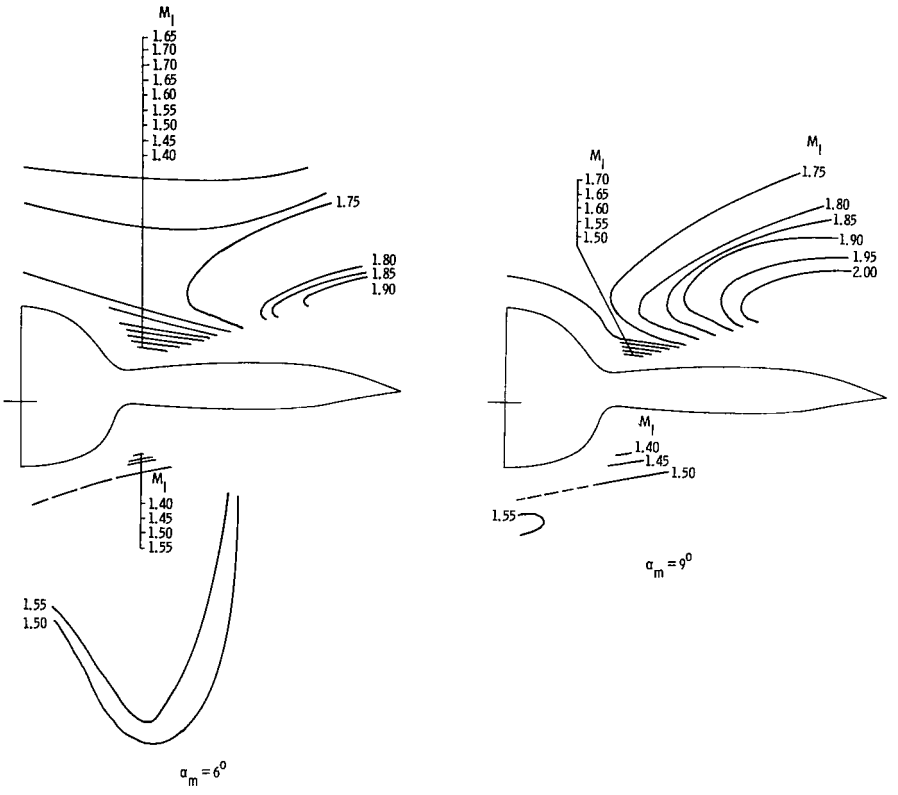

(a) Concluded.

Figure 6.- Continued.

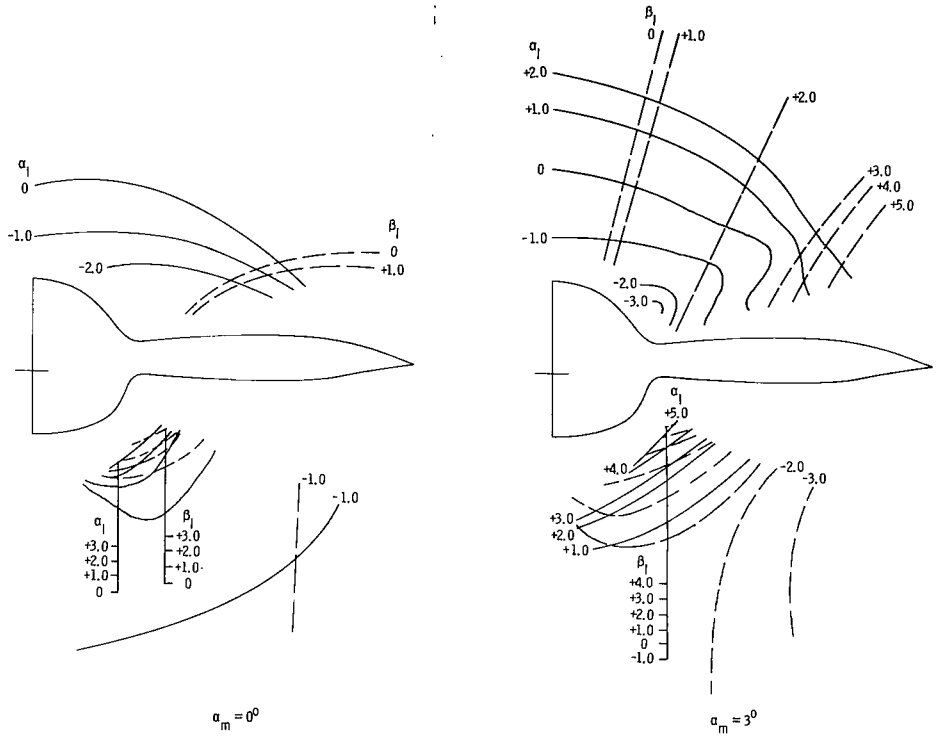

(b) Local flow angles. $\beta_m = 0^0$.

Figure 6.- Continued.

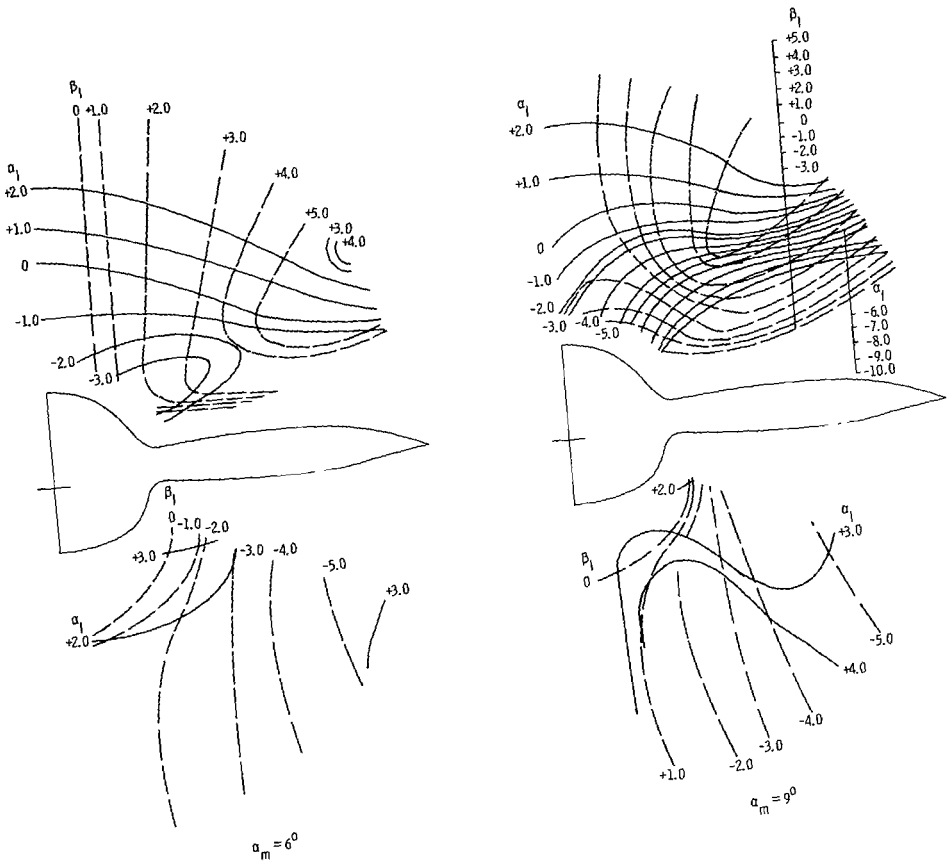

(b) Concluded.

Figure 6.- Continued.

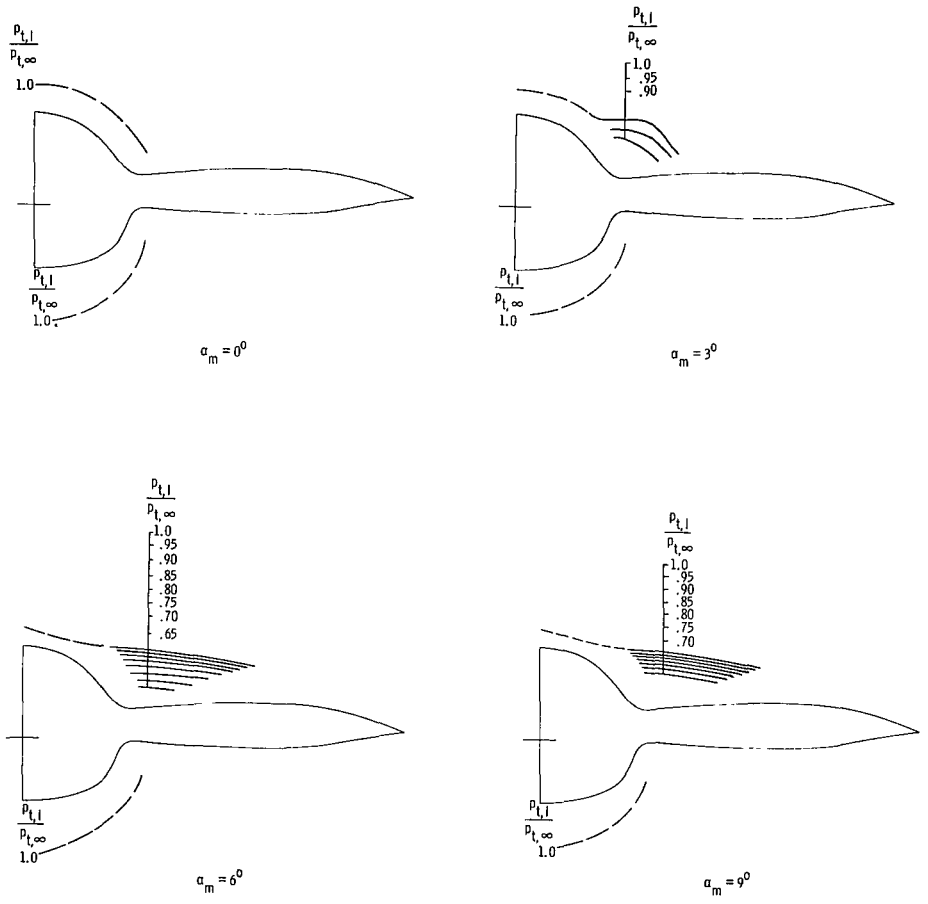

(c) Ratio of local to free-stream total pressure. $\beta_m = 0^0$.

Figure 6.- Continued.

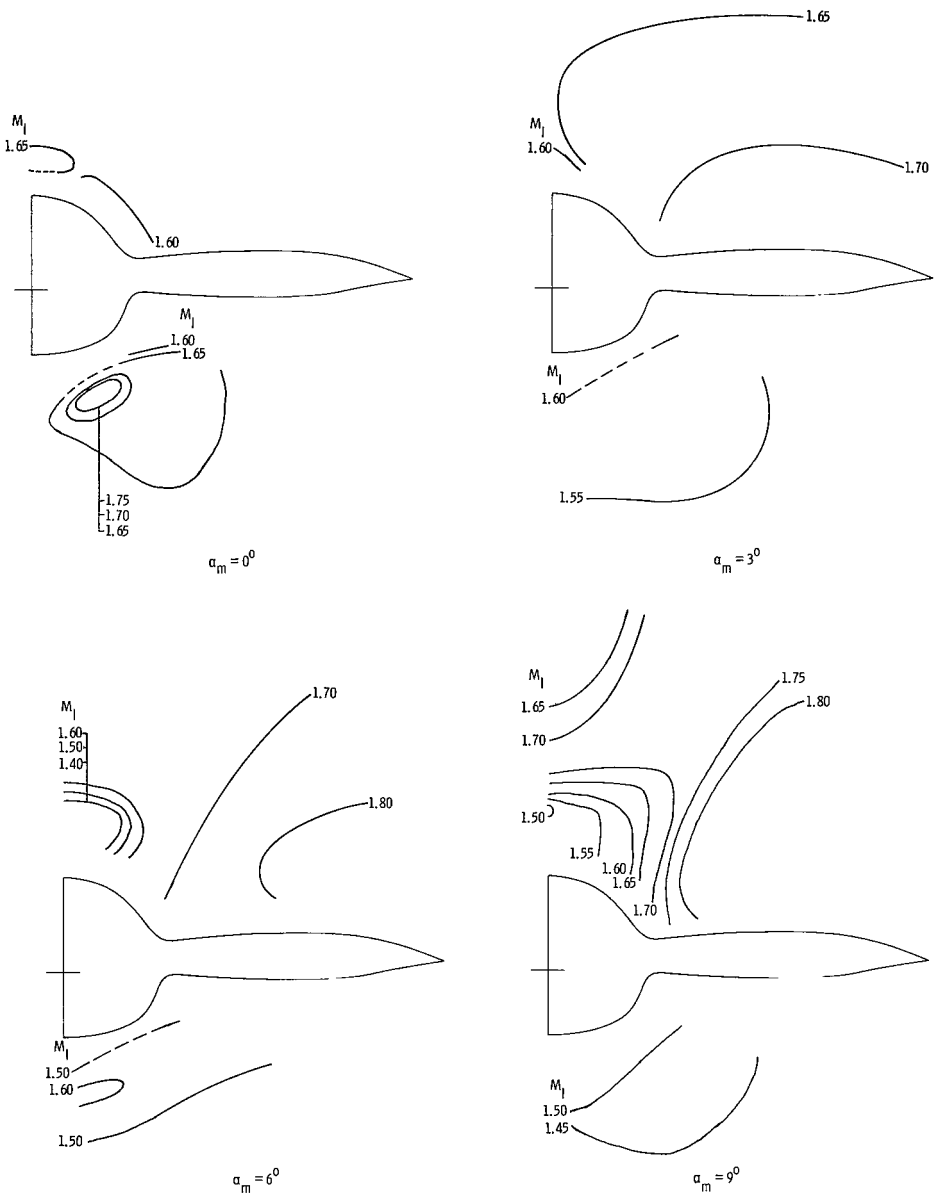

(d) Local Mach number. $\beta_m = 5^0$.

Figure 6.- Continued.

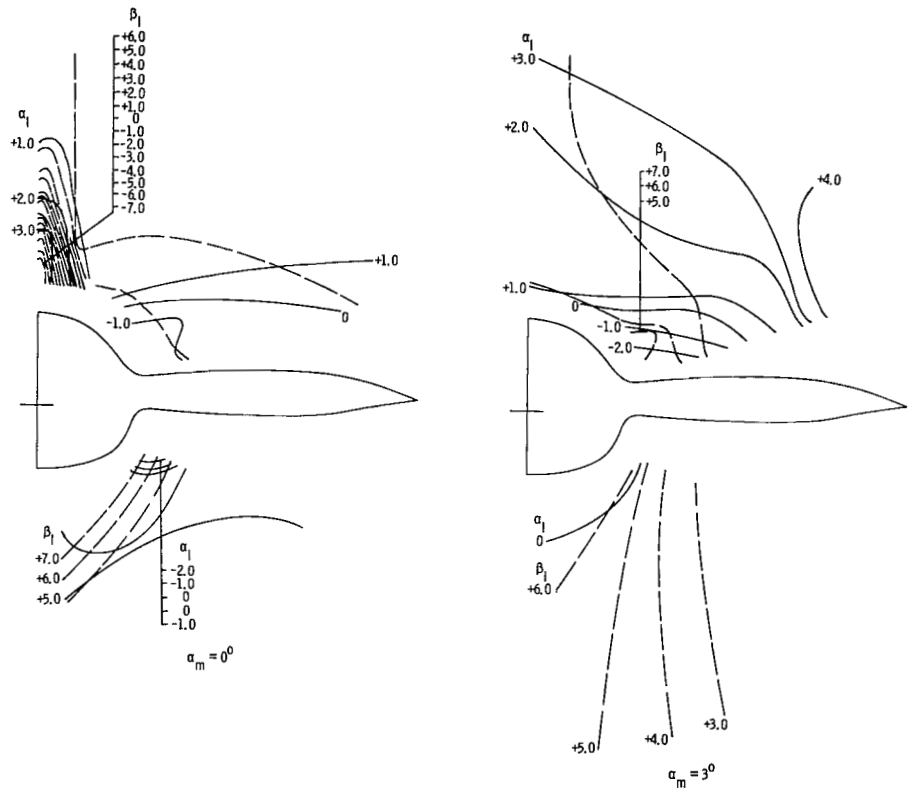

(e) Local flow angles. $\beta_m = 5^o$.

Figure 6.- Continued.

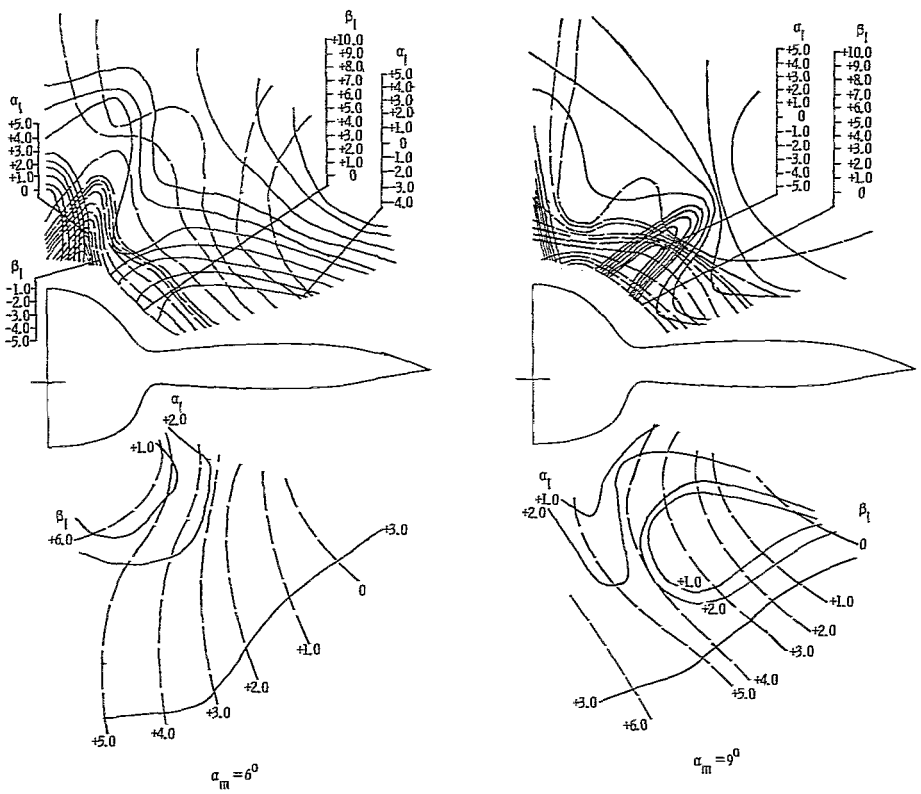

(e) Concluded.

Figure 6.- Continued.

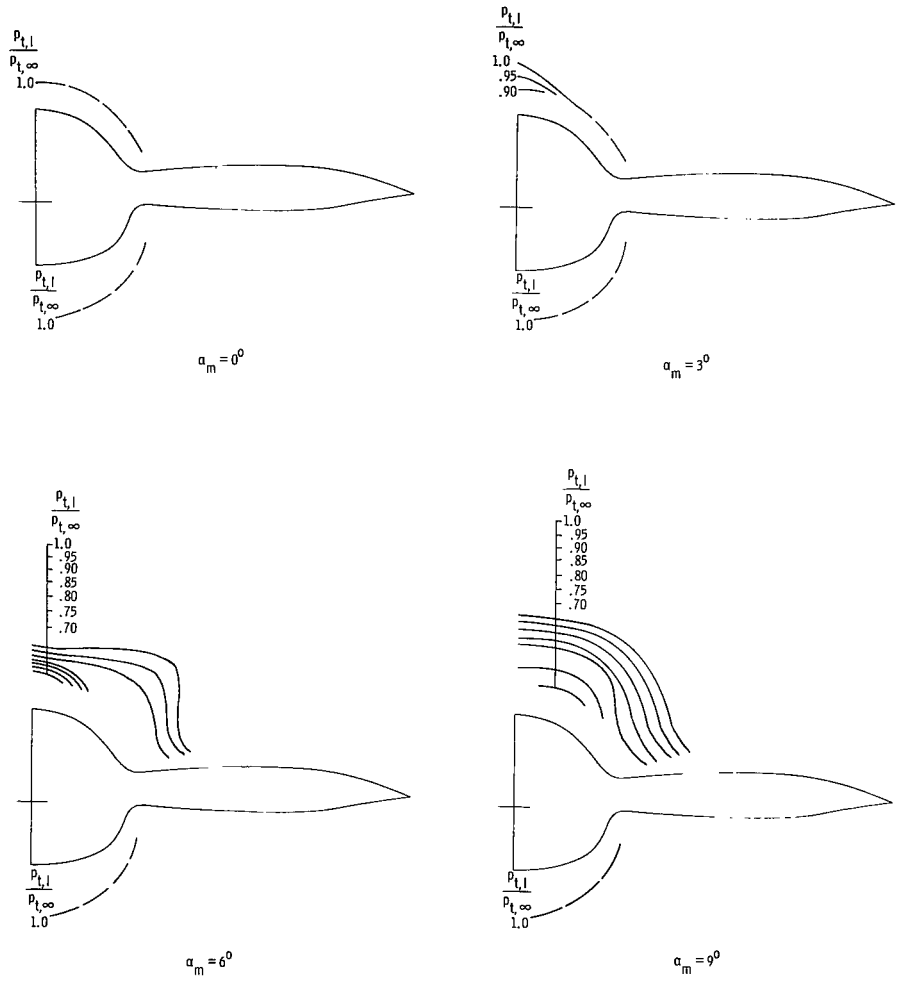

(f) Ratio of local to free-stream total pressure. $\beta_m = 5^0$.

Figure 6.- Continued.

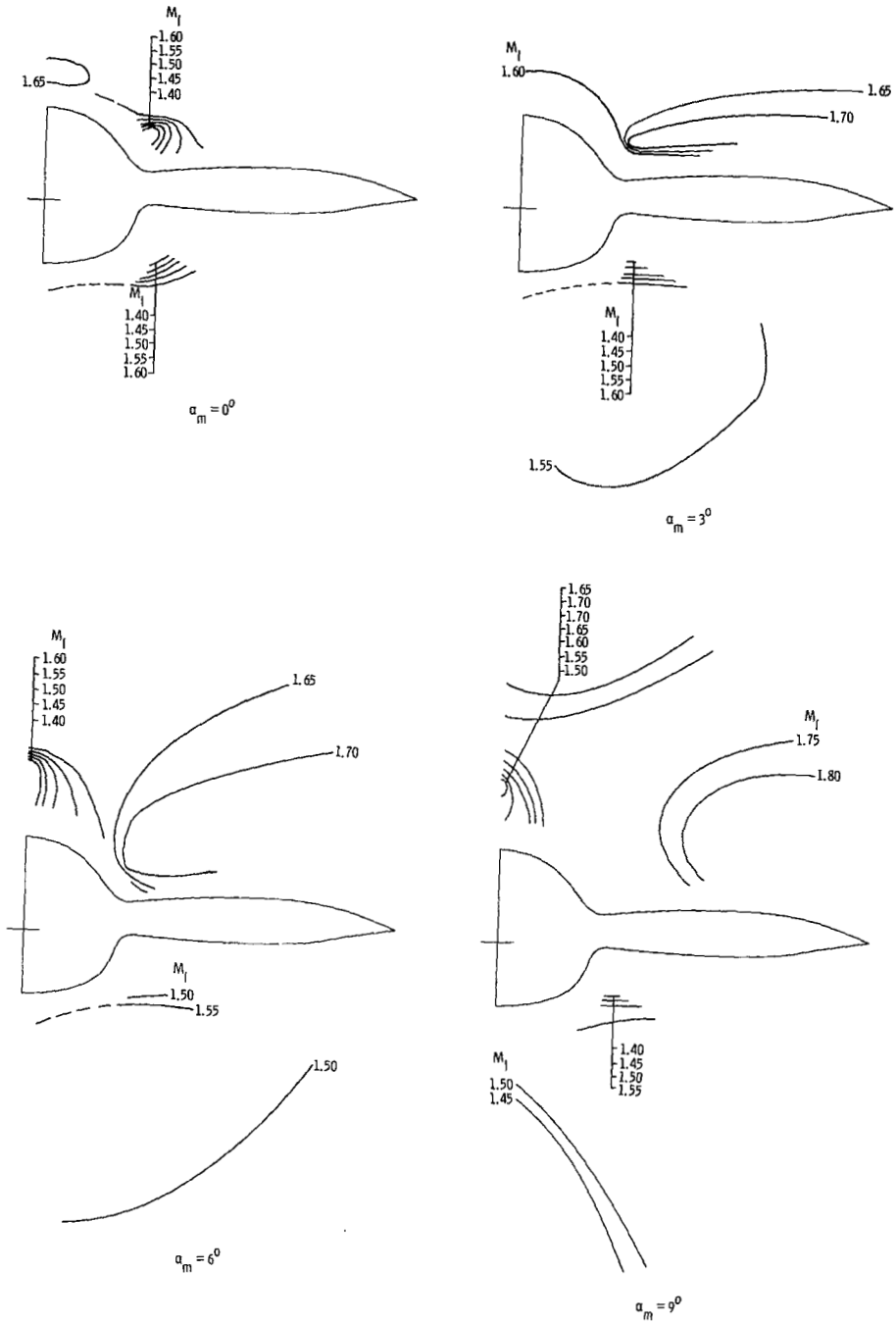

(g) Local Mach number. $\beta_m = -5^0$.

Figure 6.- Continued.

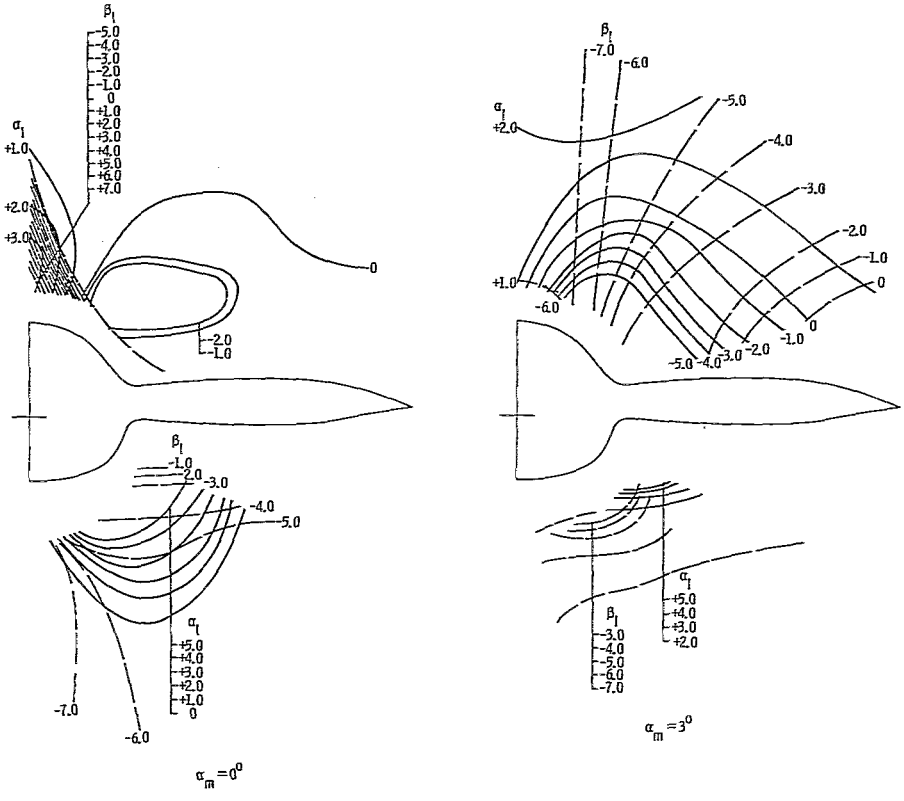

(h) Local flow angles. $\beta_m = -5^0$.

Figure 6.- Continued.

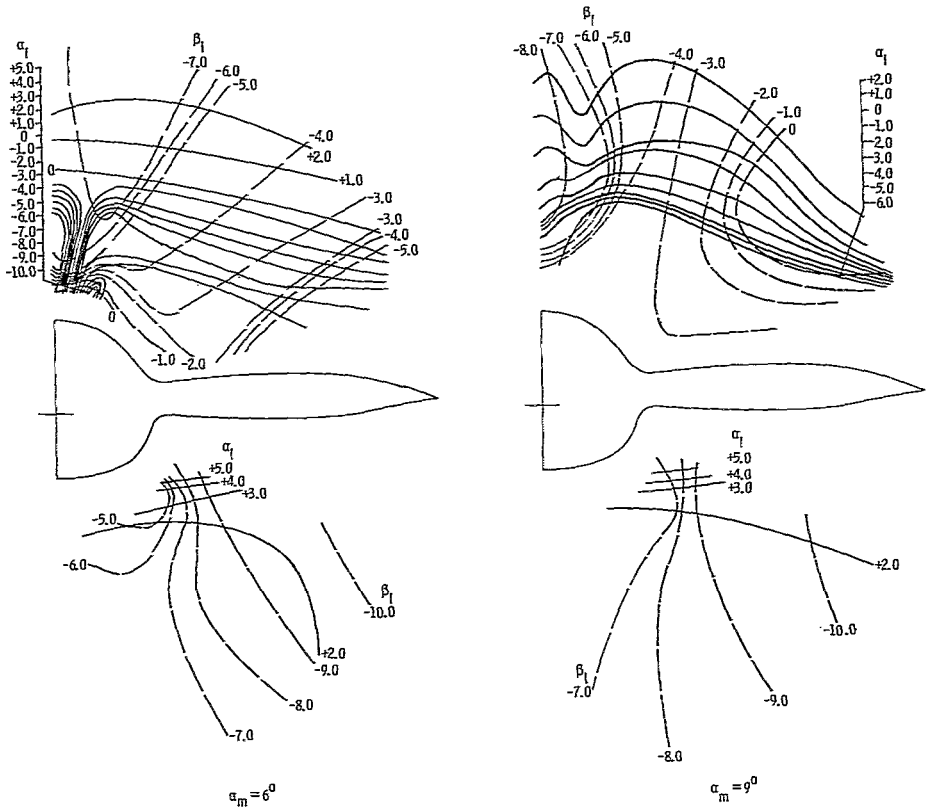

(h) Concluded.

Figure 6.- Continued.

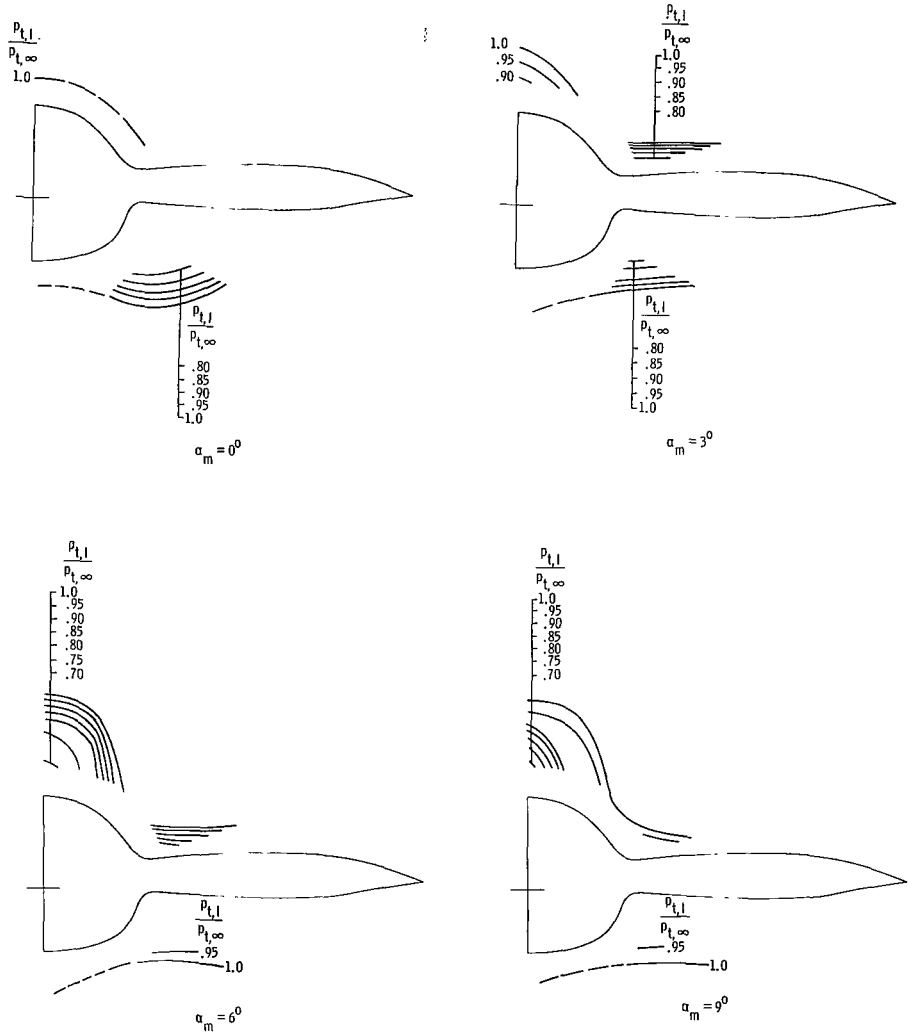

(i) Ratio of local to free-stream total pressure. $\beta_m = -5^0$.

Figure 6.- Concluded.

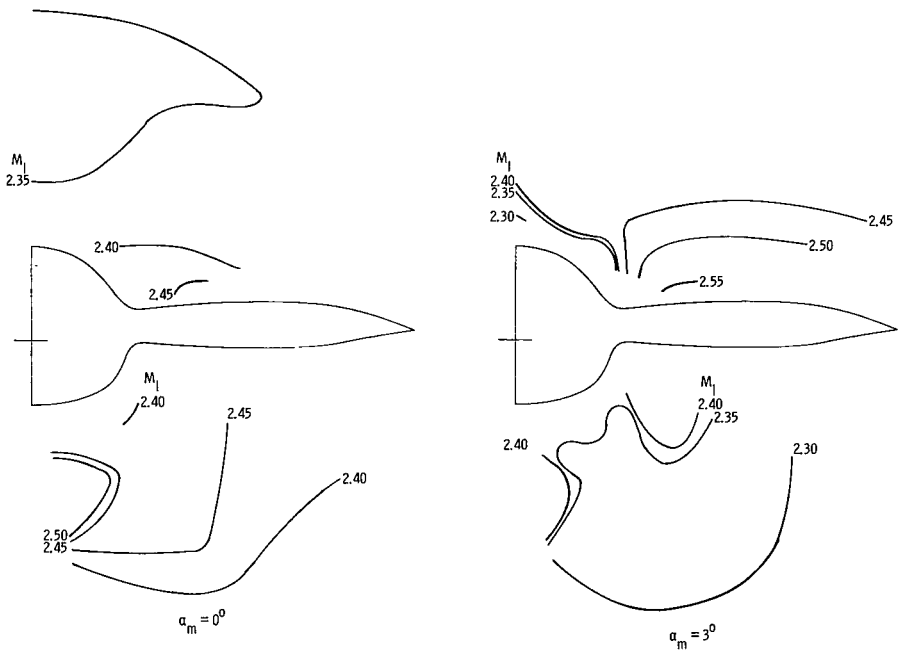

(a) Local Mach number. $\beta_m = 0^o$.

Figure 7.- Local flow parameters at $x = 80.21$ cm. $M_\infty = 2.36$.

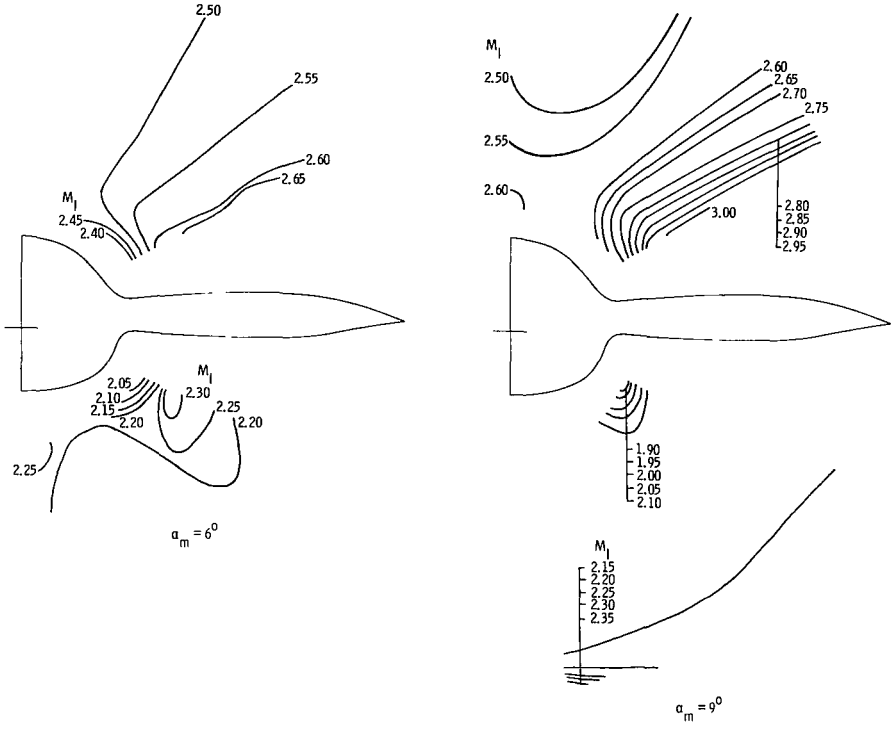

(a) Concluded.

Figure 7.- Continued.

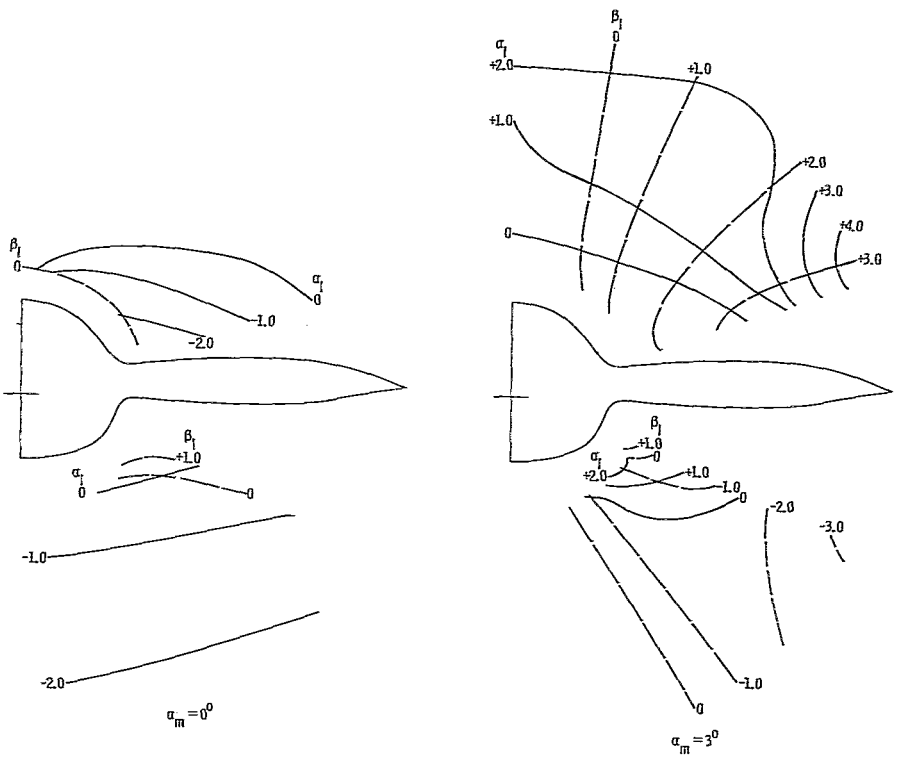

(b) Local flow angles. $\beta_m = 0^o$.

Figure 7.- Continued.

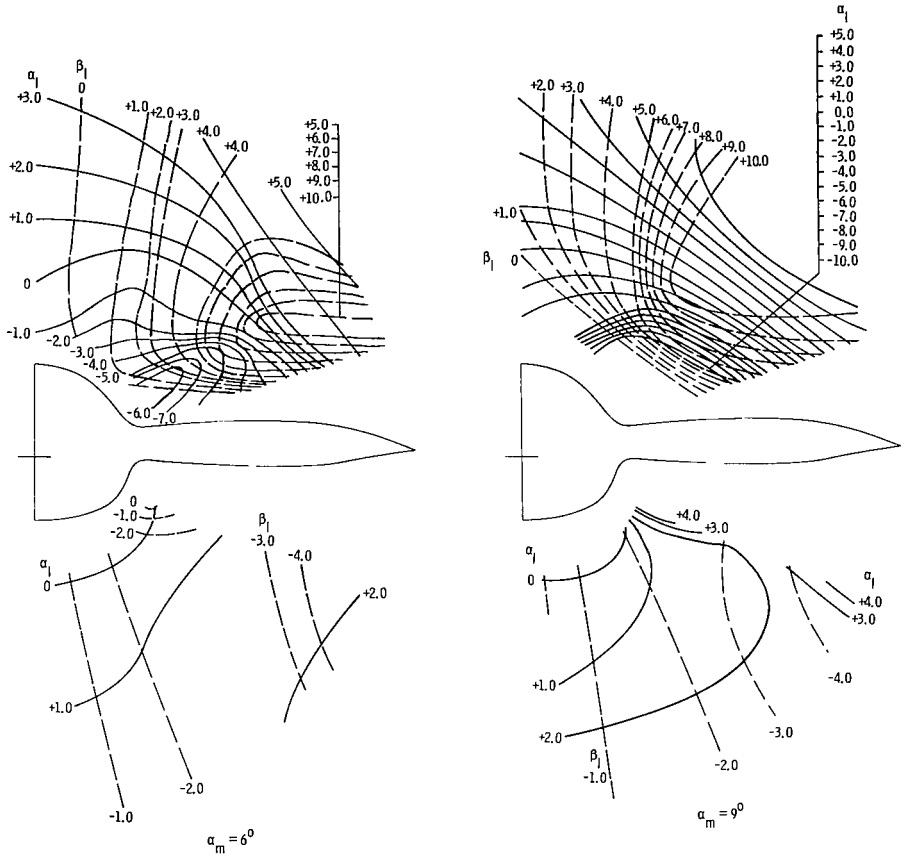

(b) Concluded.

Figure 7.- Continued.

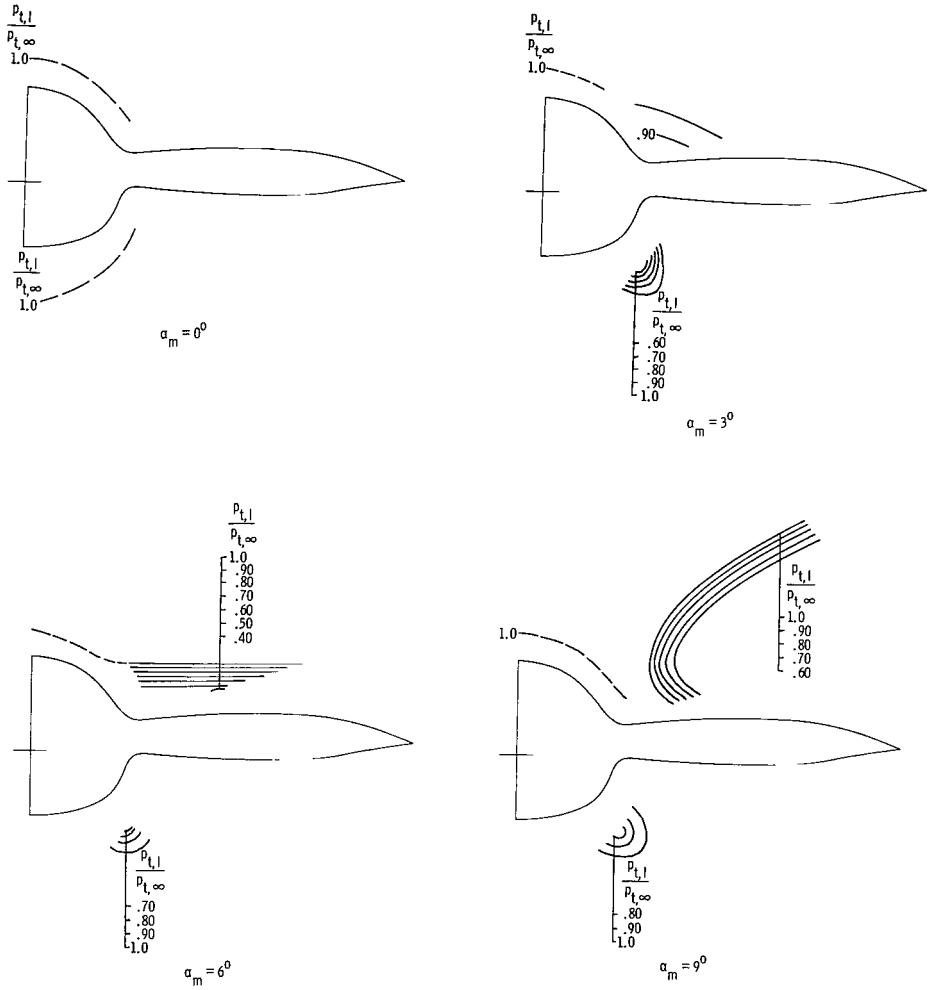

(c) Ratio of local to free-stream total pressure. $\beta_m = 0^0$.

Figure 7.- Continued

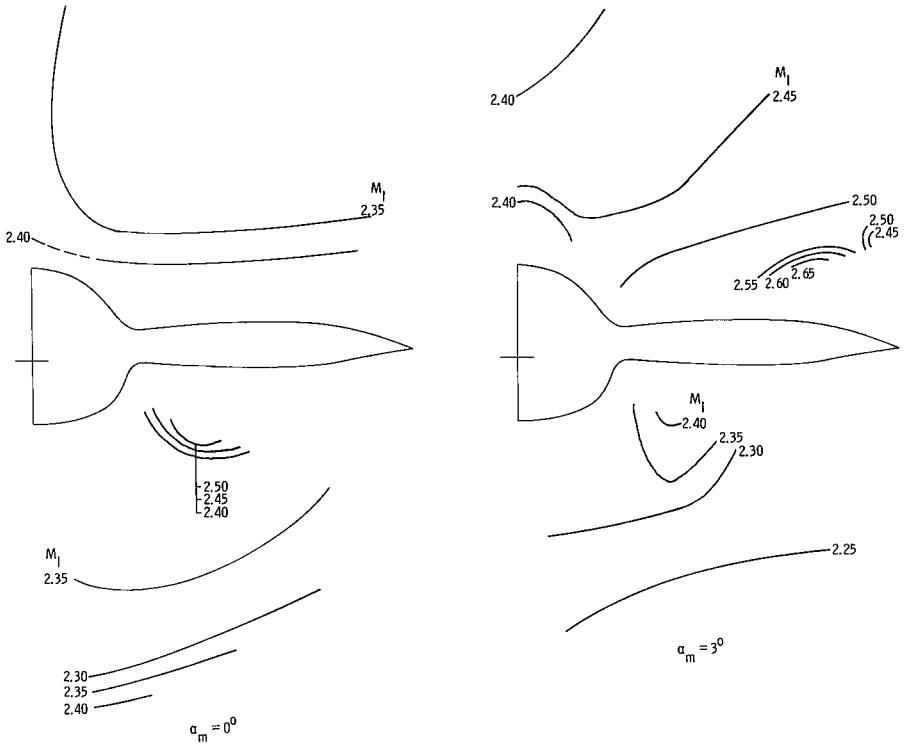

(d) Local Mach number. $\beta_m = 5^0$.

Figure 7.- Continued.

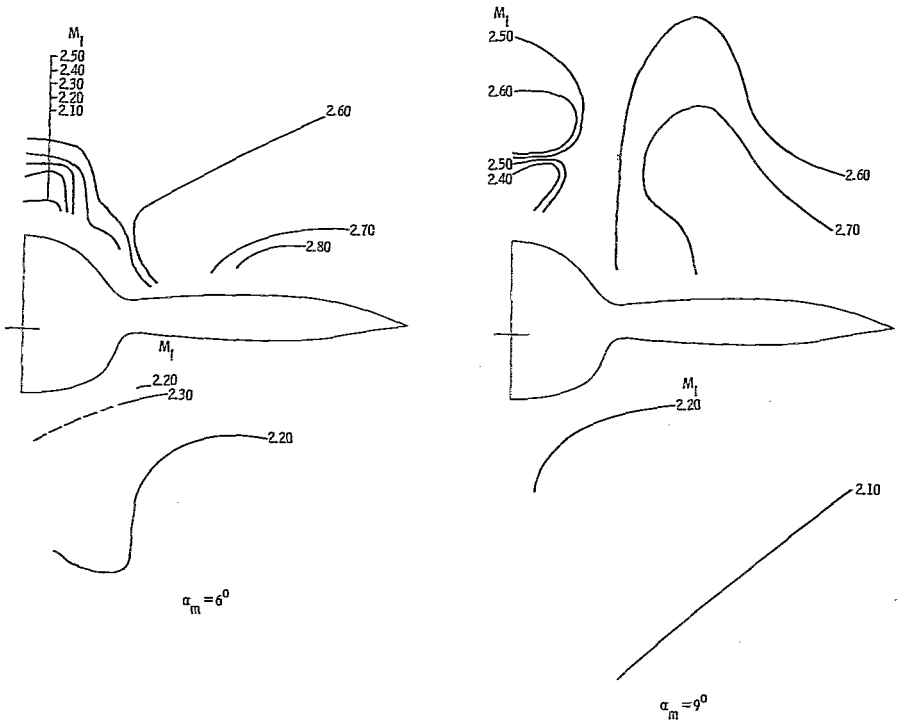

(d) Concluded.

Figure 7.- Continued.

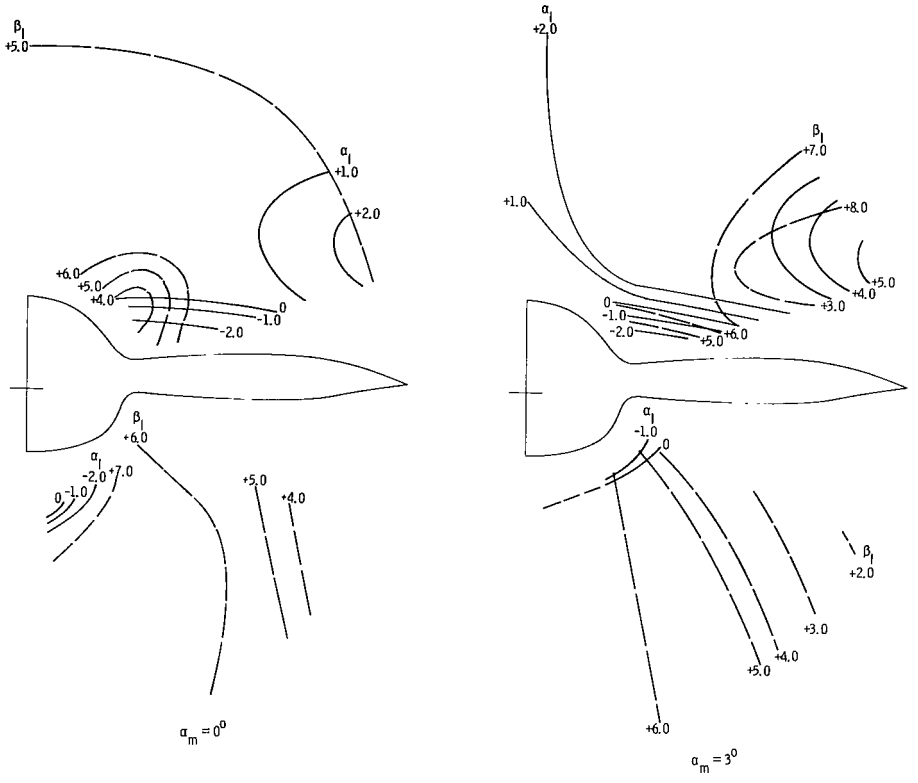

(e) Local flow angles. $\beta_m = 5^o$.

Figure 7.- Continued.

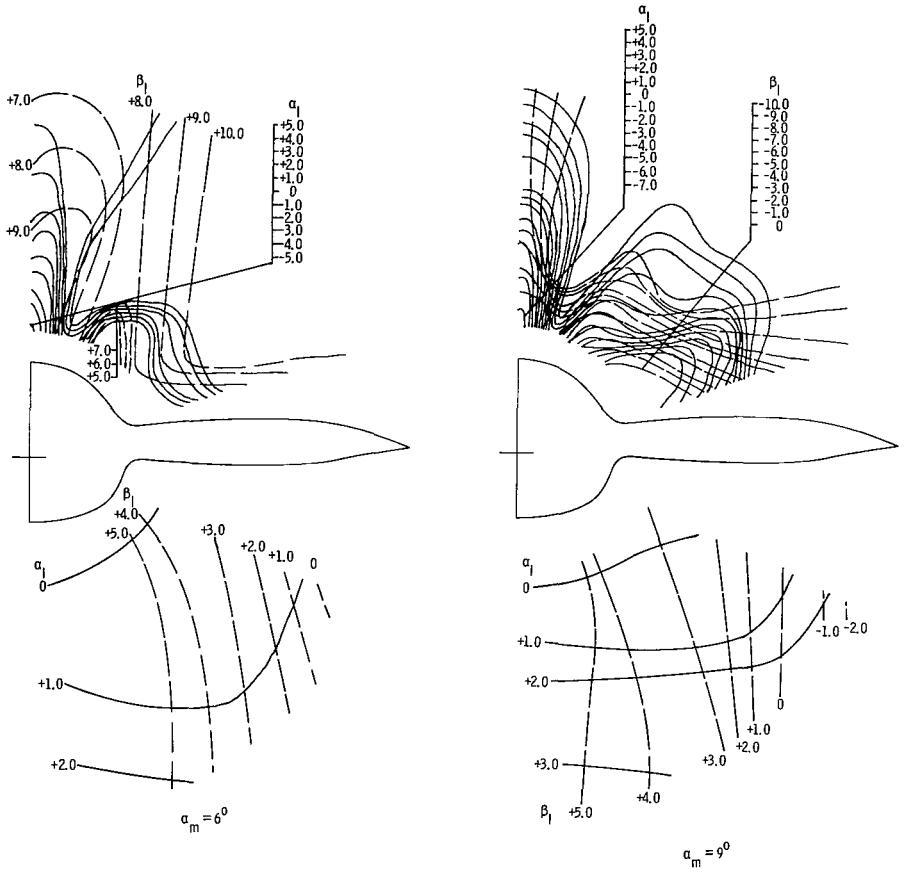

(e) Concluded.

Figure 7.- Continued.

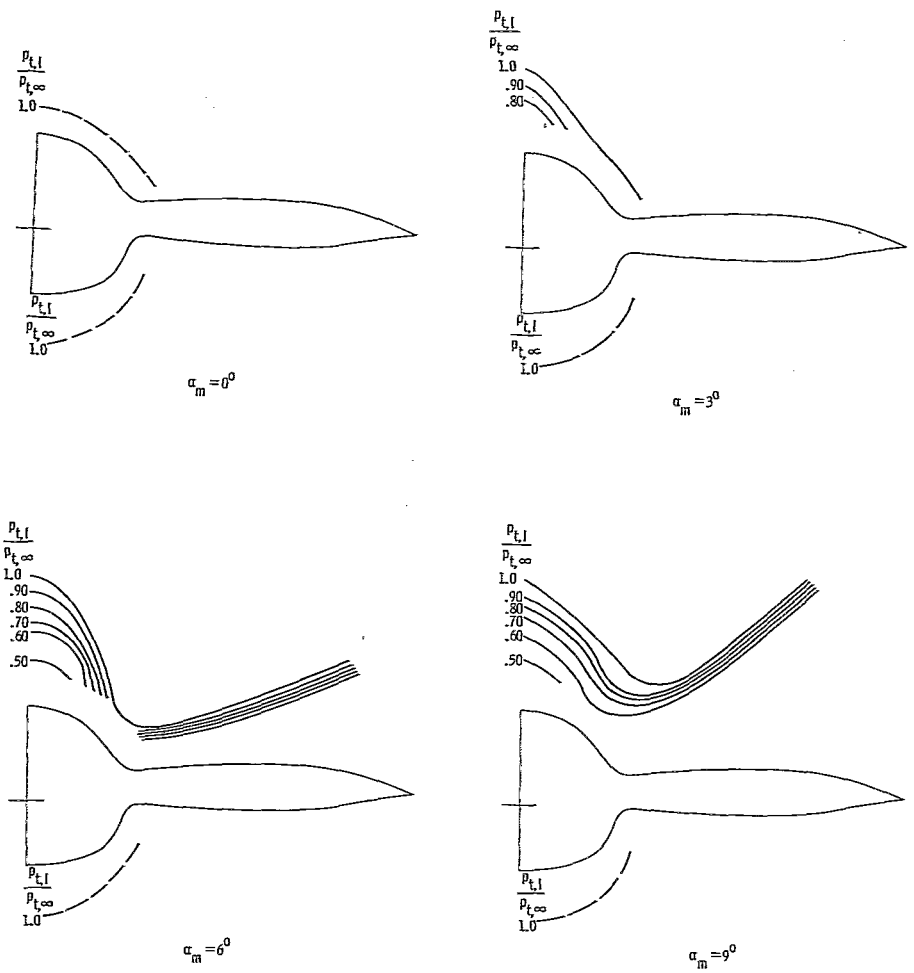

(f) Ratio of local to free-stream total pressure. $\beta_m = 5^0$.

Figure 7.- Continued.

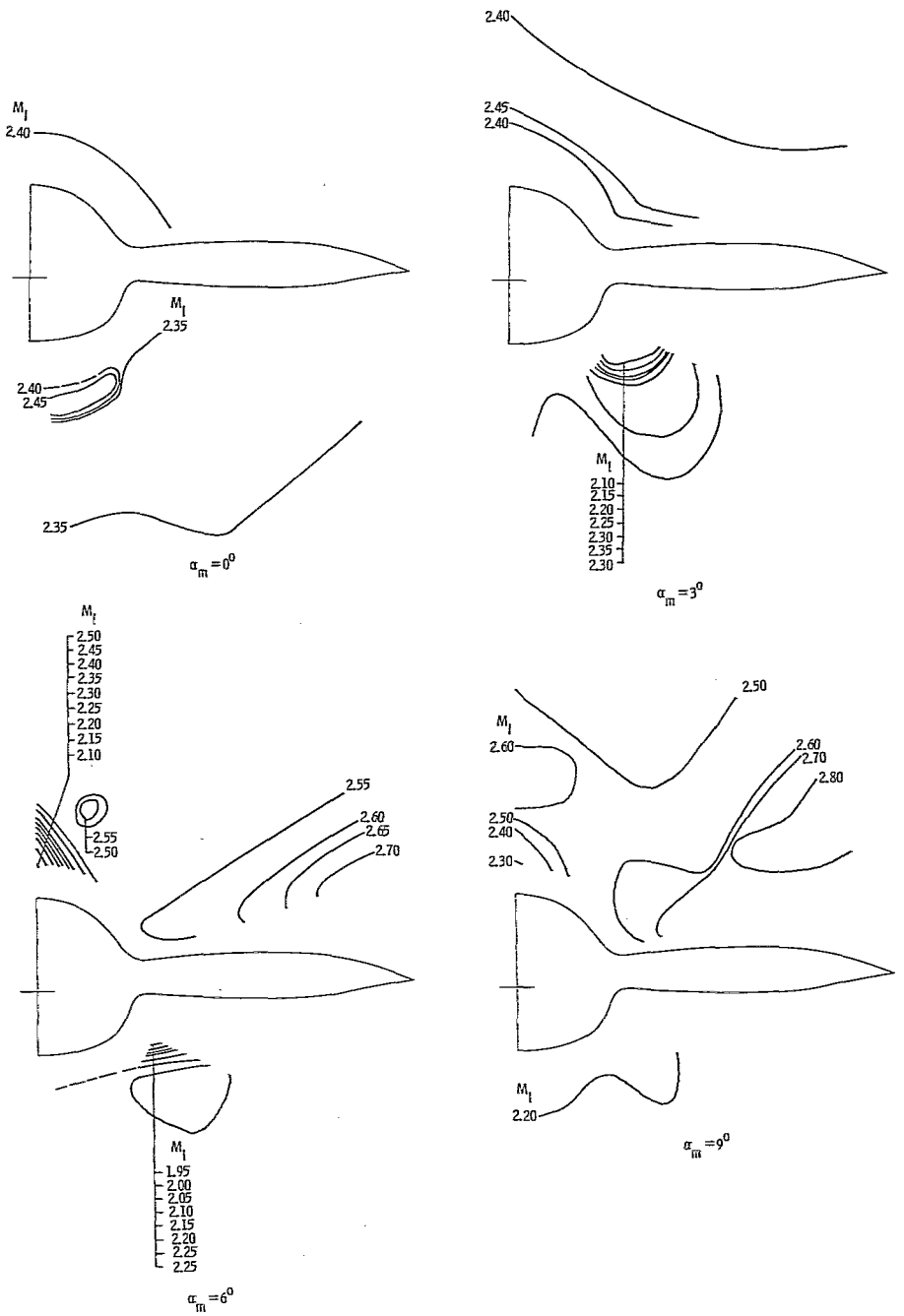

(g) Local Mach number. $\beta_m = -5^0$.

Figure 7.- Continued.

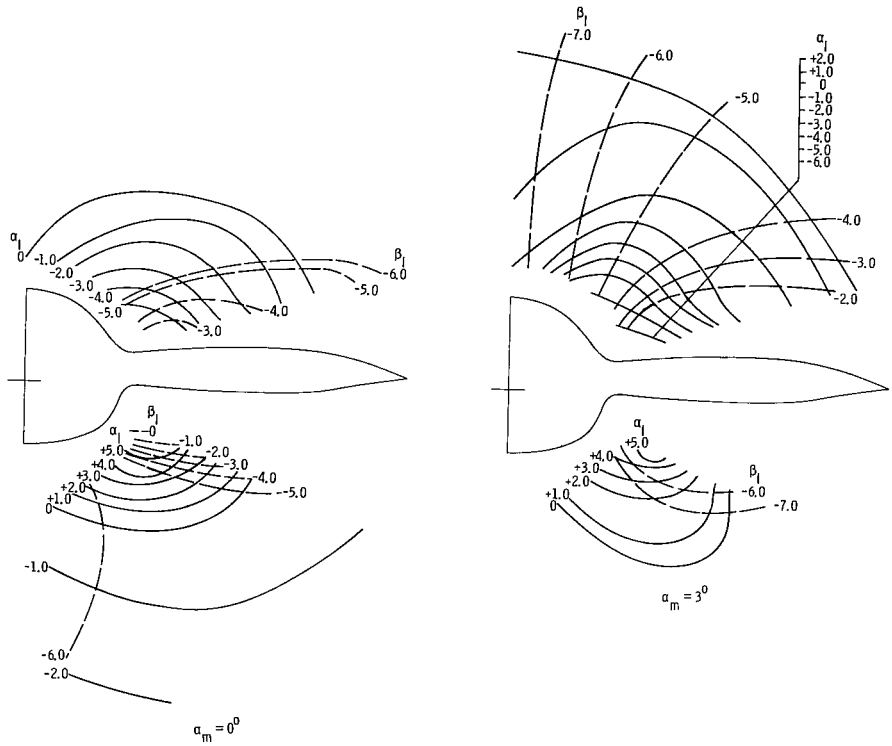

(h) Local flow angles. $B_m = -5^0$.

Figure 7.- Continued.

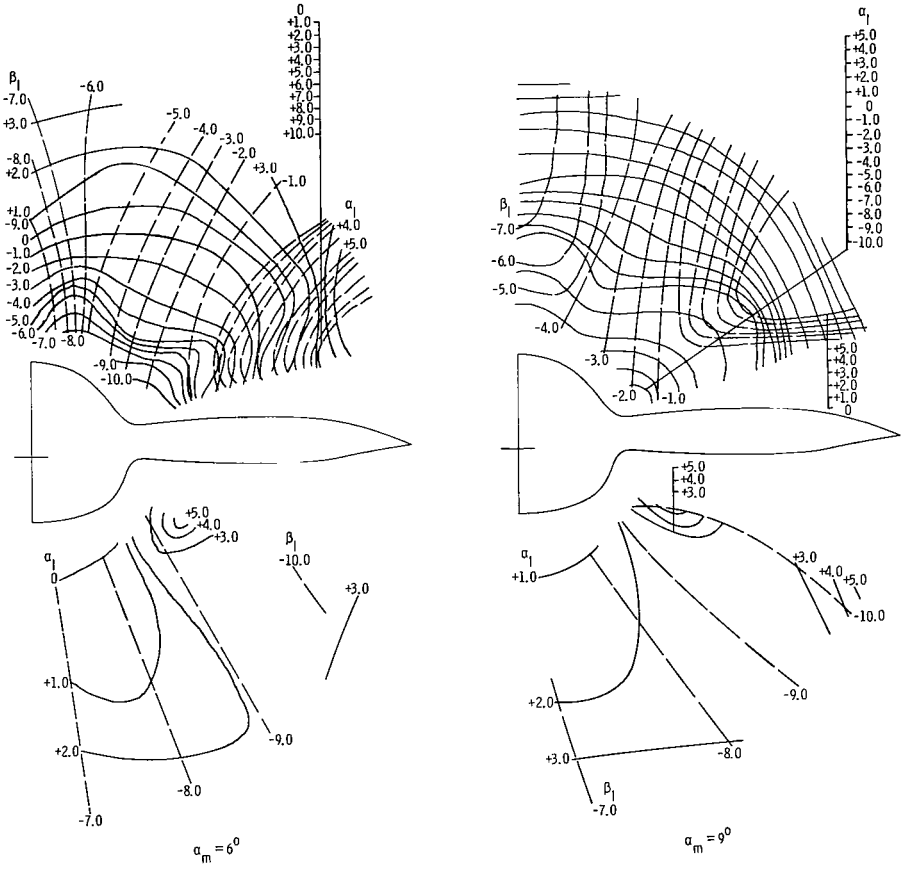

(h) Concluded.

Figure 7.- Continued.

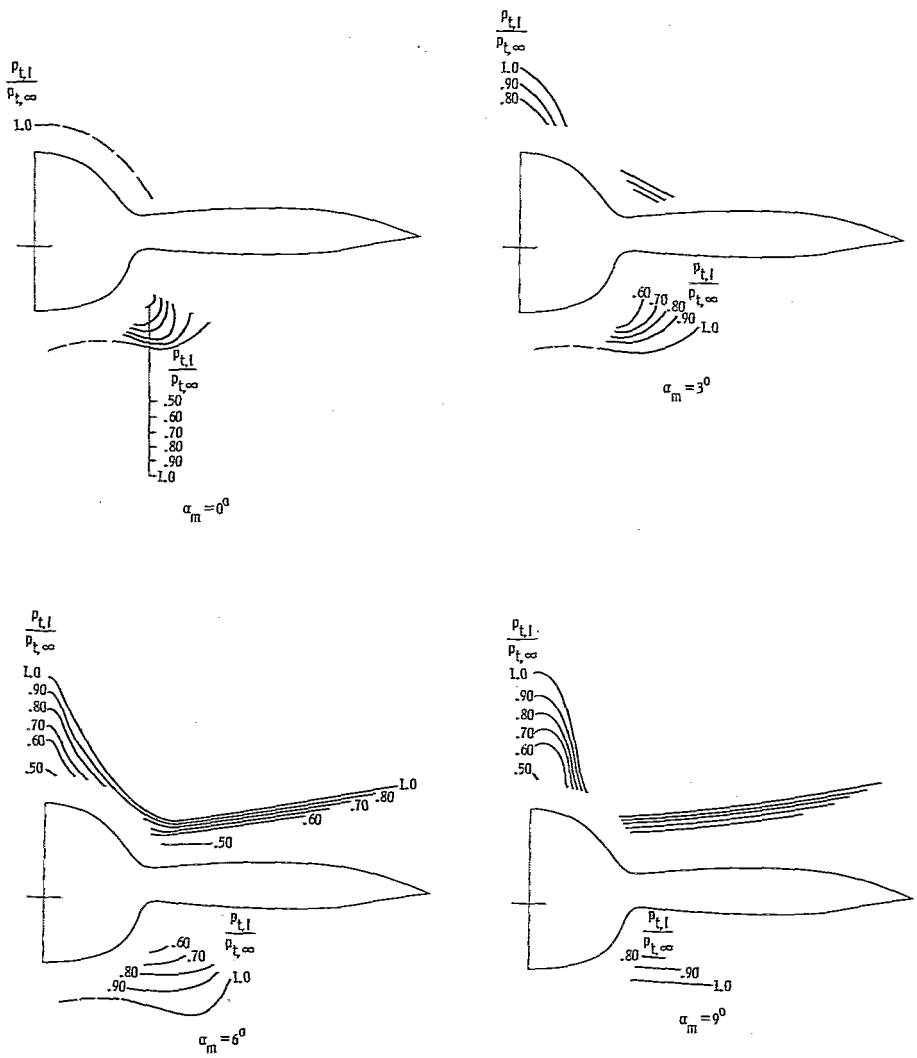

(i) Ratio of local to free-stream total pressure. $\beta_m = -5^0$.

Figure 7.- Concluded.

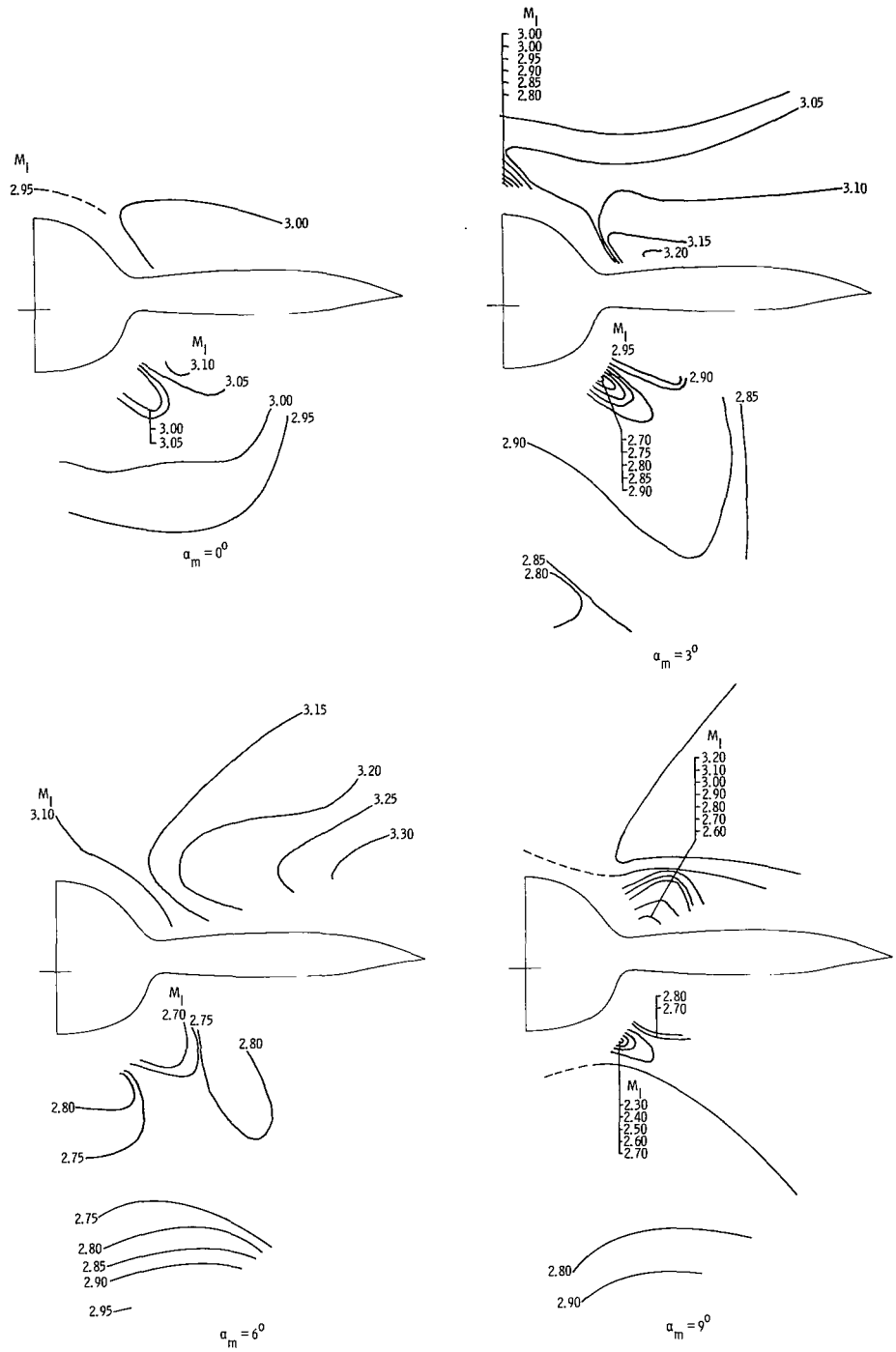

(a) Local Mach number. $\beta_m = 0^o$.

Figure 8.- Local flow parameters at x = 80.21 cm. $M_\infty = 2.96$.

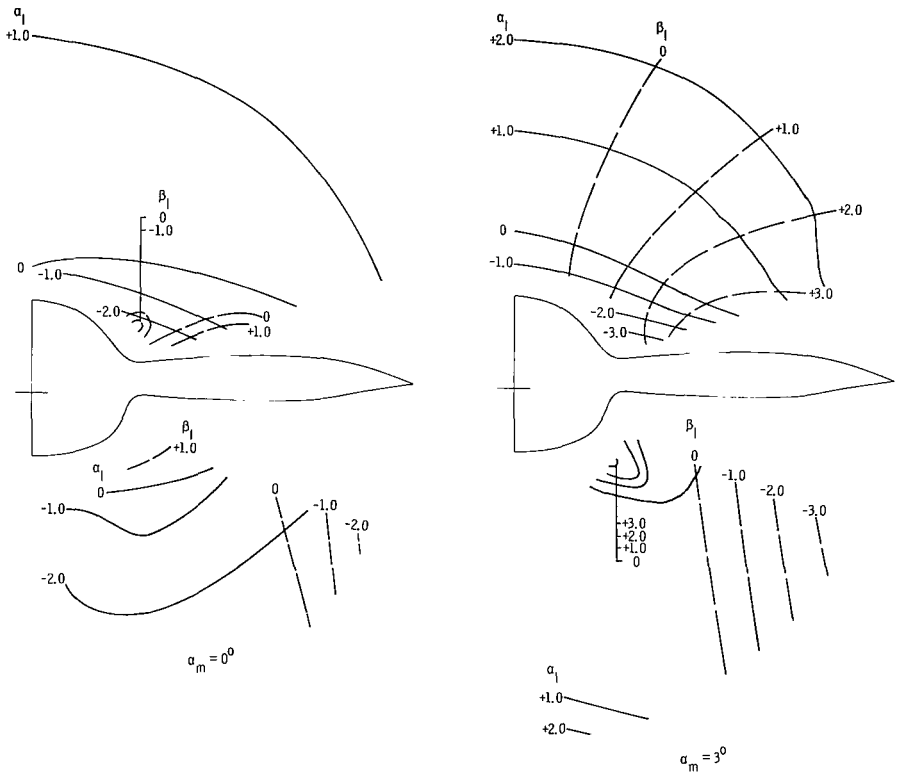

(b) Local flow angles. $\beta_m = 0^o$.

Figure 8.- Continued.

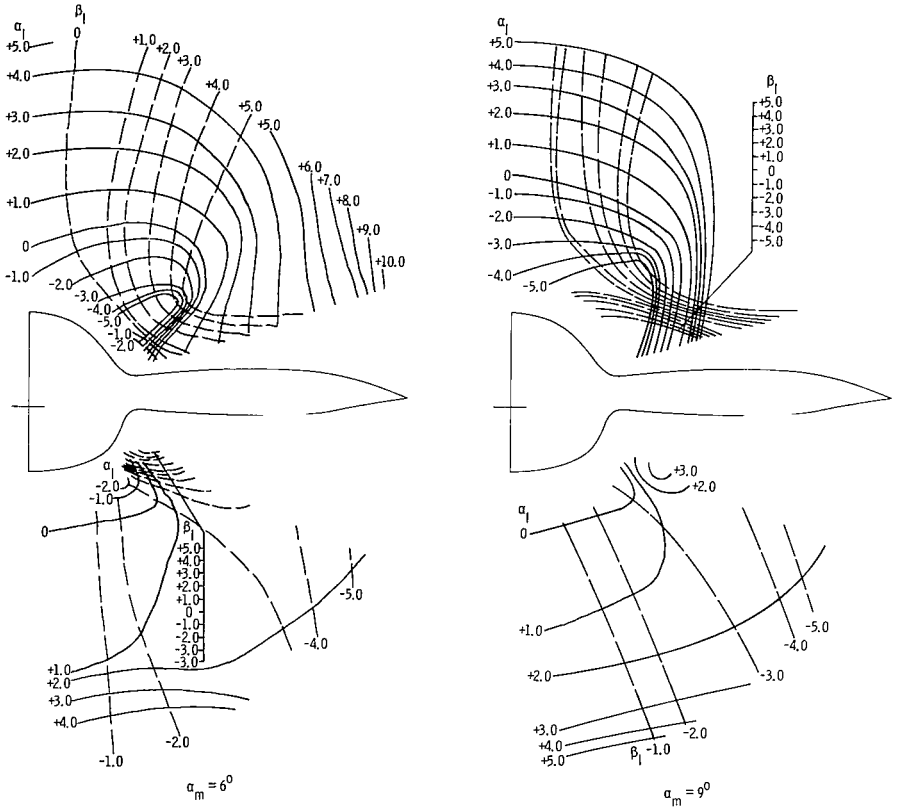

(b) Concluded.

Figure 8.- Continued.

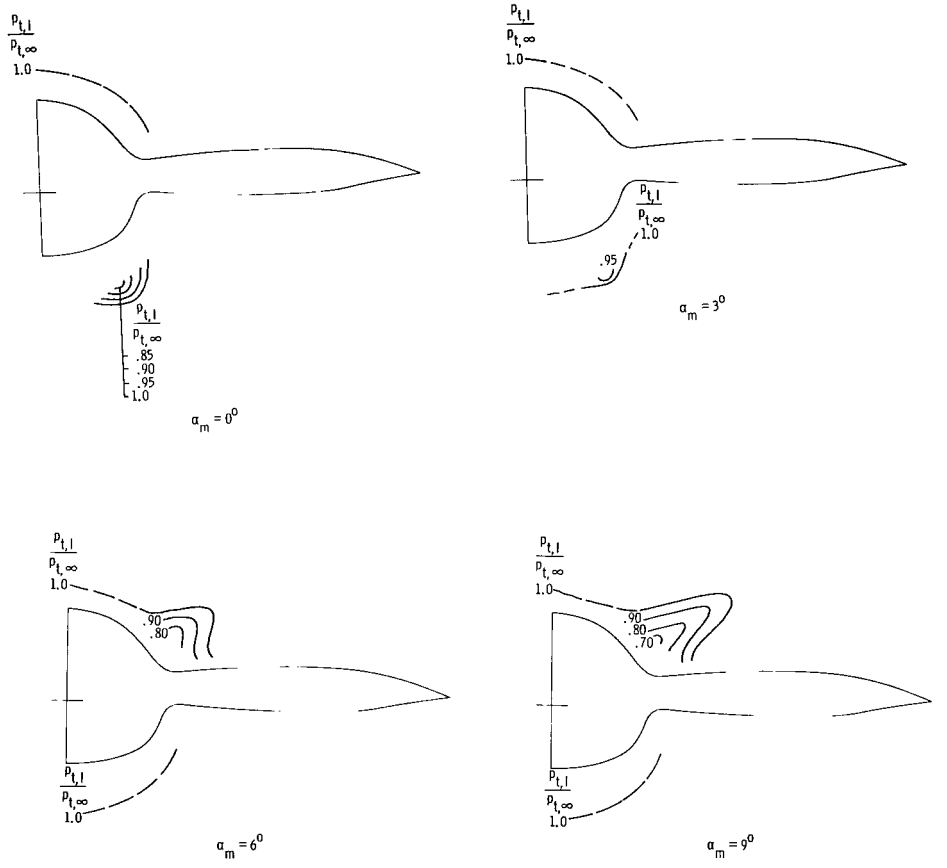

(c) Ratio of local to free-stream total pressure. $\beta_m = 0^0$.

Figure 8.- Continued.

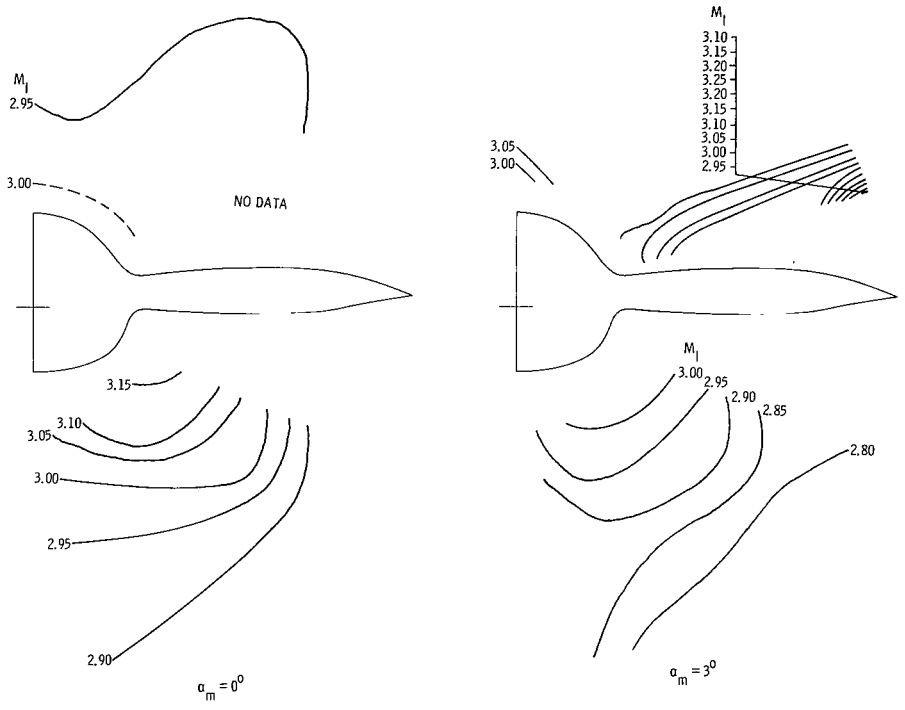

(d) Local Mach number. $\beta_m = 5^0$.

Figure 8.- Continued.

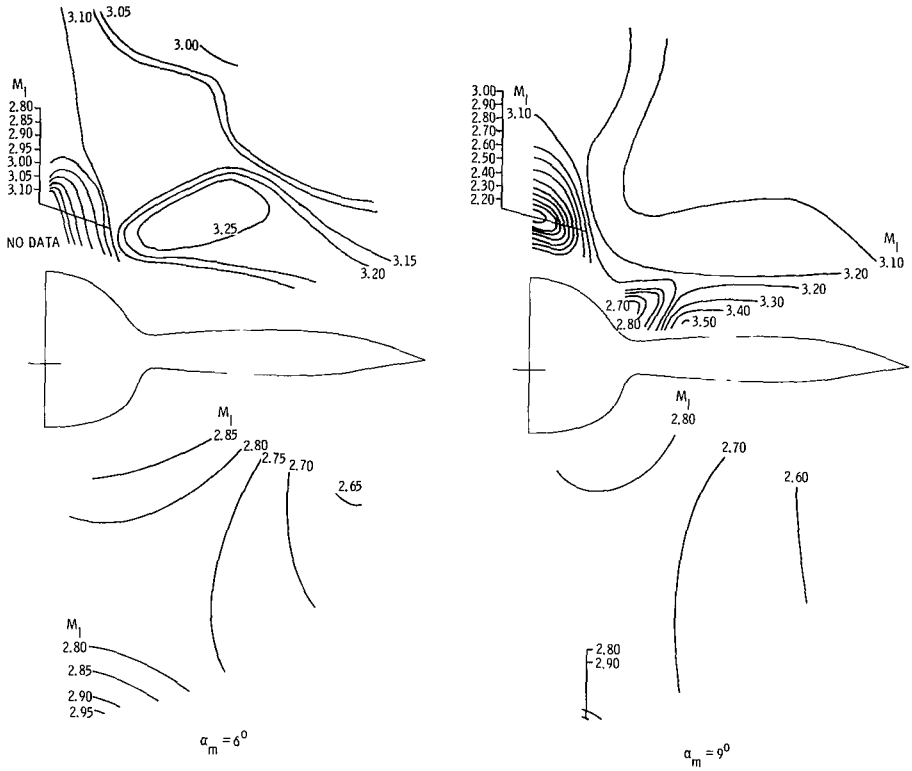

(d) Concluded.

Figure 8.- Continued.

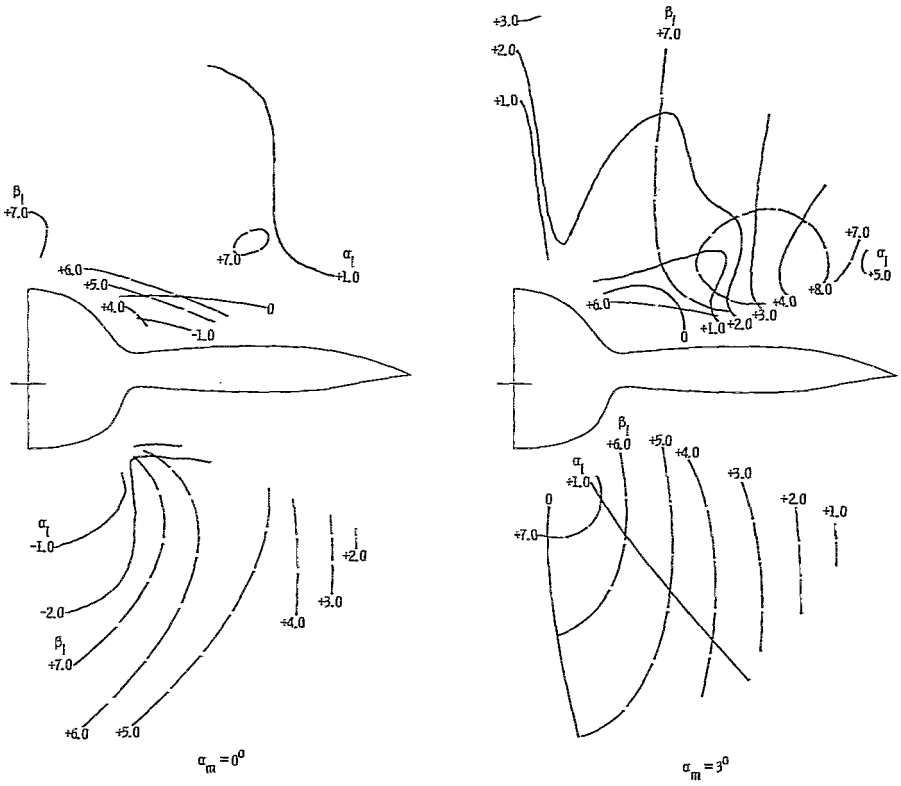

(e) Local flow angles. $\beta_m = 5^0$.

Figure 8.- Continued.

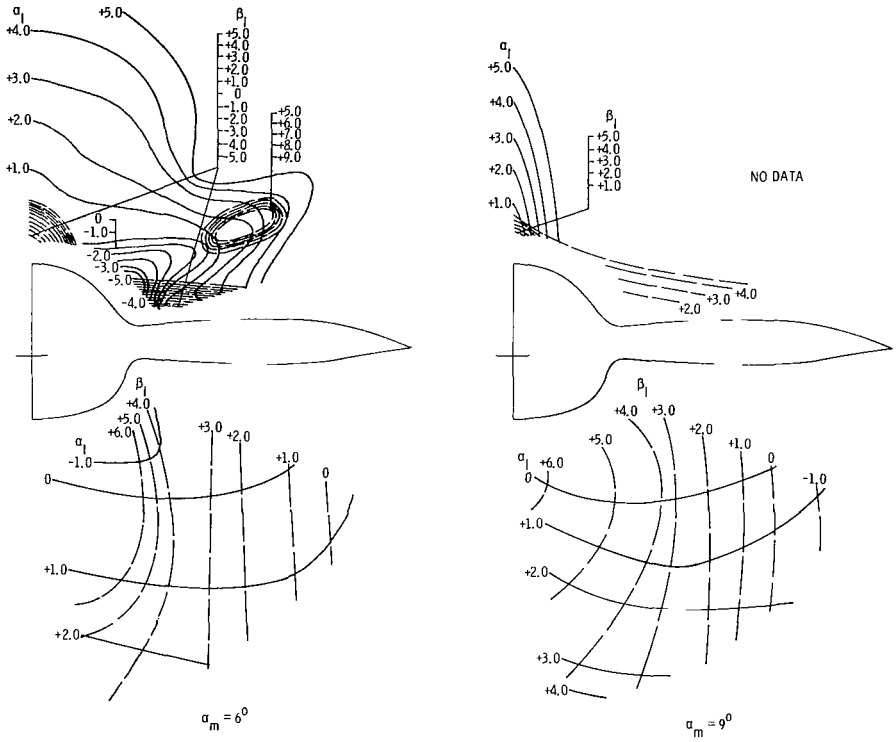

(e) Concluded.

Figure 8.- Continued.

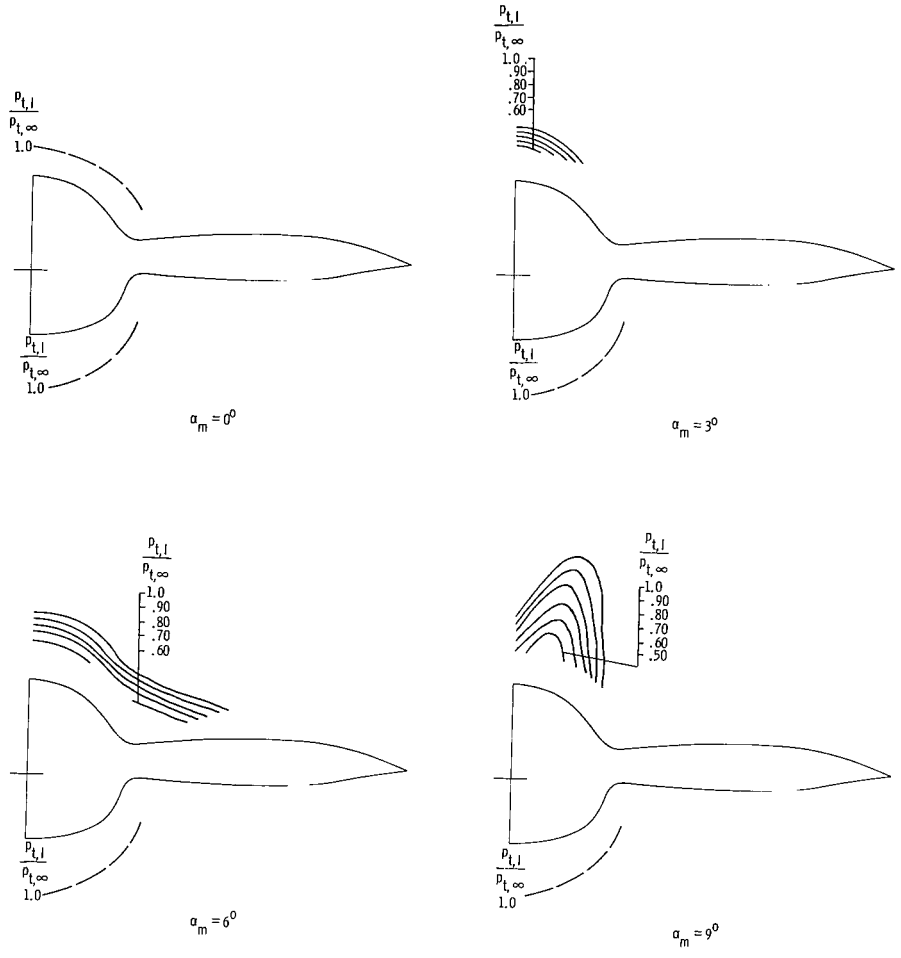

(f) Ratio of local to free-stream total pressure. $\beta_m = 5^0$.

Figure 8.- Continued.

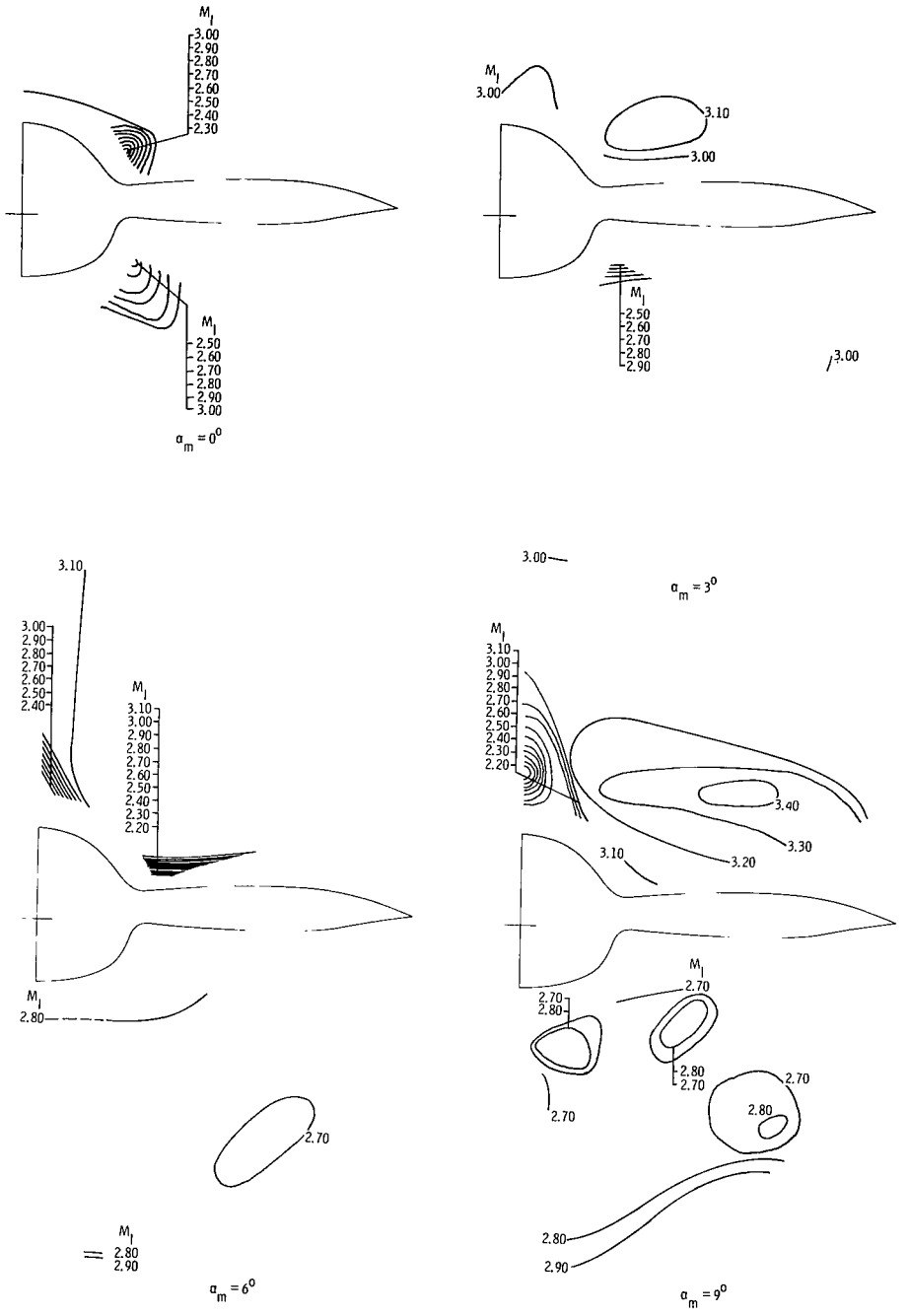

(g) Local Mach number. $\beta_m = -5^0$.

Figure 8.- Continued.

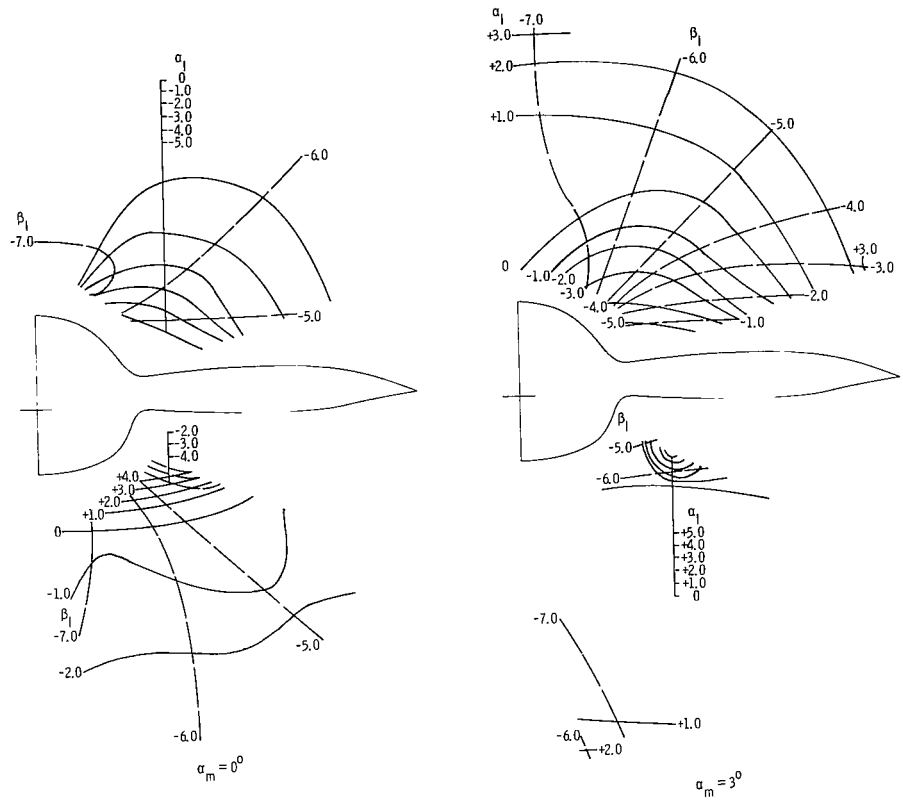

(h) Local flow angles. $\beta_m = -5^o$.

Figure 8.- Continued.

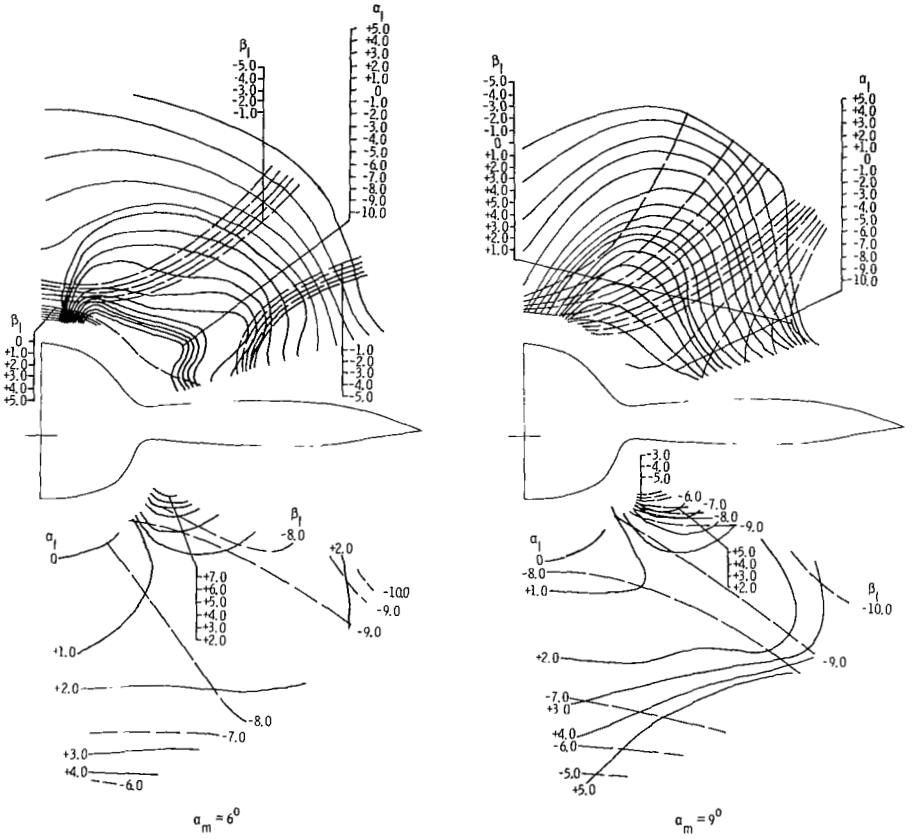

(h) Concluded.

Figure 8.- Continued.

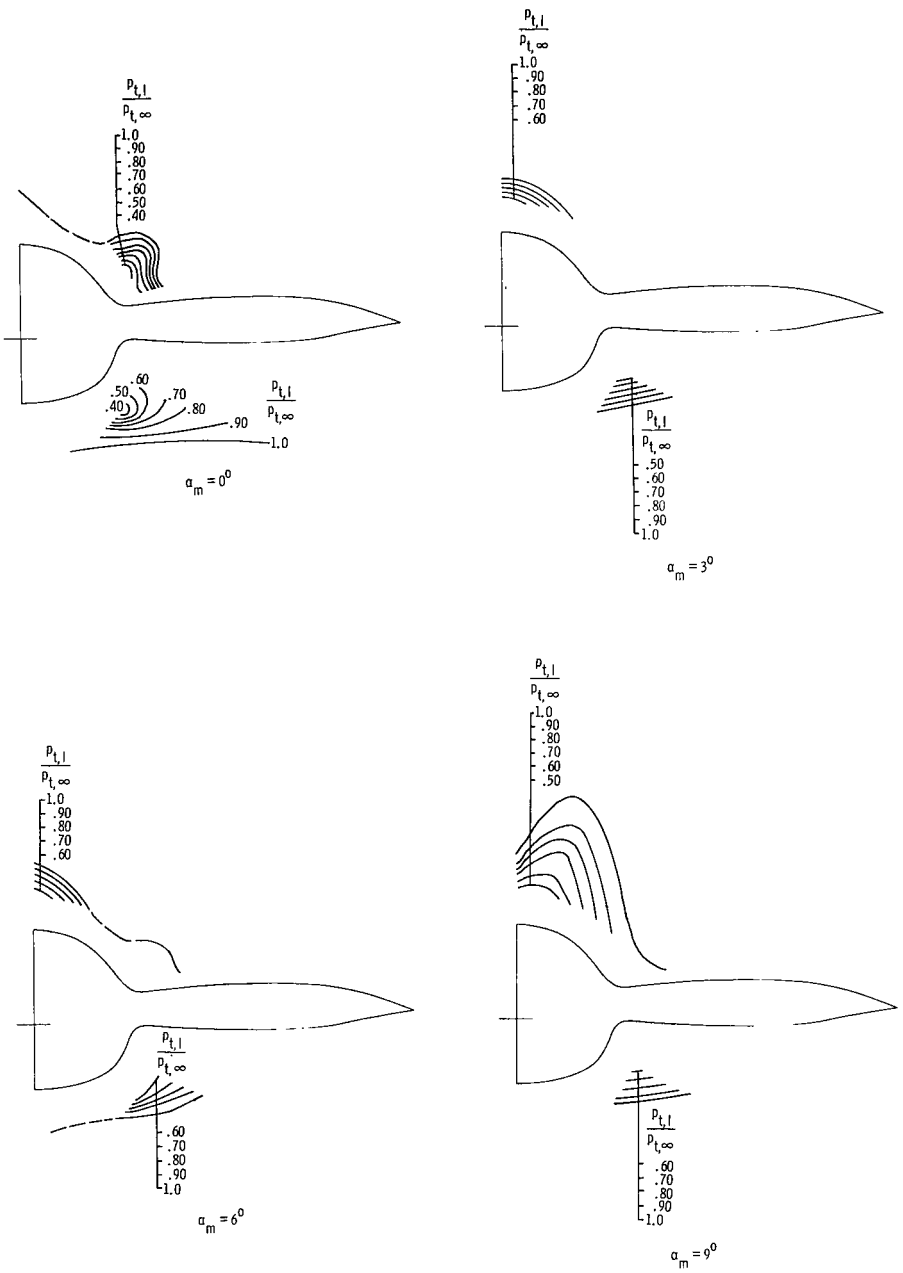

(i) Ratio of local to free-stream total pressure. $\beta_m = -5^0$.

Figure 8.- Concluded.

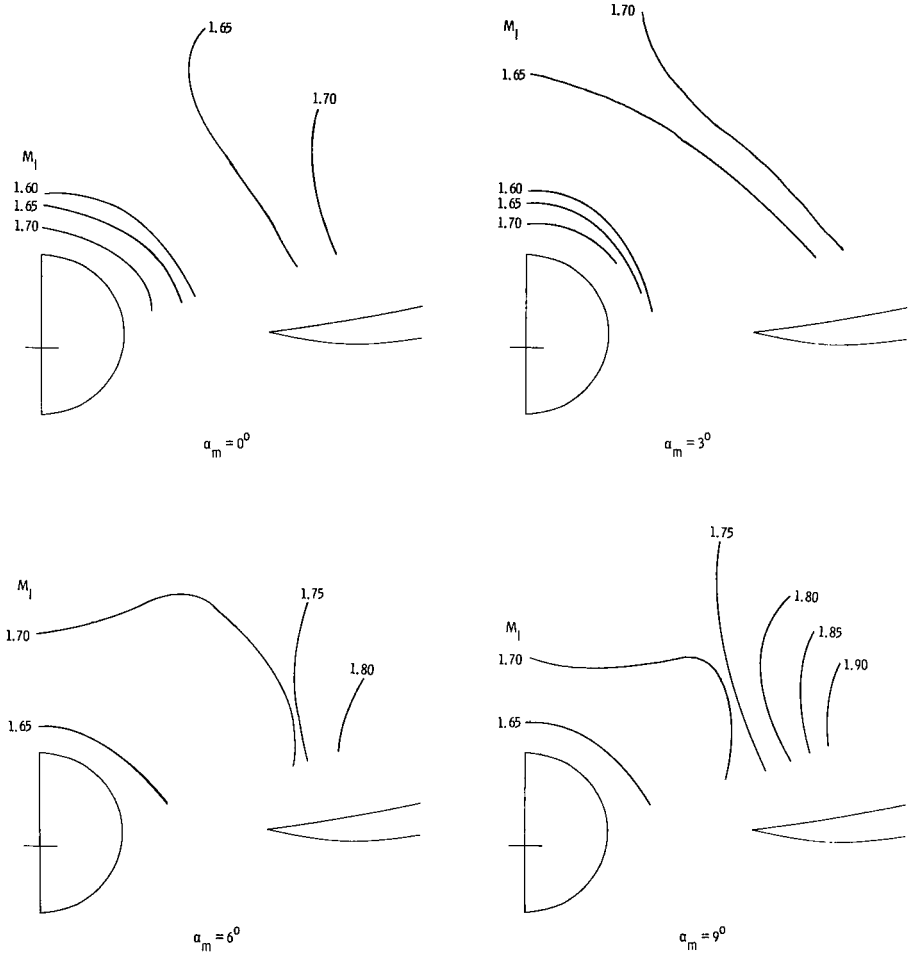

(a) Local Mach number.

Figure 9.- Local flow parameters at x = 97.49 cm. $\beta_m = 0^0$; $M_\infty = 1.60$.

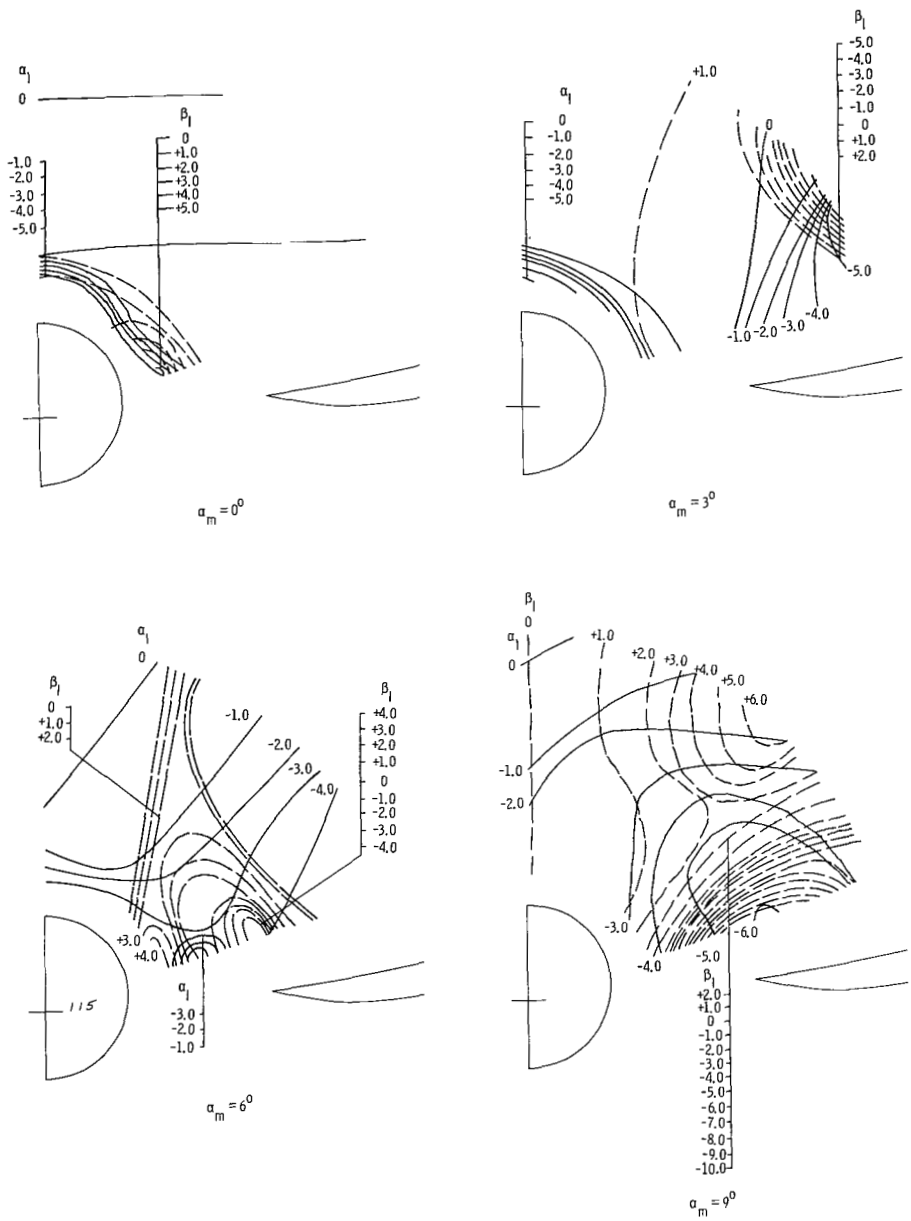

(b) Local flow angles.

Figure 9.- Continued.

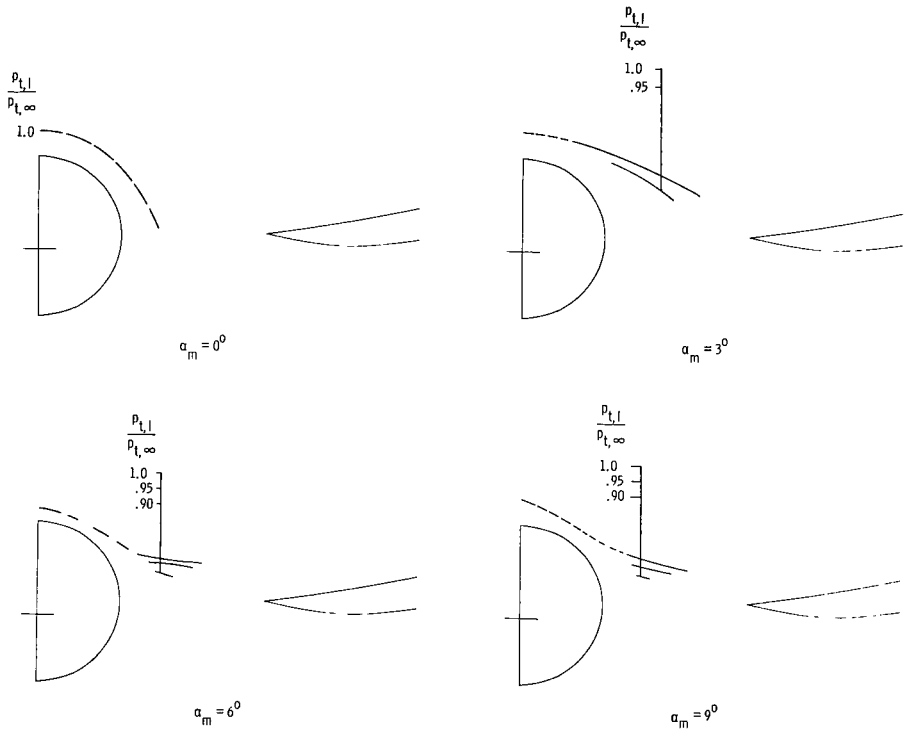

(c) Ratio of local to free-stream total pressure.

Figure 9.- Concluded.

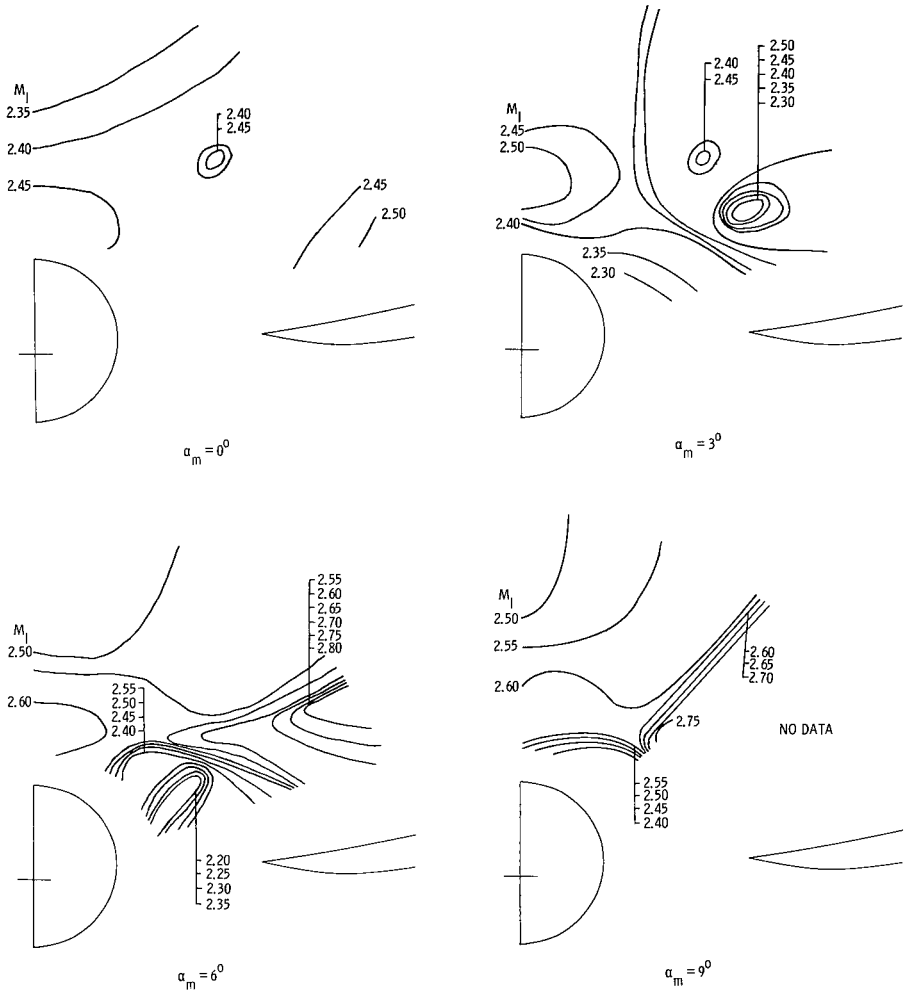

(a) Local Mach number.

Figure 10.- Local flow parameters at $x = 97.49$ cm. $\beta_m = 0^0$; $M_\infty = 2.36$.

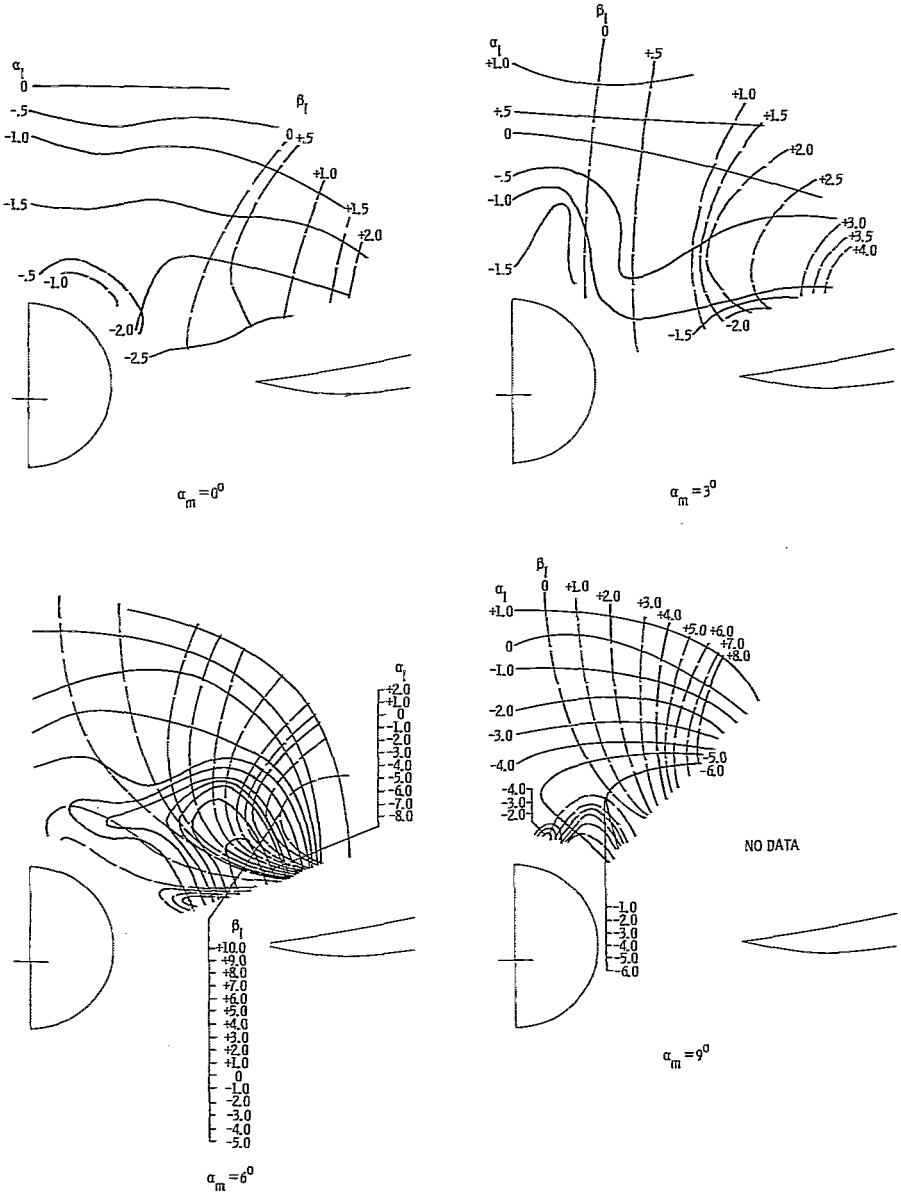

(b) Local flow angles.

Figure 10.- Continued.

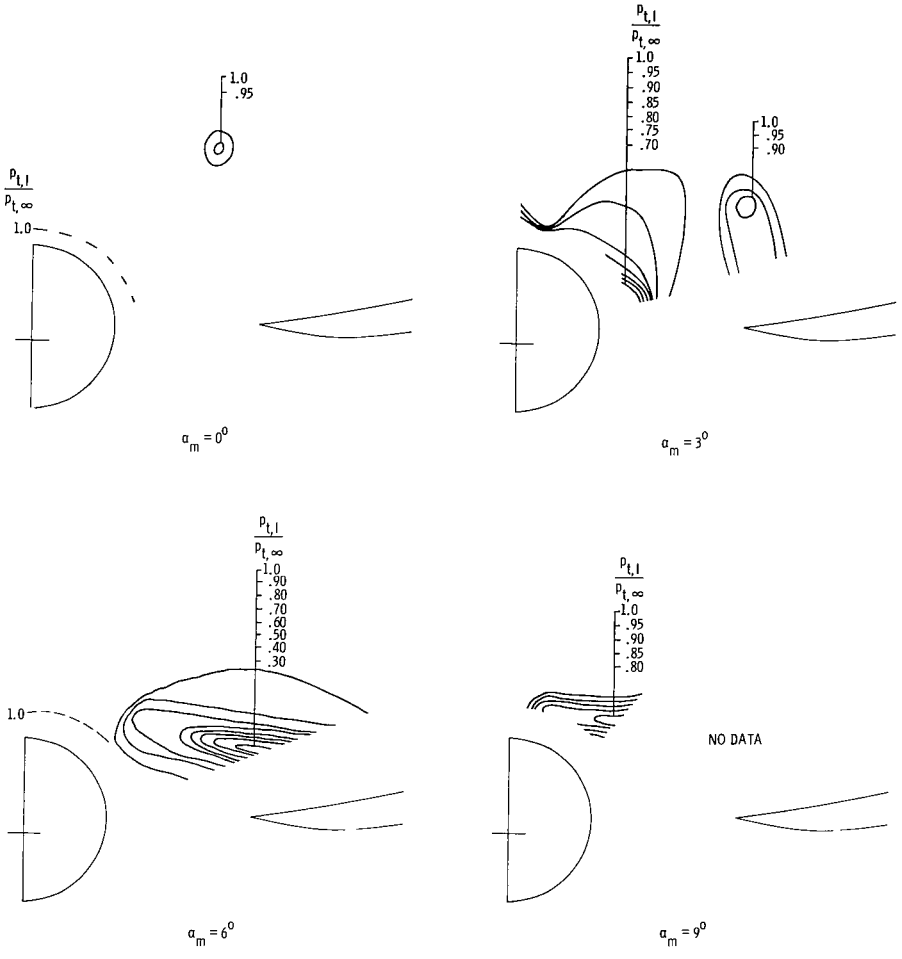

(c) Ratio of local to free-stream total pressure.

Figure 10.- Concluded.

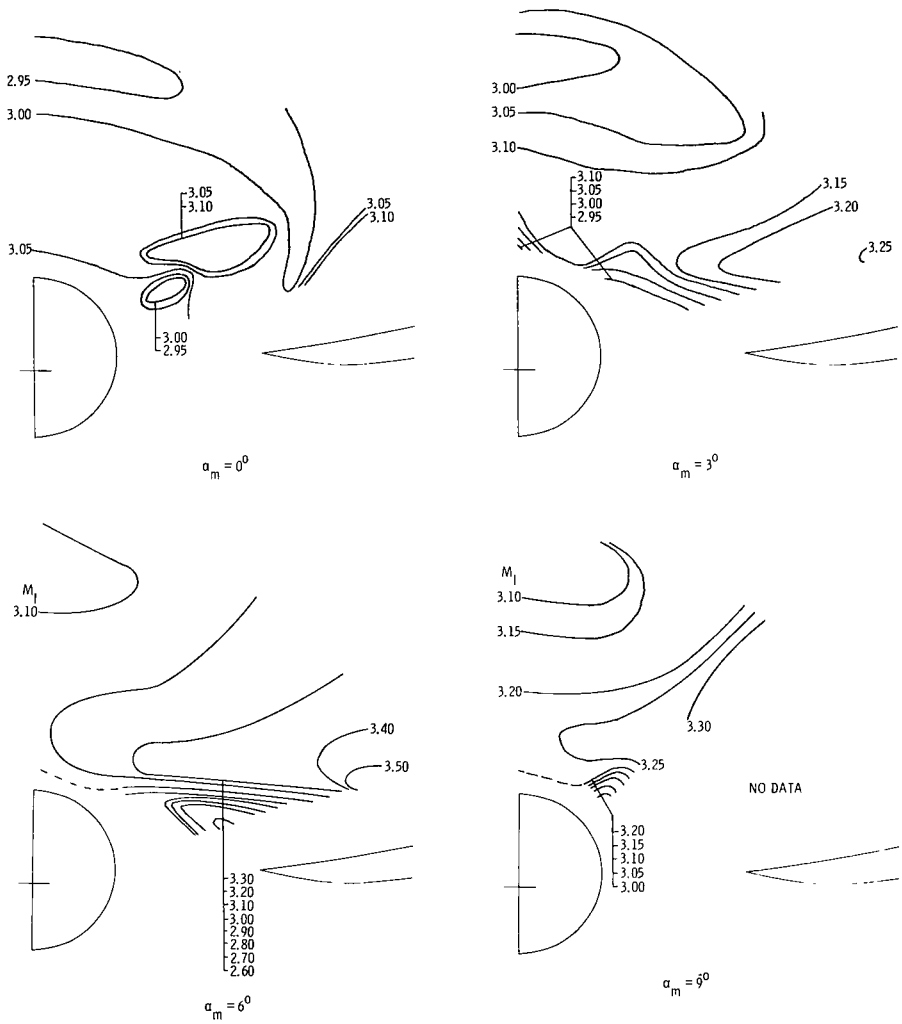

(a) Local Mach number.

Figure 11.- Local flow parameters at x = 97.49 cm. $\beta_m = 0^0$; $M_\infty = 2.96$.

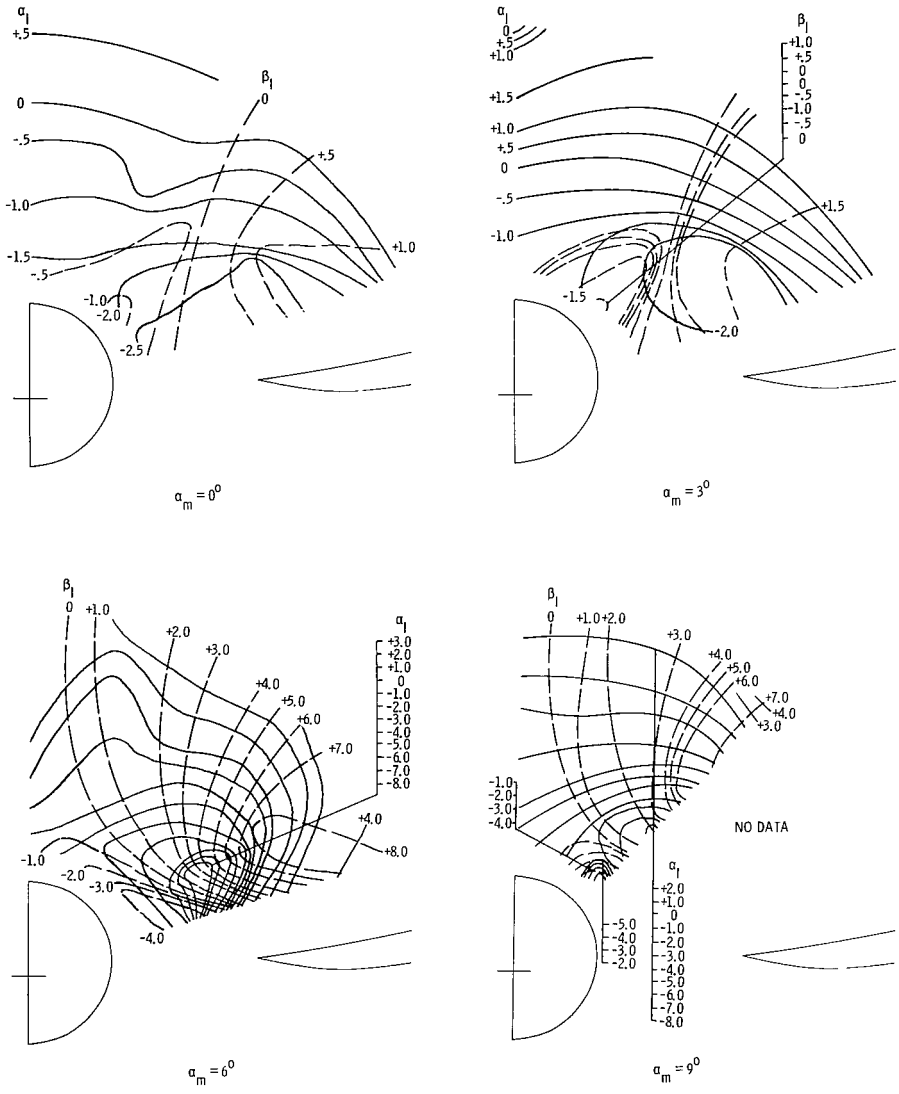

(b) Local flow angles.

Figure 11.- Continued.

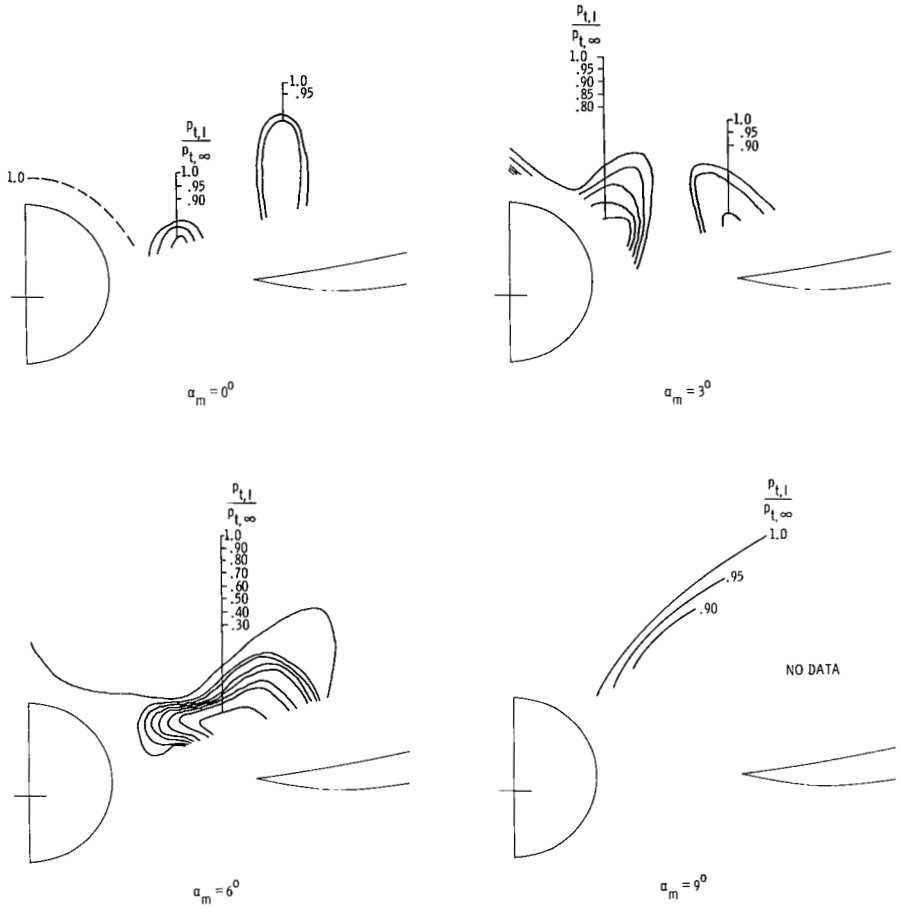

(c) Ratio of local to free-stream total pressure.

Figure 11.- Concluded.

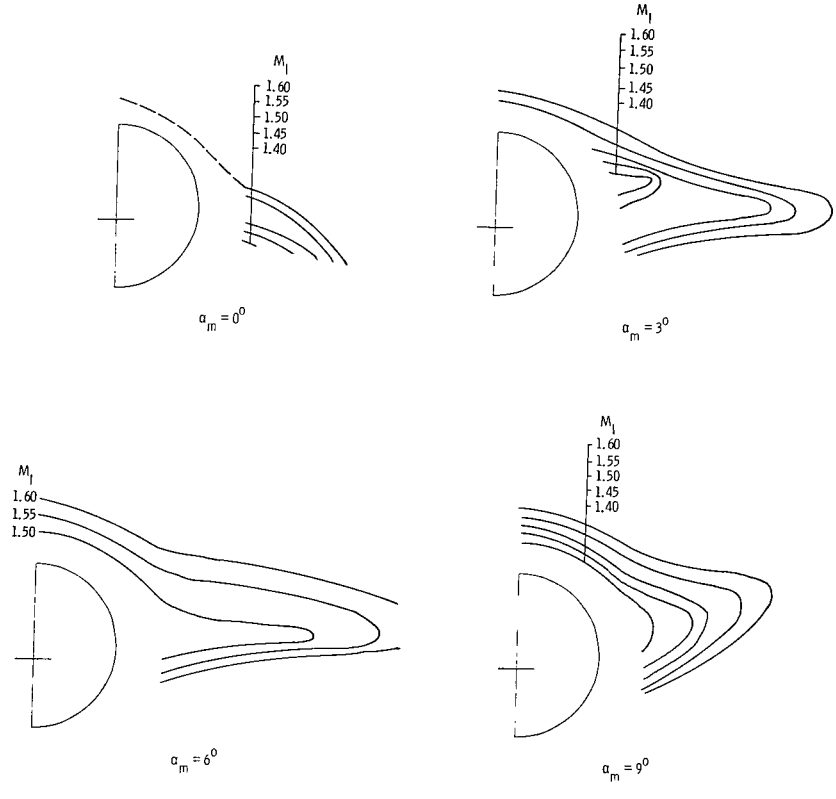

(a) Local Mach number. $\beta_m = 0^0$.

Figure 12.- Local flow parameters at $x = 115.14$ cm. $M_\infty = 1.60$.

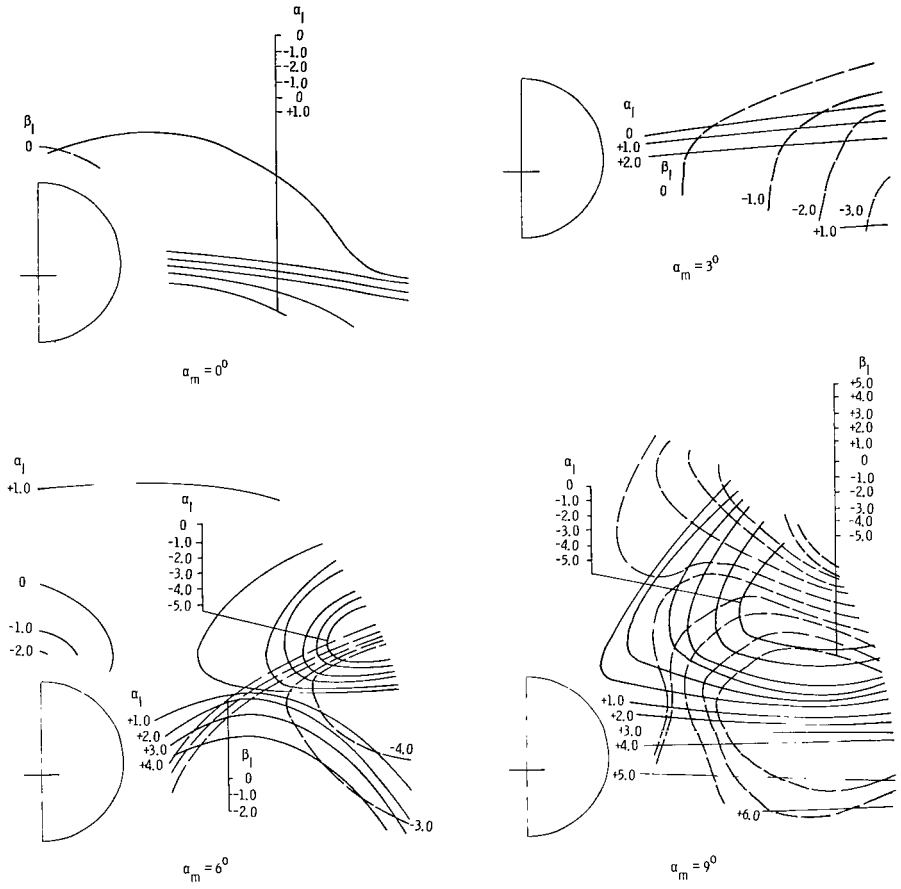

(b) Local flow angles. $\beta_m = 0^0$.

Figure 12.- Continued.

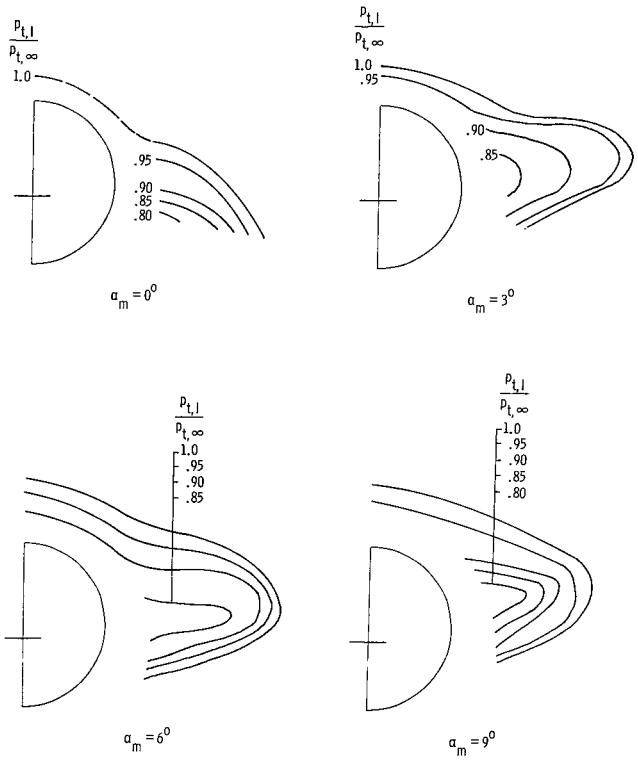

(c) Ratio of local to free-stream total pressure. $\beta_m = 0^o$.

Figure 12.- Continued.

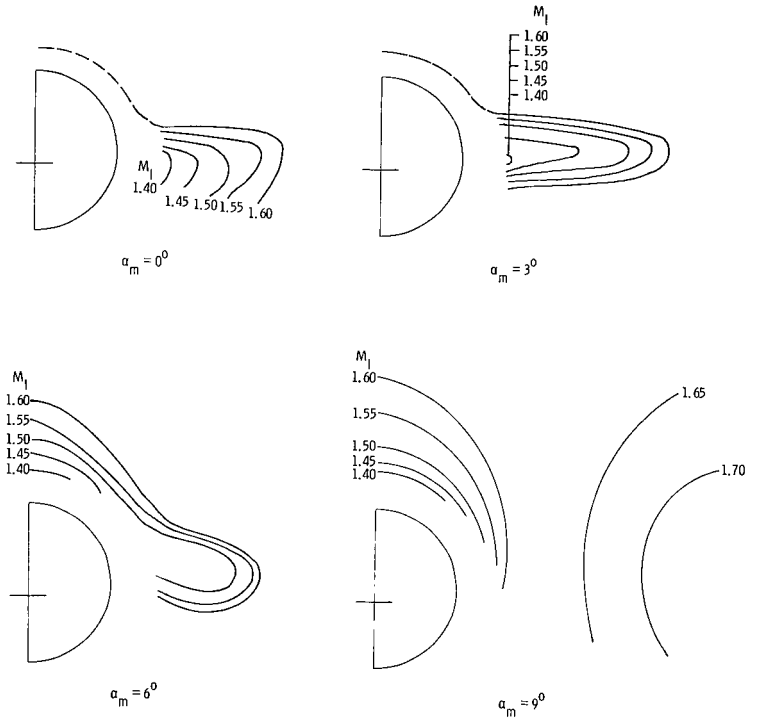

(d) Local Mach number. $\beta_m = 5^o$.

Figure 12.- Continued.

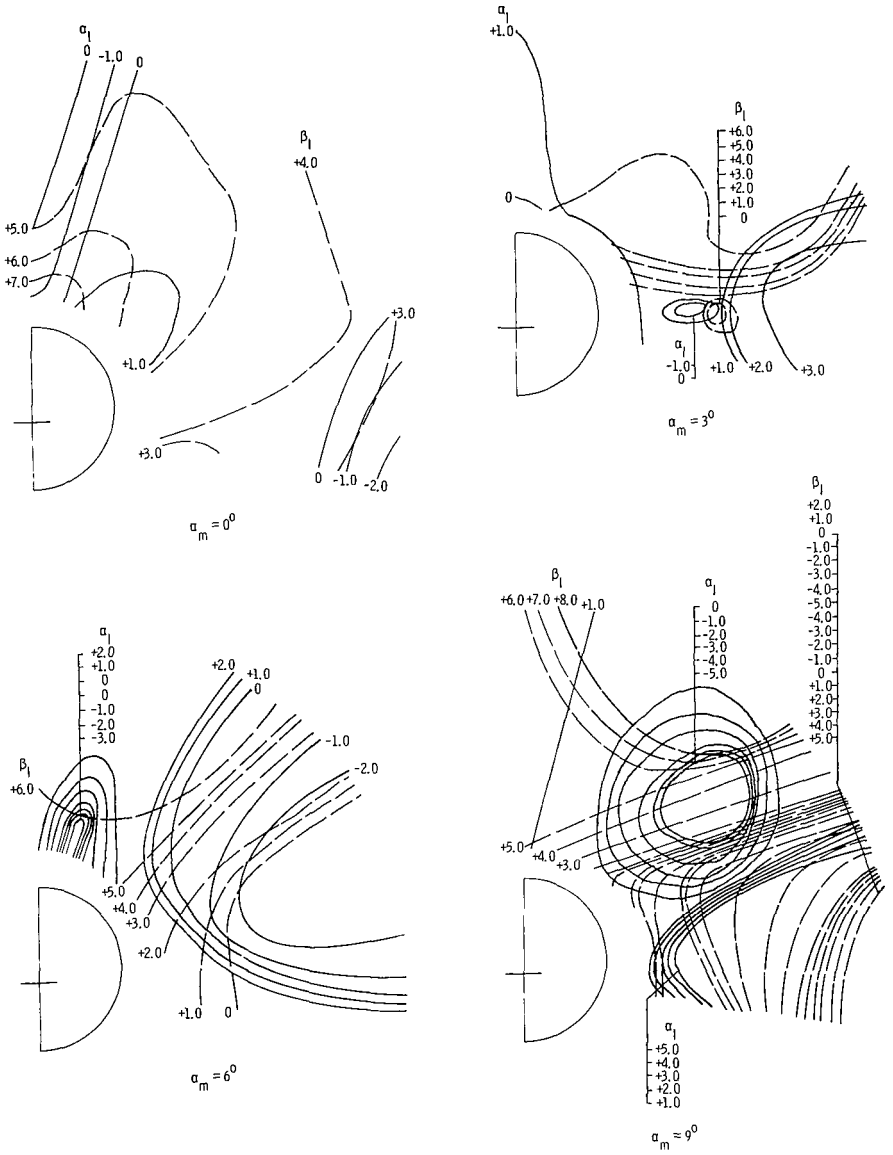

(e) Local flow angles. $\beta_m = 5^0$.

Figure 12.- Continued.

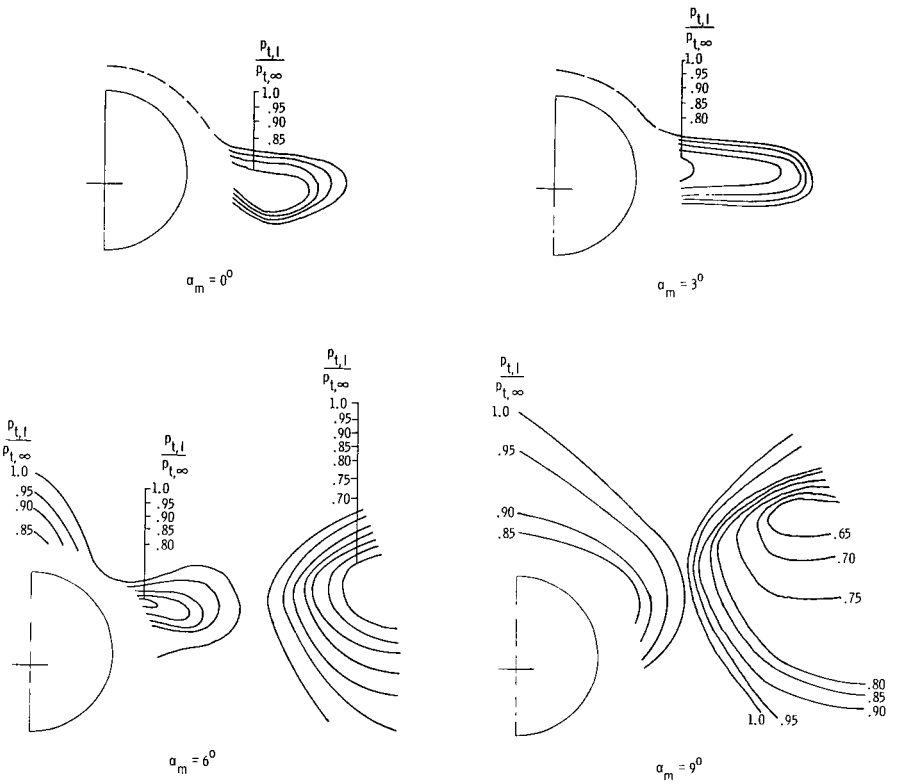

(f) Ratio of local to free-stream total pressure. $\beta_m = 5^0$.

Figure 12.- Continued.

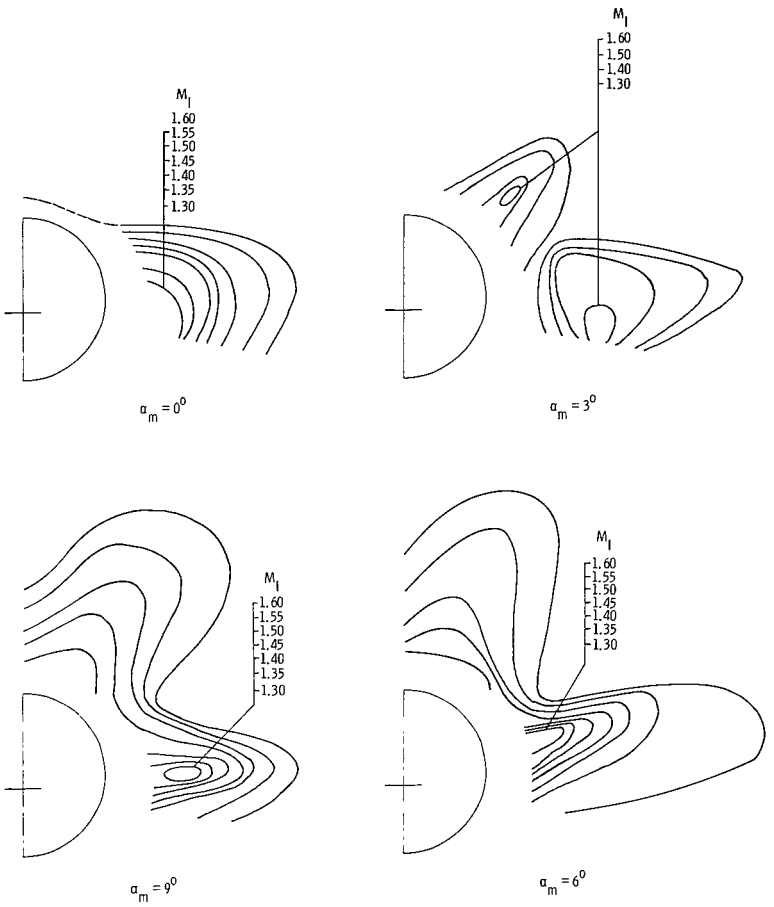

(g) Local Mach number. $\beta_m = -5^0$.

Figure 12.- Continued.

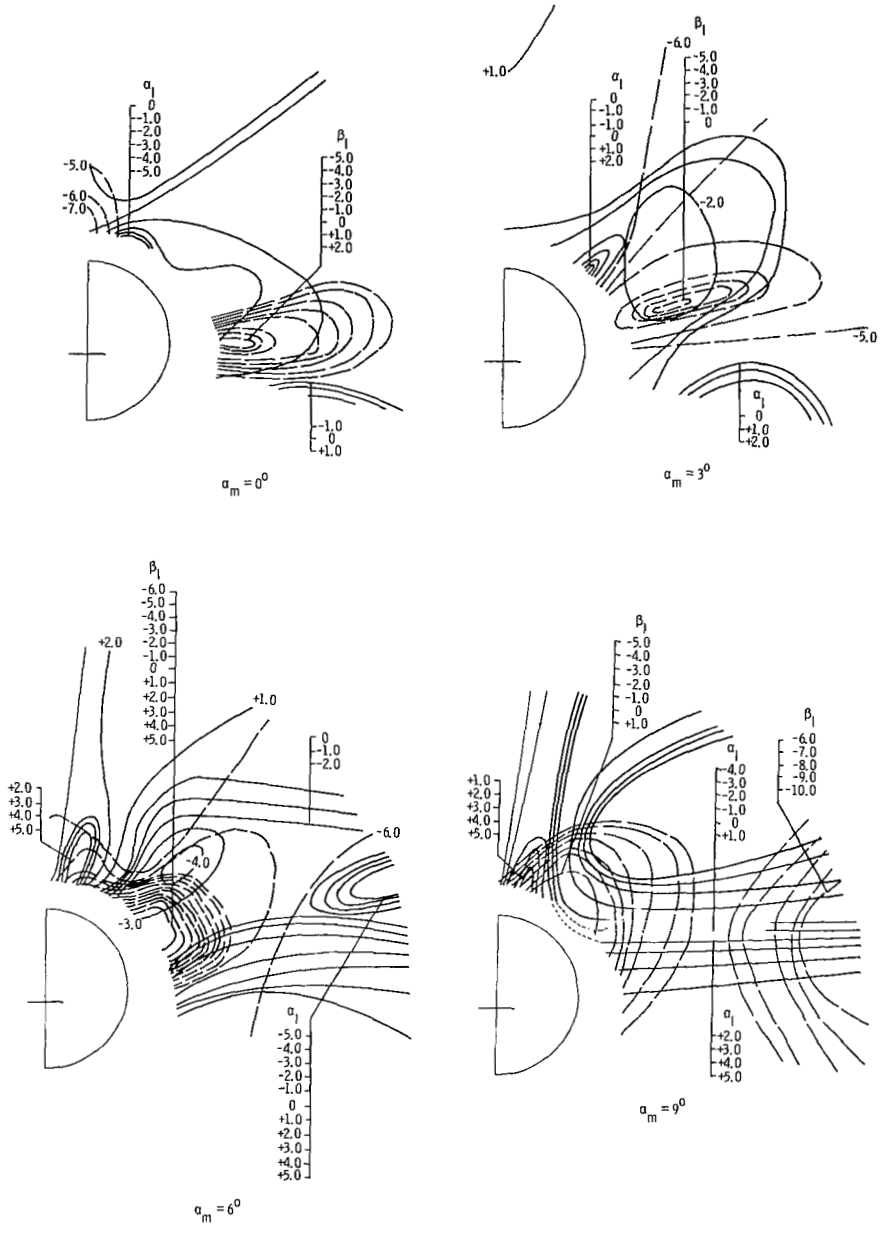

(h) Local flow angles. $\beta_m = -5^0$.

Figure 12.- Continued.

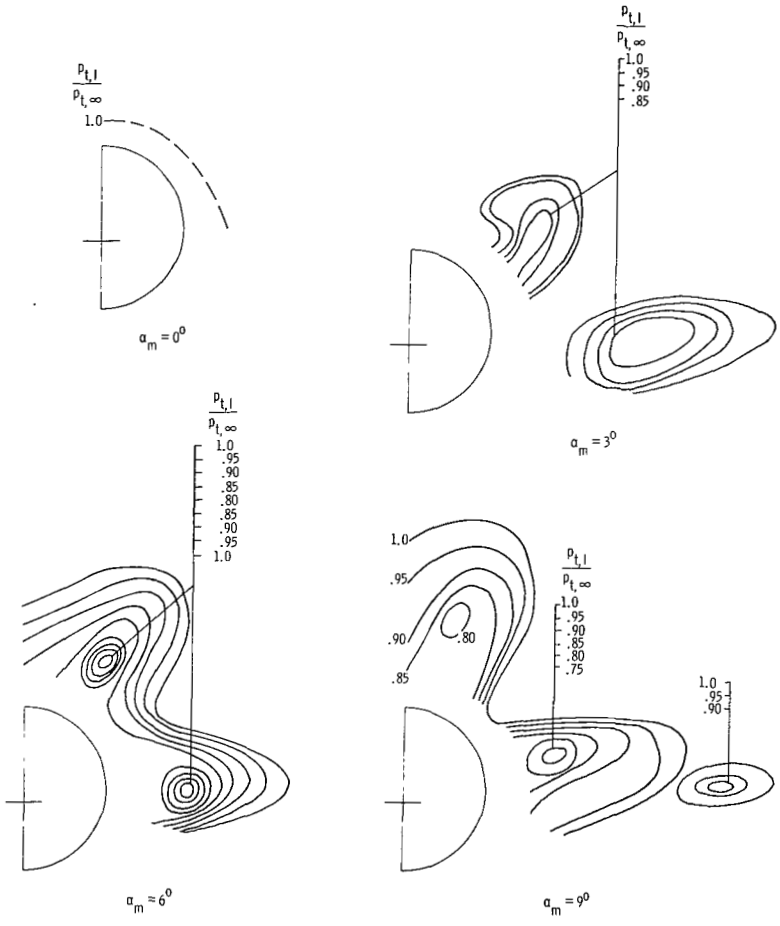

(i) Ratio of local to free-stream total pressure. $\beta_m = -5^0$.

Figure 12.- Concluded.

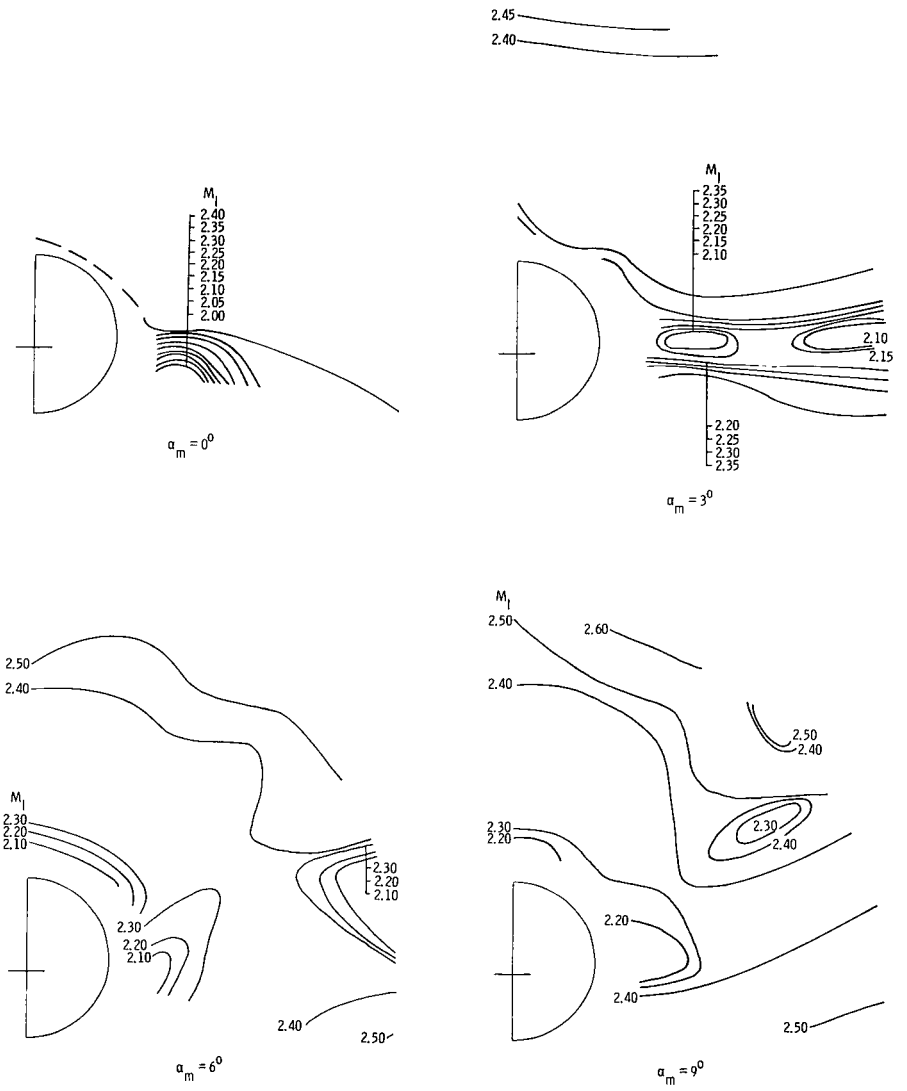

(a) Local Mach number. $\beta_m = 0^0$.

Figure 13.- Local flow parameters at $x = 115.14$ cm. $M_\infty = 2.36$.

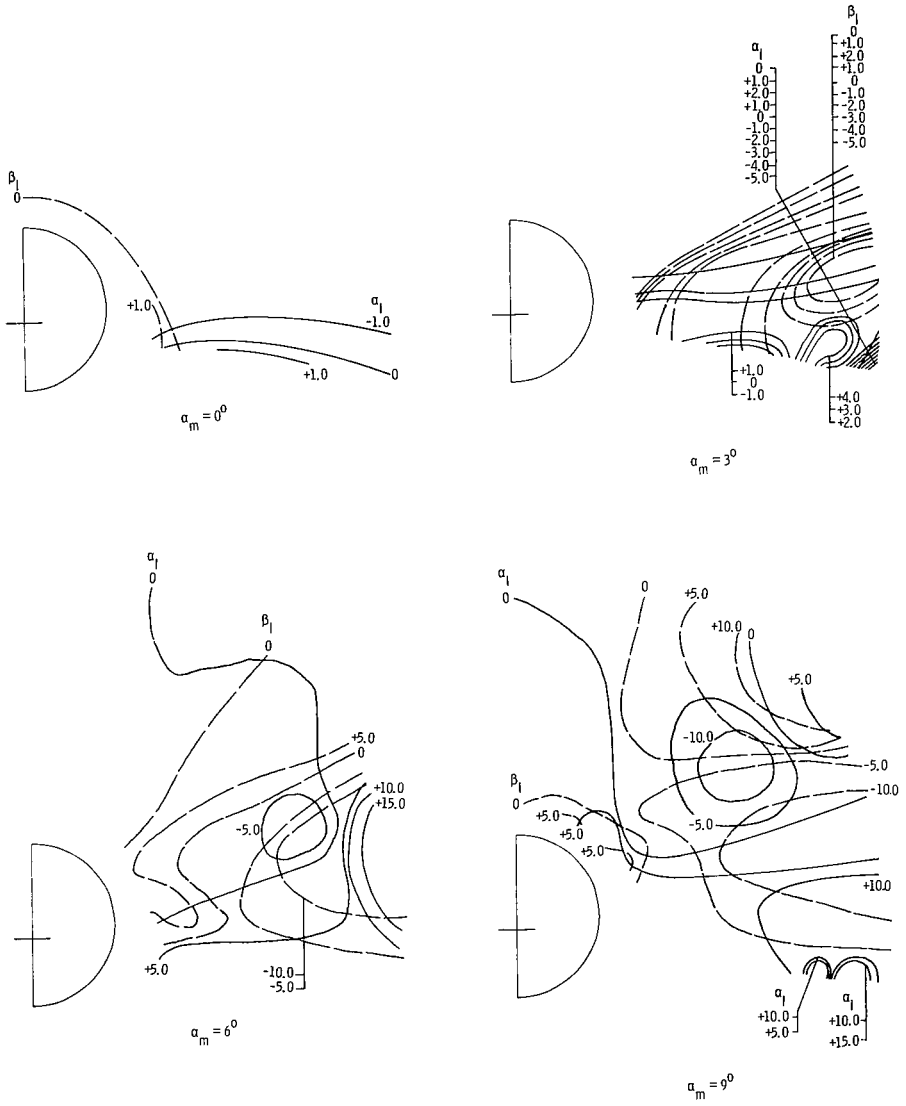

(b) Local flow angles. $\beta_m = 0^0$.

Figure 13.- Continued.

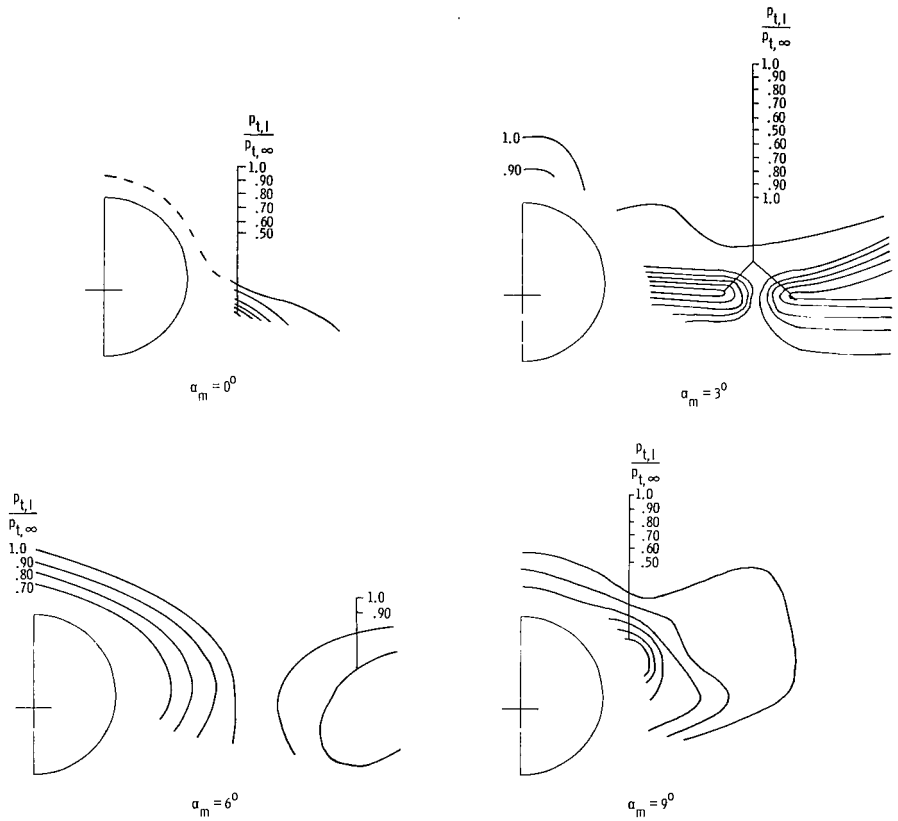

(c) Ratio of local to free-stream total pressure. $\beta_m = 0^0$.

Figure 13.- Continued.

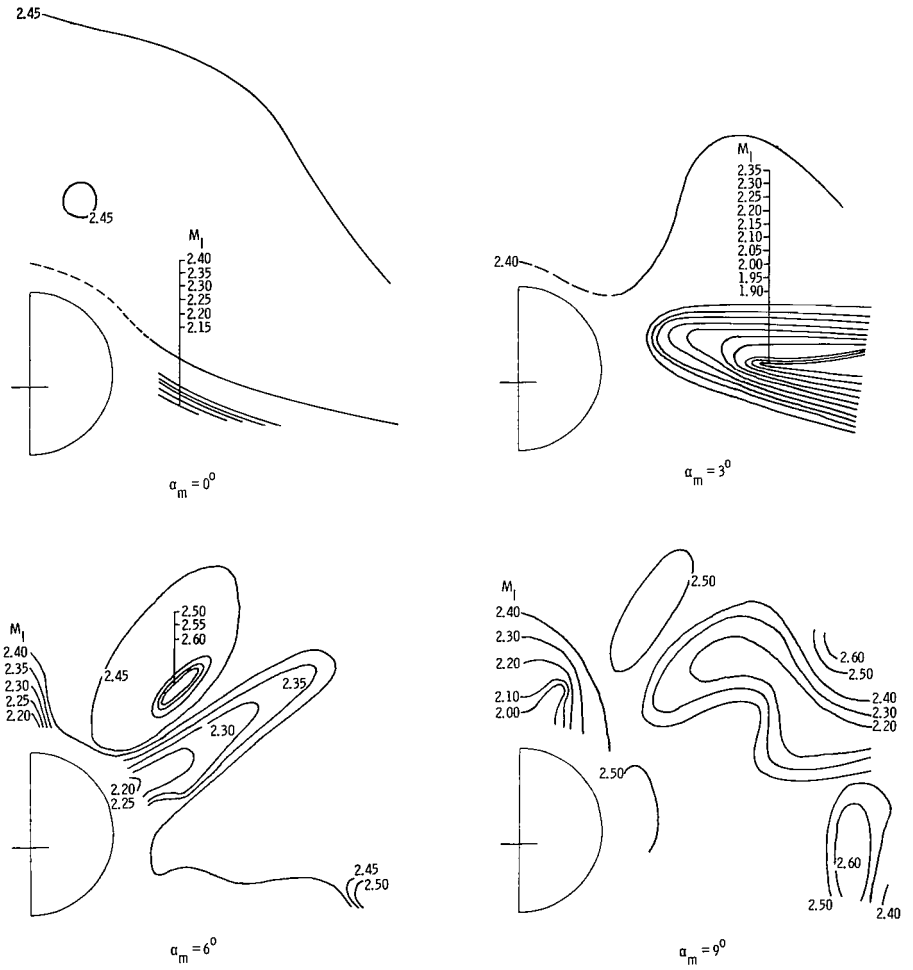

(d) Local Mach number. $\beta_m = 5^0$.

Figure 13.- Continued.

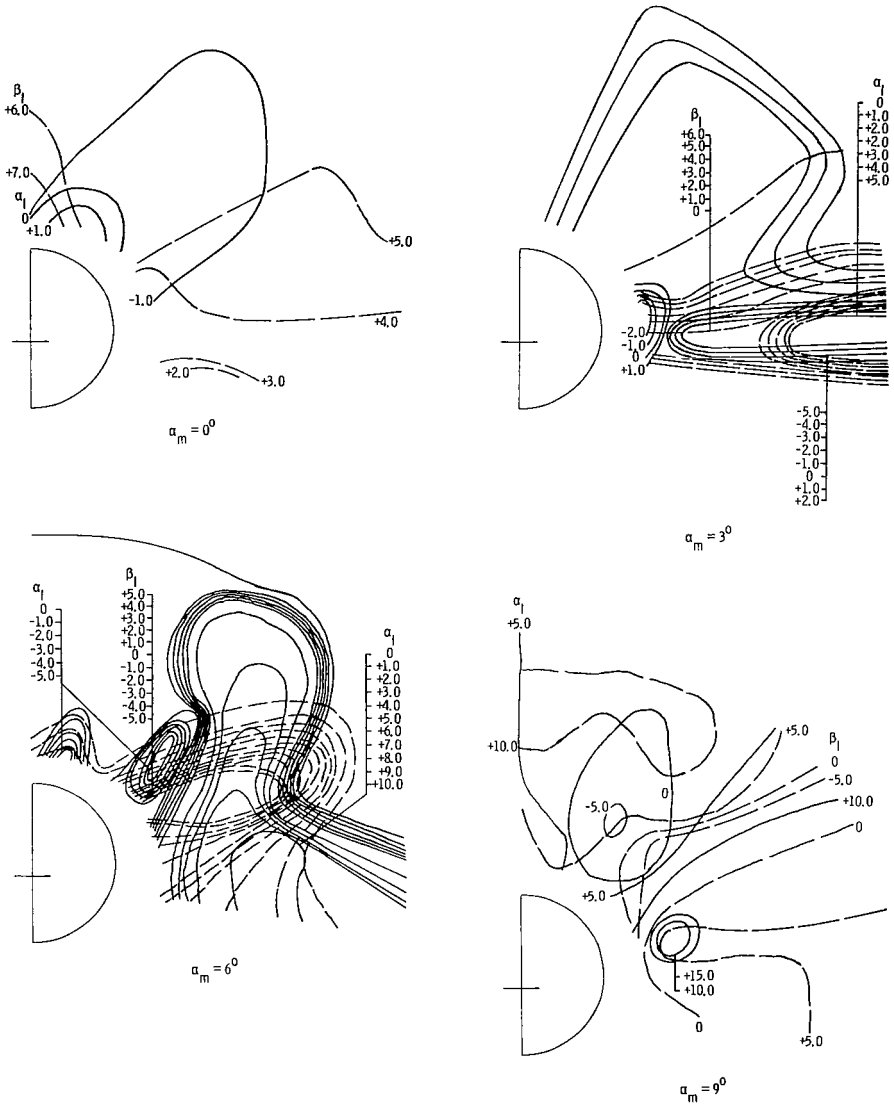

(e) Local flow angles. $\beta_m = 5^o$.

Figure 13.- Continued.

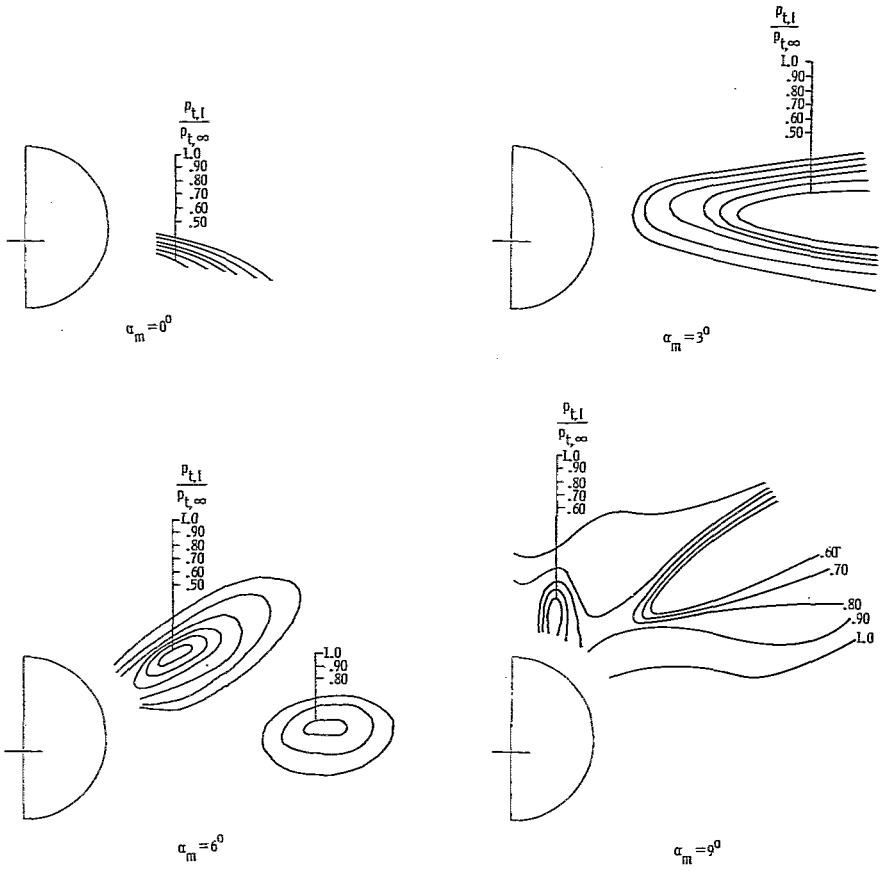

(f) Ratio of local to free-stream total pressure. $\beta_m = 5^0$.

Figure 13.- Continued.

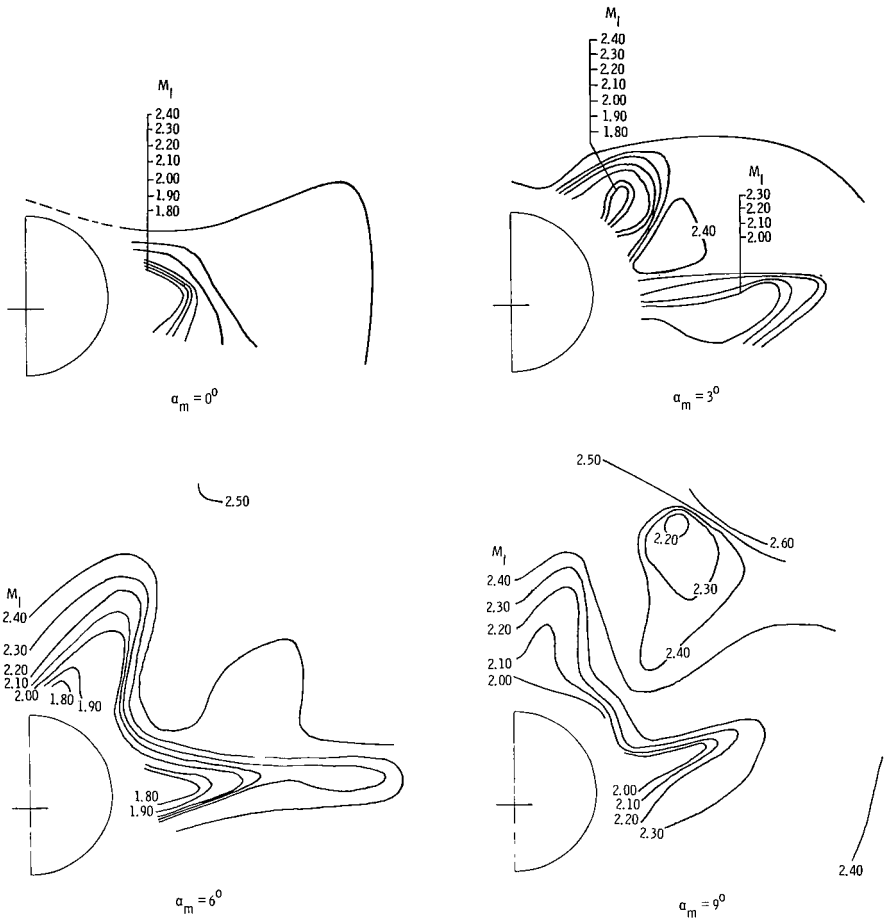

(g) Local Mach number. $\beta_m = -5^0$.

Figure 13.- Continued.

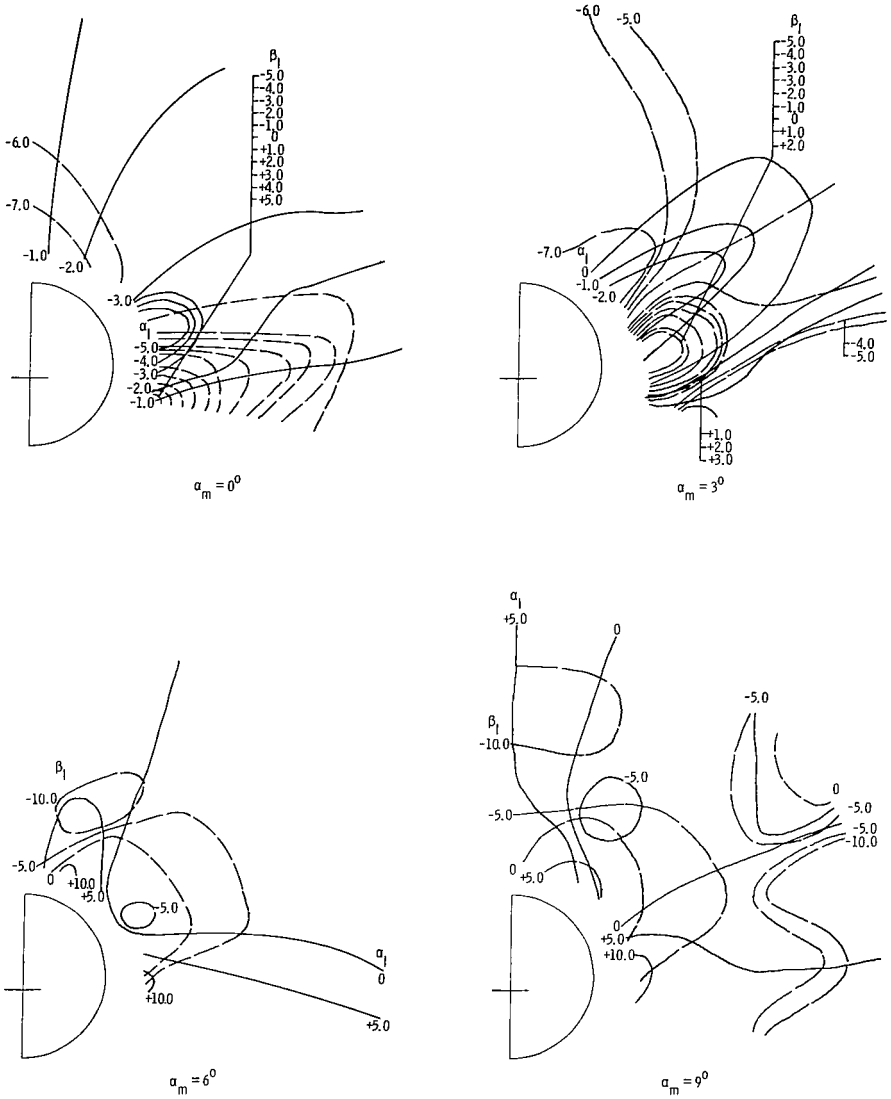

(h) Local flow angles. $\beta_m = -5^0$.

Figure 13.- Continued.

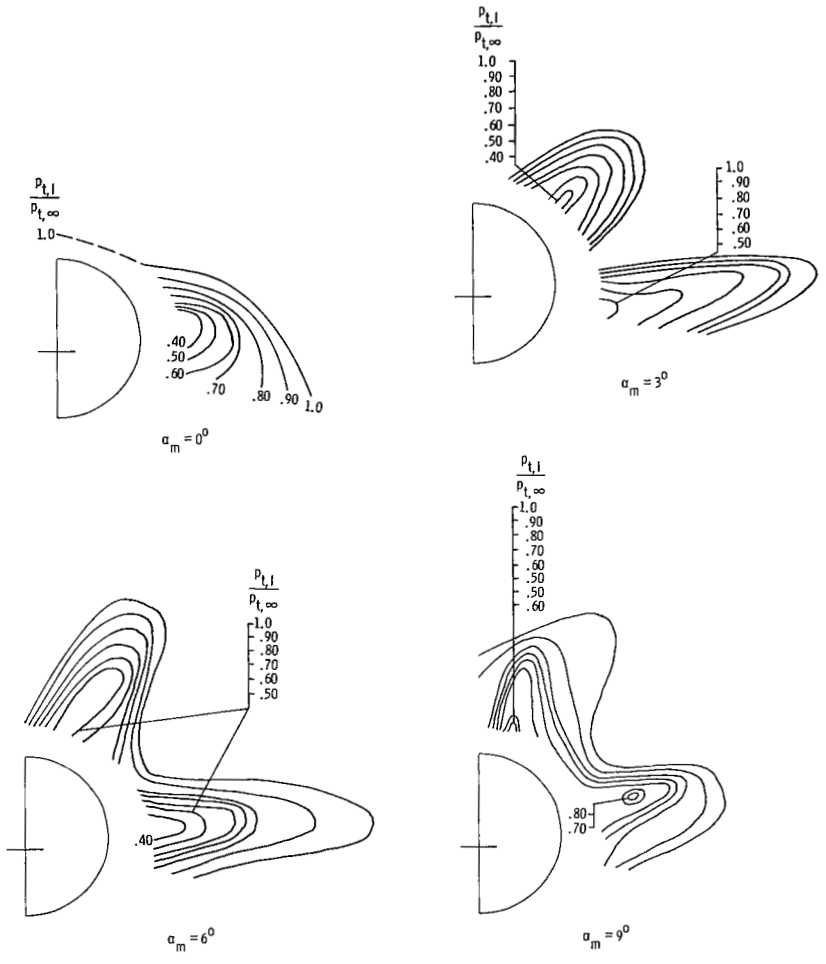

(i) Ratio of local to free-stream total pressure. $\beta_m = -5^0$.

Figure 13.- Concluded.

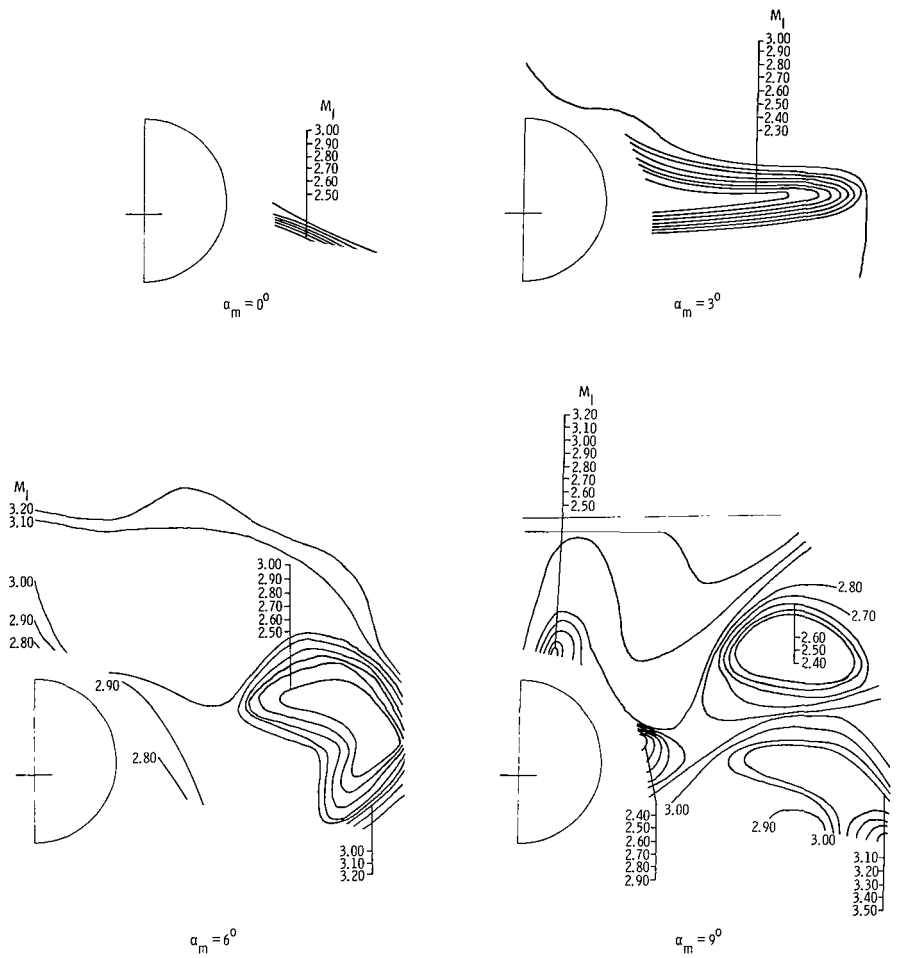

(a) Local Mach number. $\beta_m = 0^0$.

Figure 14.- Local flow parameters at $x = 115.14$ cm. $M_\infty = 2.96$.

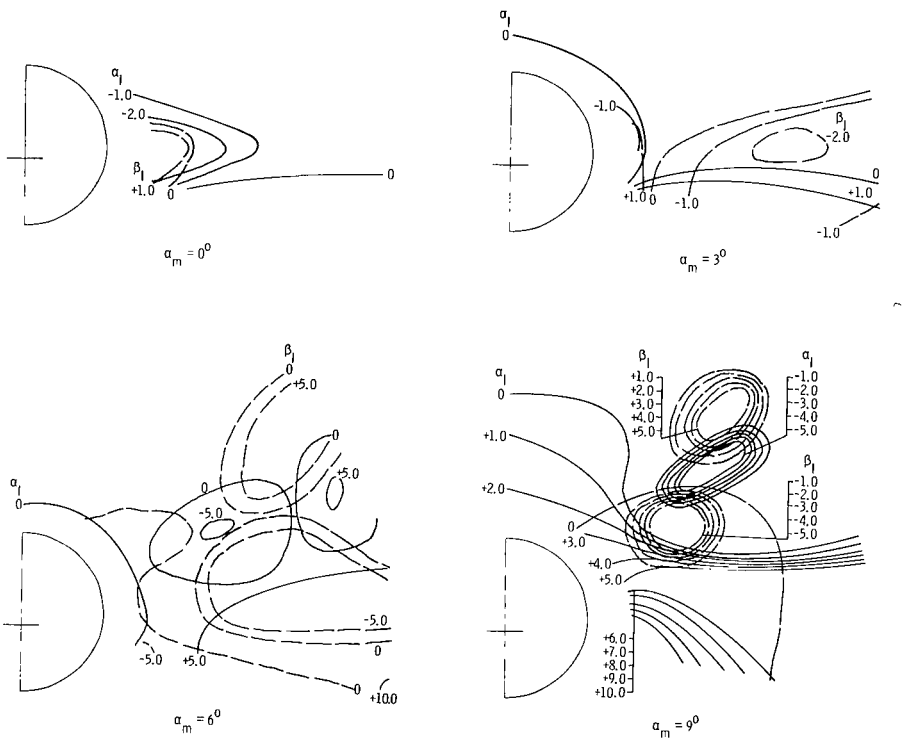

(b) Local flow angles. $\beta_m = 0^0$.

Figure 14.- Continued.

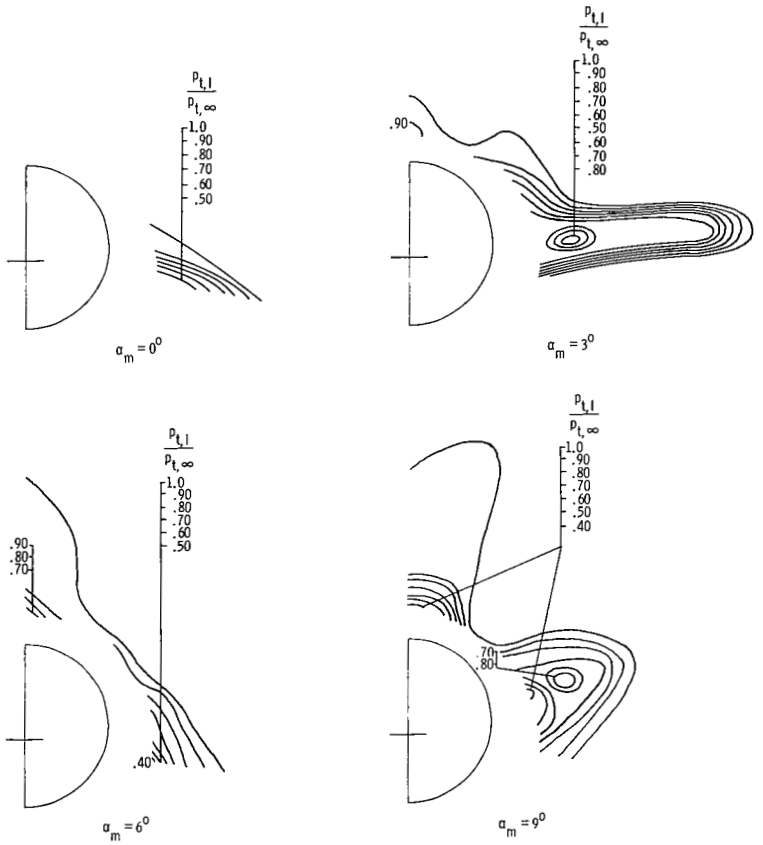

(c) Ratio of local to free-stream total pressure. $\beta_m = 0^o$.

Figure 14.- Continued.

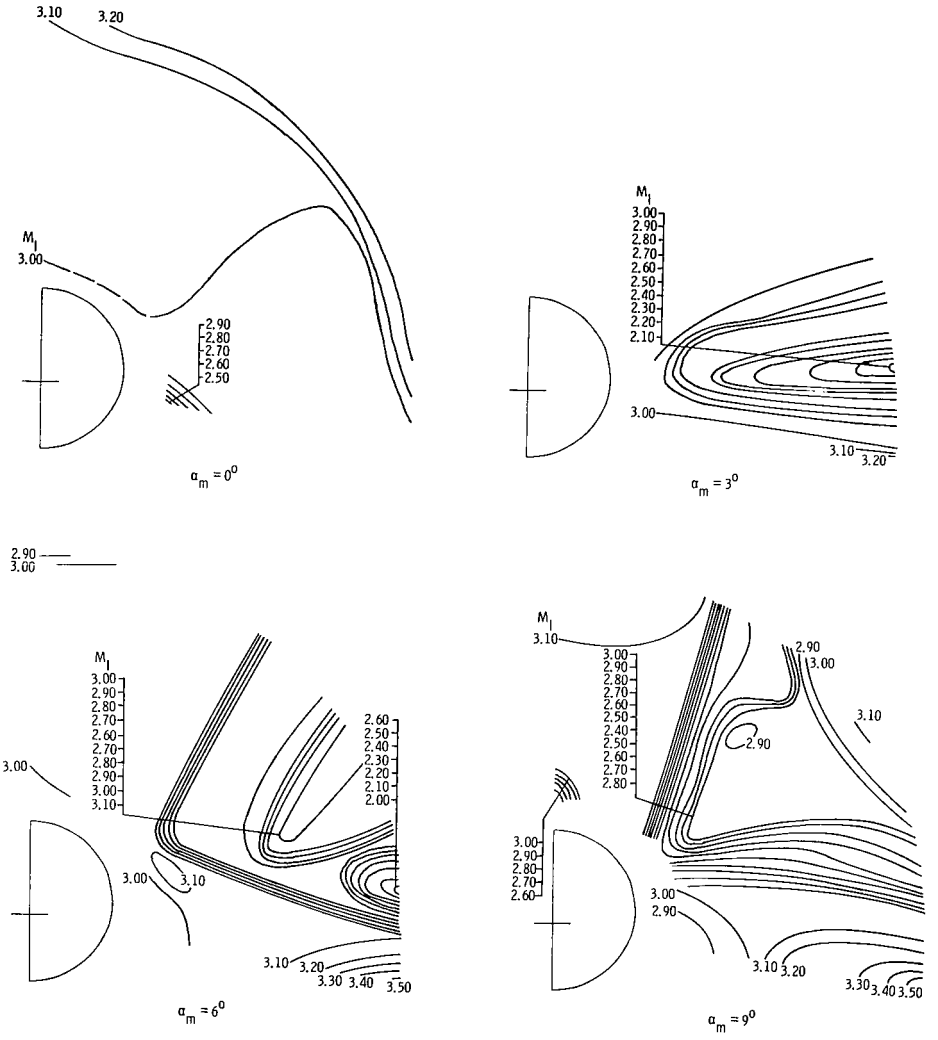

(d) Local Mach number. $\beta_m = 5^0$.

Figure 14.- Continued.

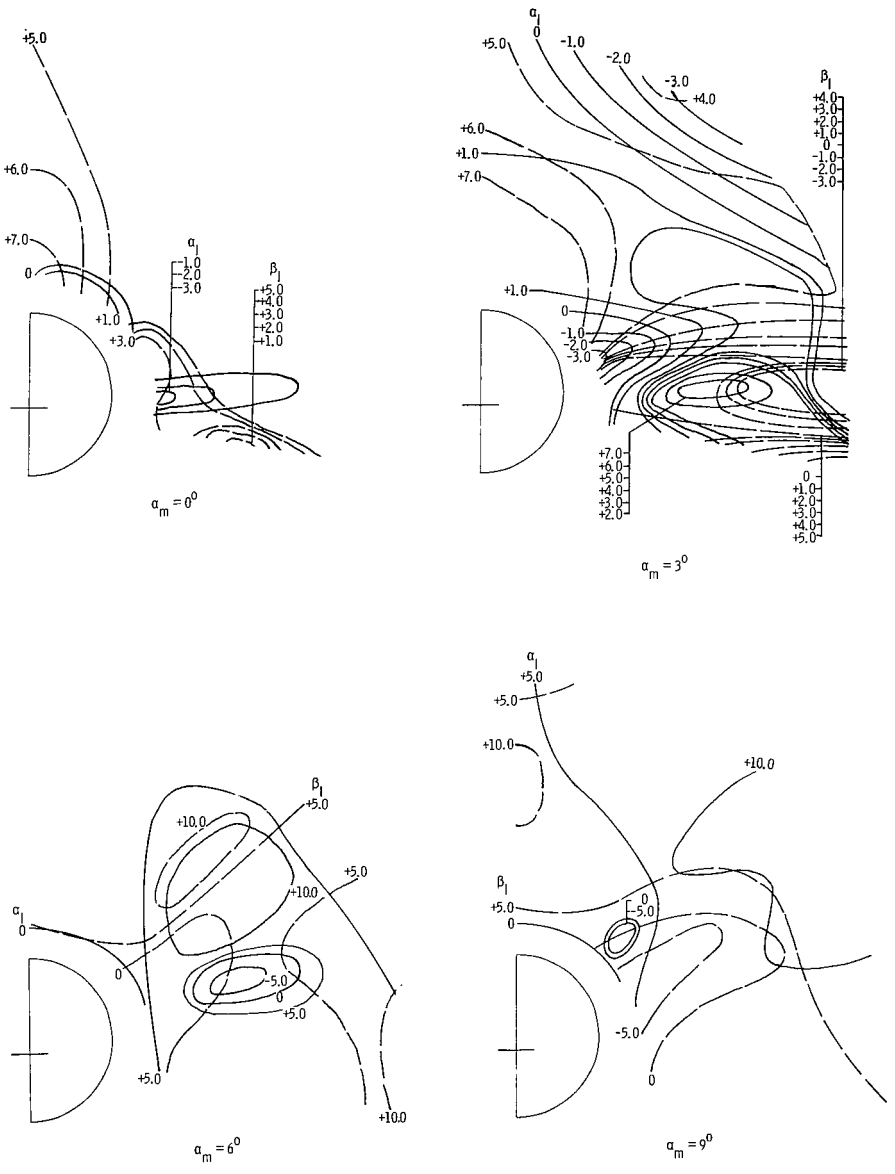

(e) Local flow angles. $\beta_m = 5^0$.

Figure 14.- Continued.

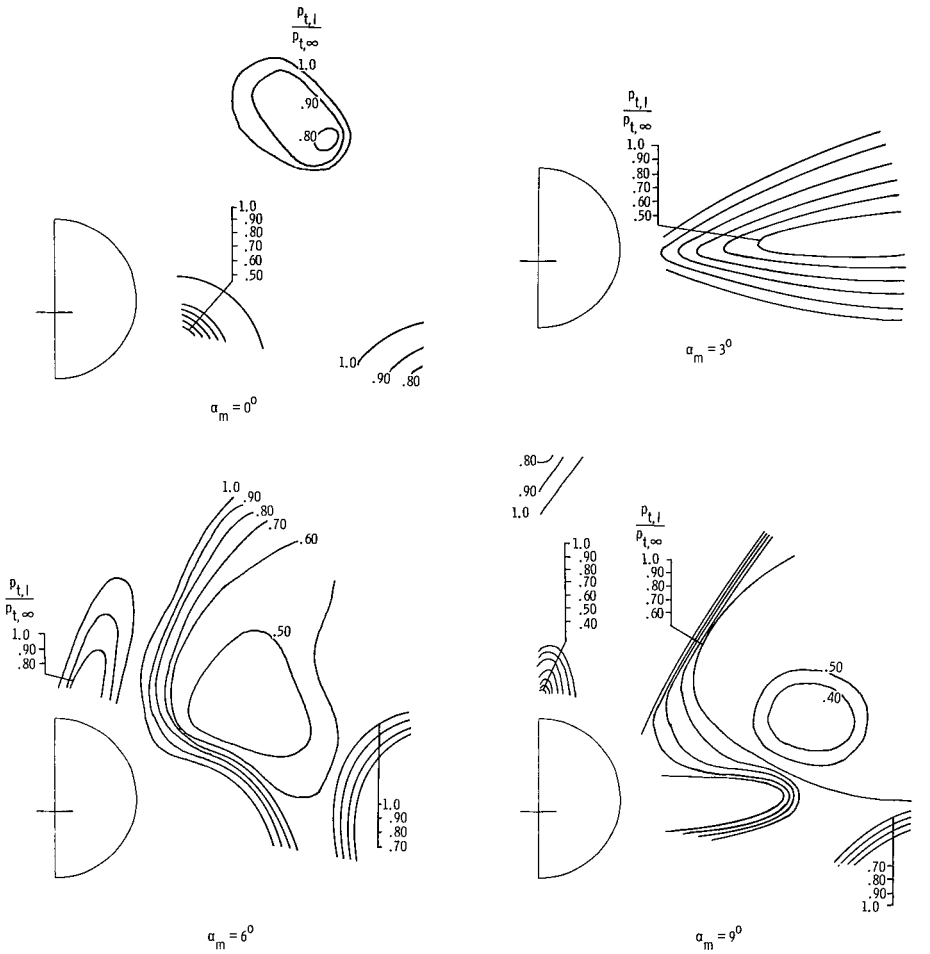

(f) Ratio of local to free-stream total pressure. $\beta_m = 5^o$.

Figure 14.- Continued.

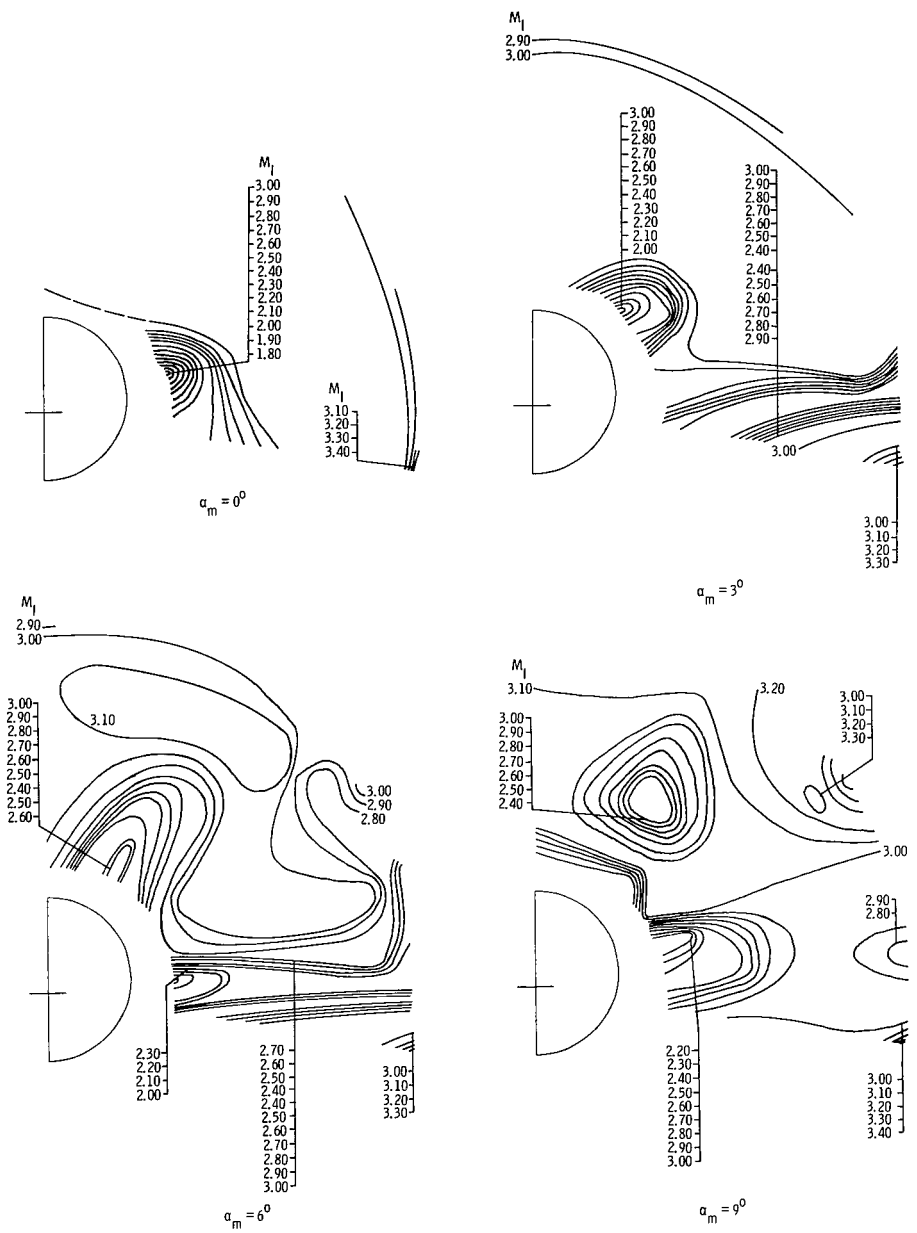

(g) Local Mach number. $\beta_m = -5^0$.

Figure 14.- Continued.

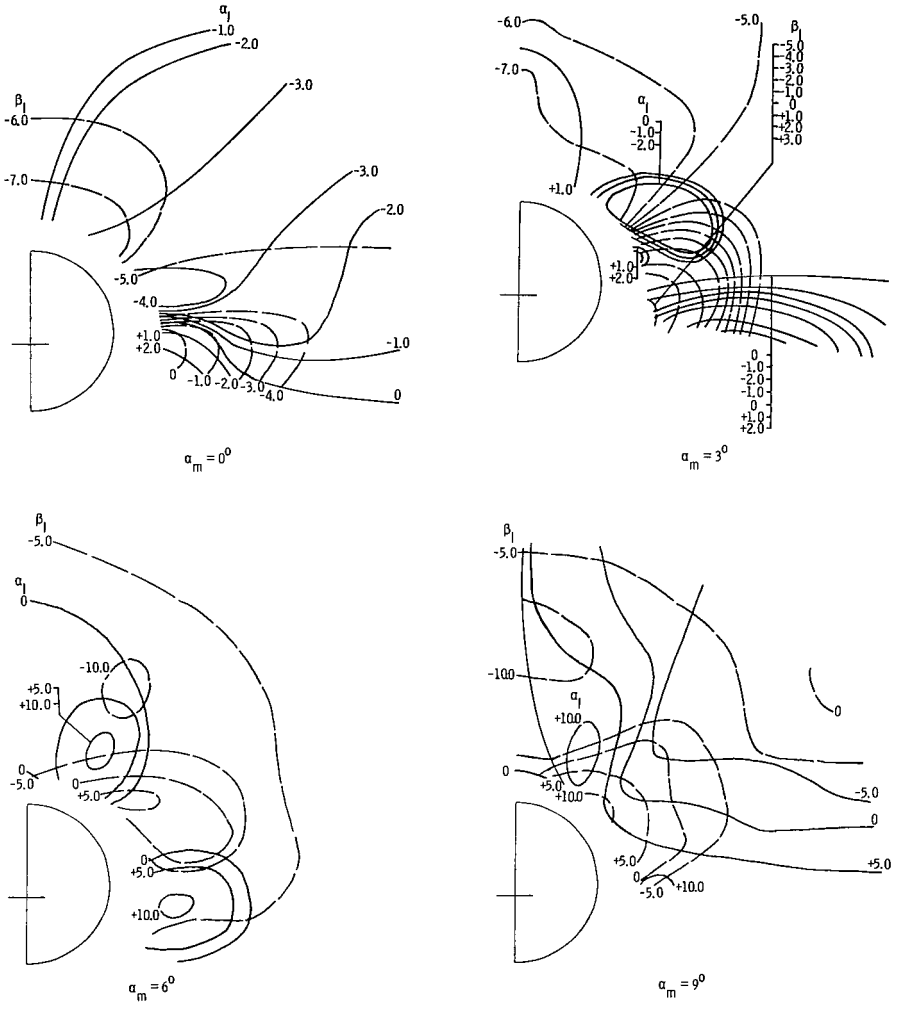

(h) Local flow angles. $\beta_m = -5^o$.

Figure 14.- Continued.

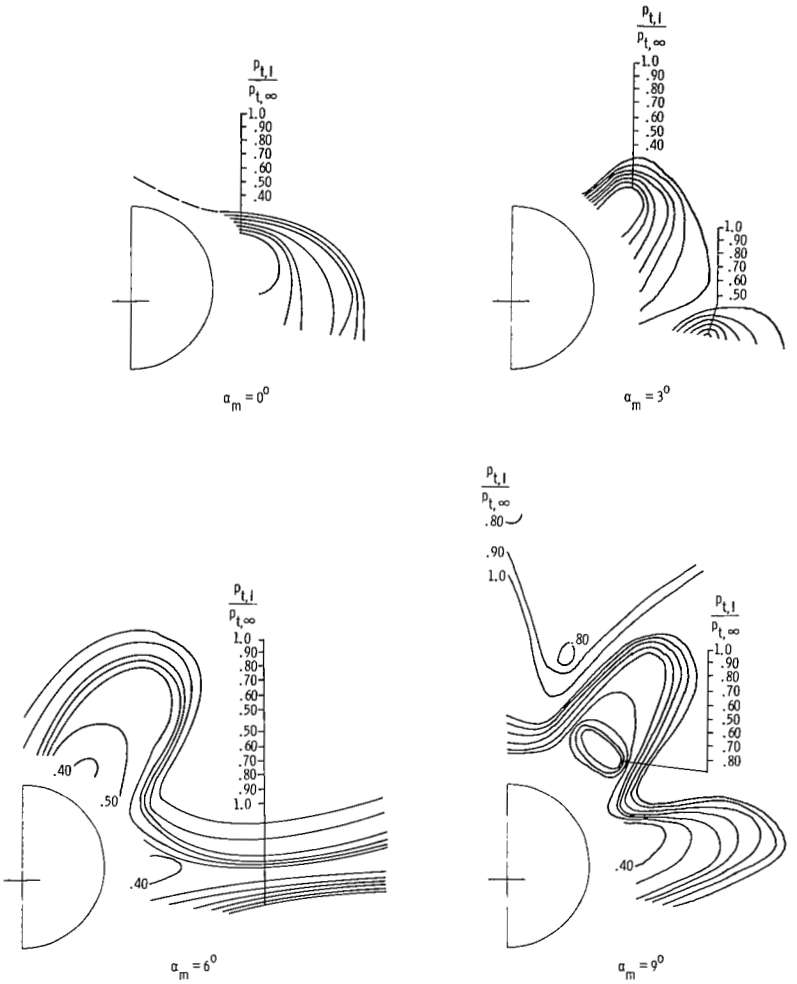

(i) Ratio of local to free-stream total pressure. $\beta_m = -5^0$.

Figure 14.- Concluded.

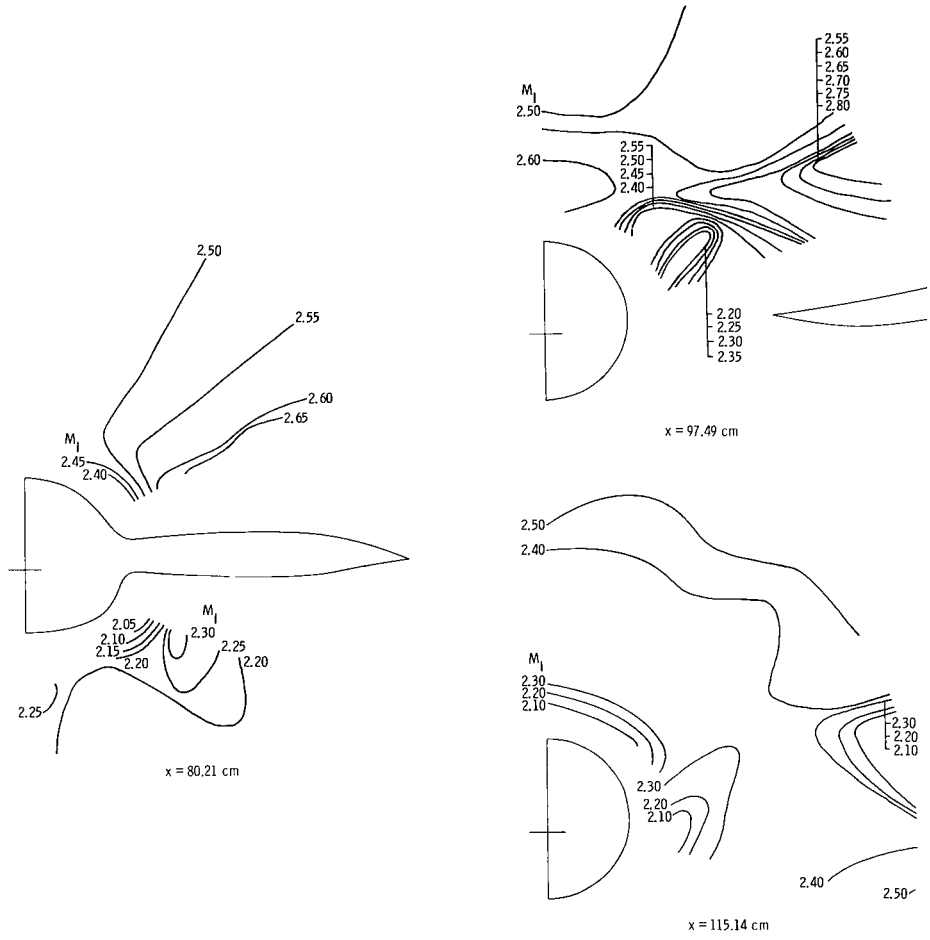

(a) Local Mach number.

Figure 15.- Typical local flow properties at three longitudinal stations. $M_\infty = 2.36$; $\alpha_m = 6^0$; $\beta_m = 0^0$.

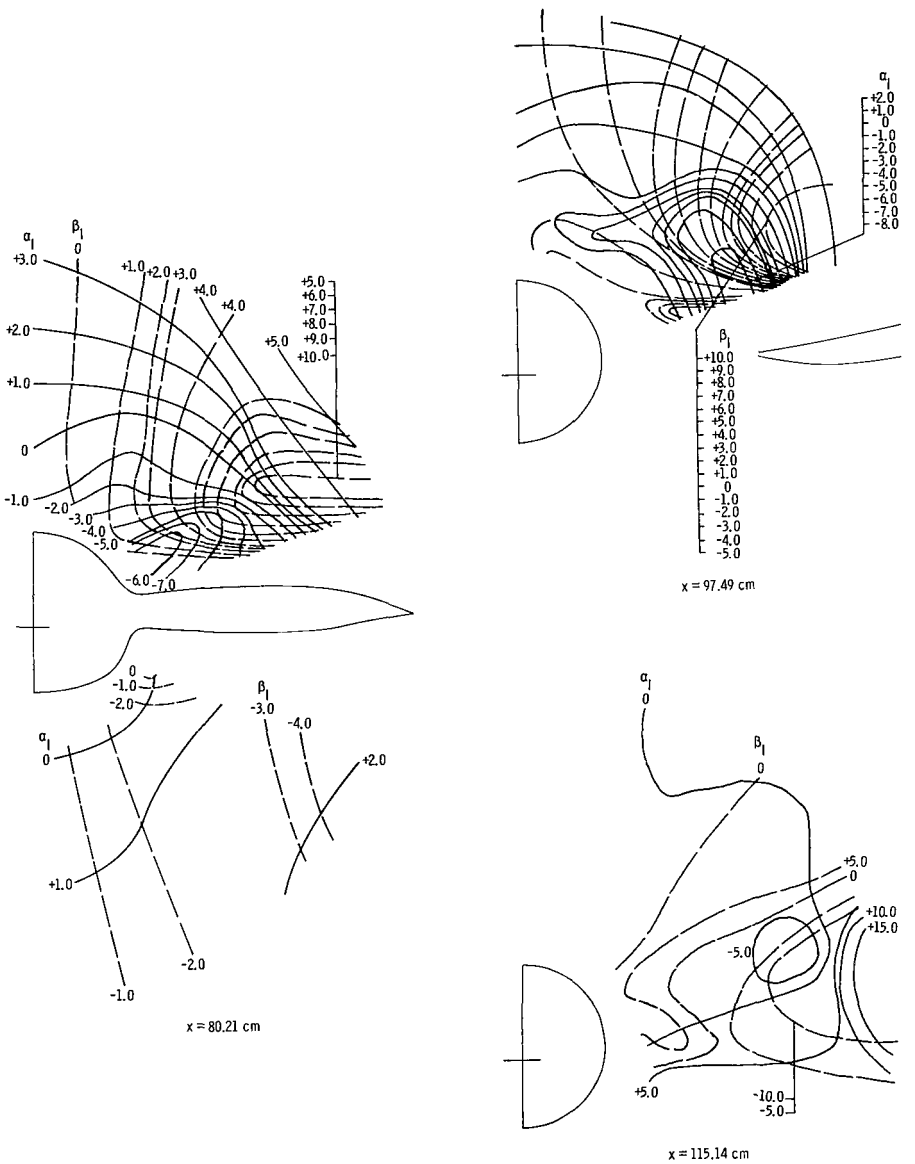

(b) Local flow angles.

Figure 15.- Continued.

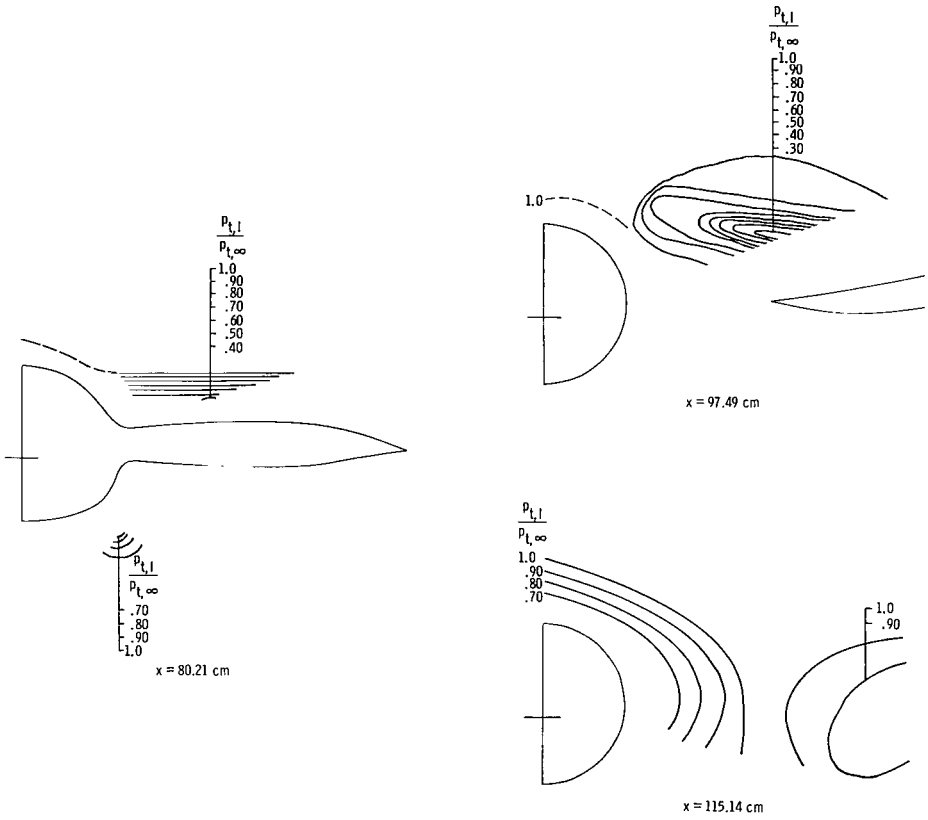

(c) Ratio of local to free-stream total pressure.

Figure 15.- Concluded.

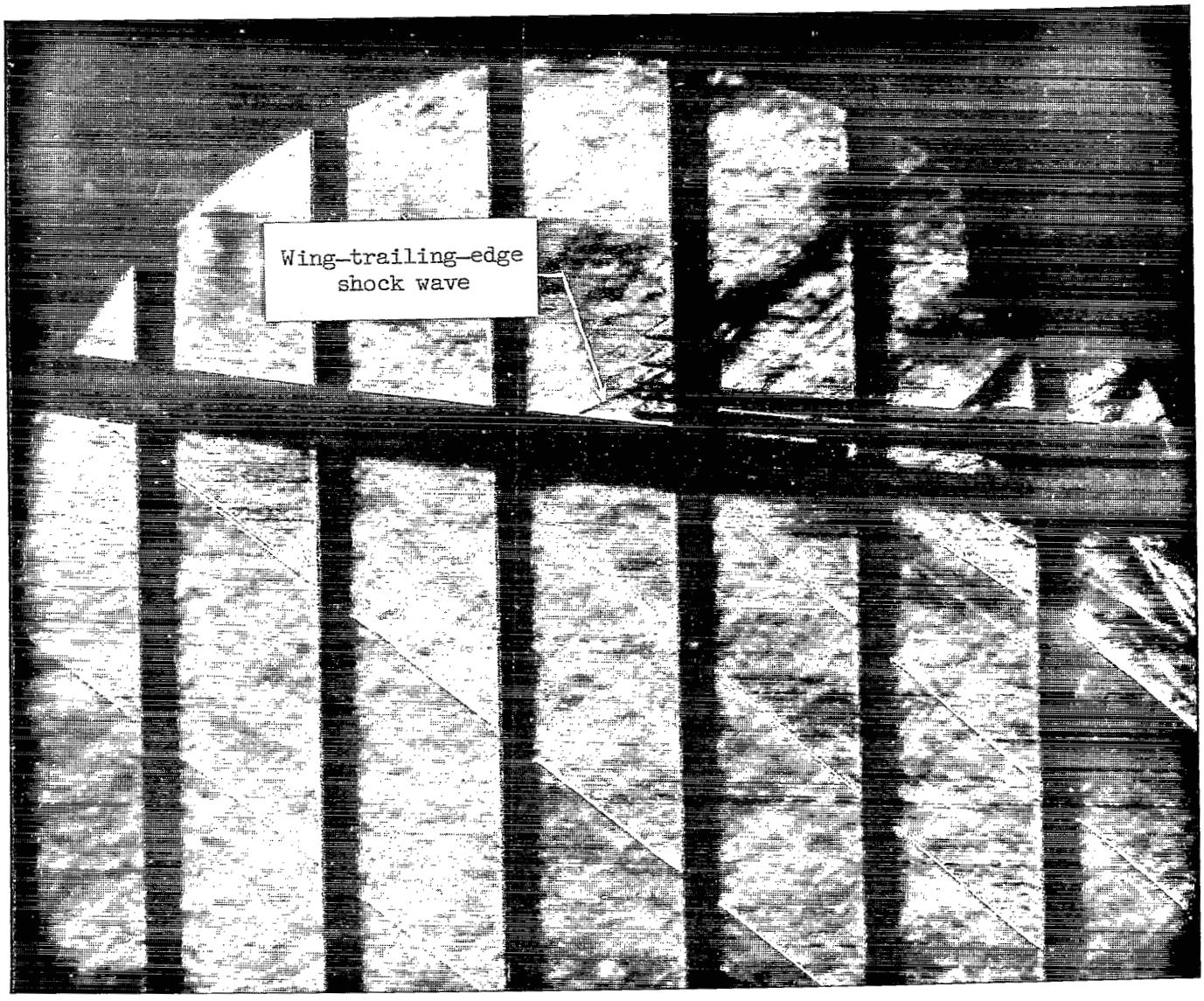

Figure 16.- Schlieren photograph of model. $M_\infty = 1.60$; $\alpha = 6^0$; $\beta_m = 0^0$; $x = 97.49$ cm. L-68-5647

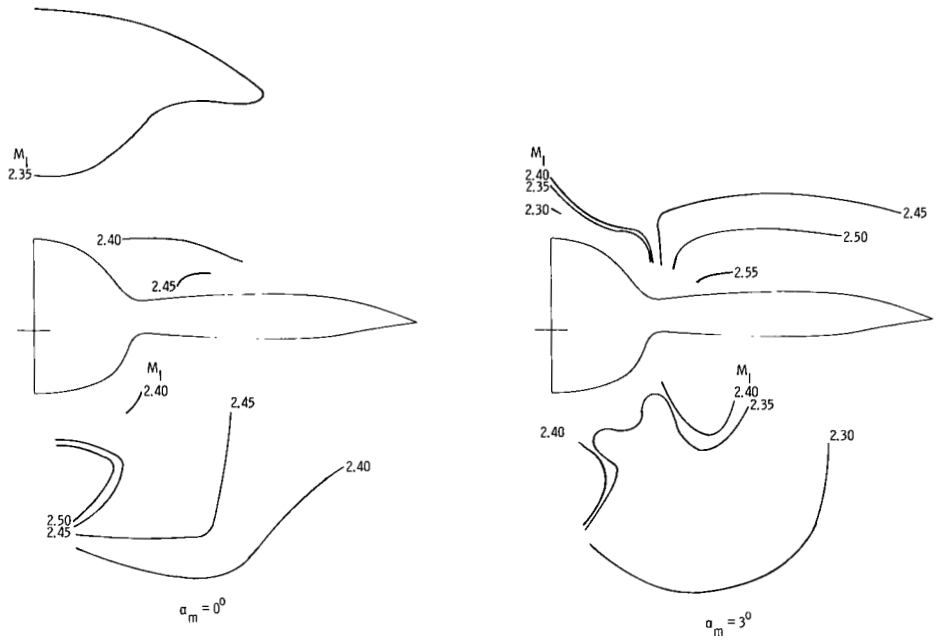

(a) Local Mach number. x = 80.21 cm.

Figure 17.- Effects of model angle of attack on local flow parameters. $M_\infty = 2.36$; $\beta_m = 0^\circ$.

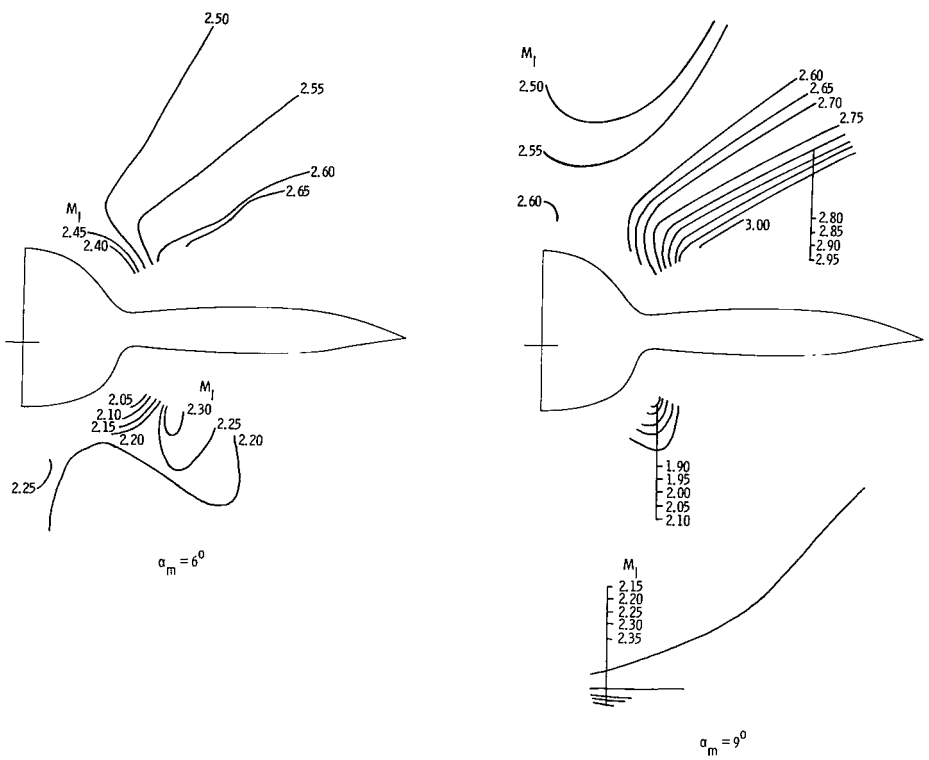

(a) Concluded.

Figure 17.- Continued.

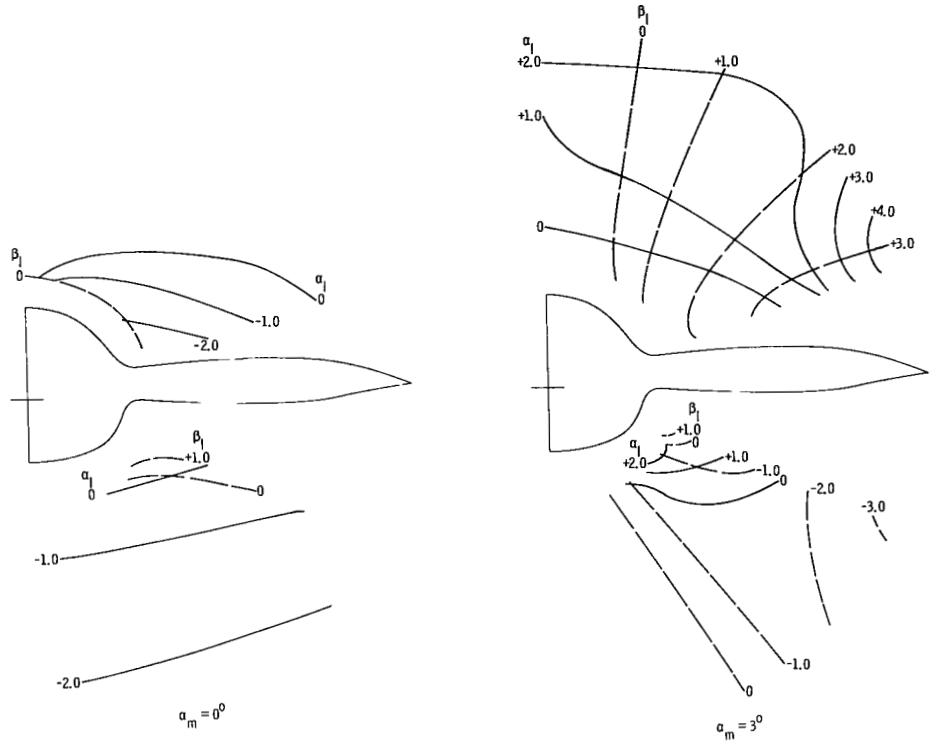

(b) Local flow angles. x = 80.21 cm.

Figure 17.- Continued.

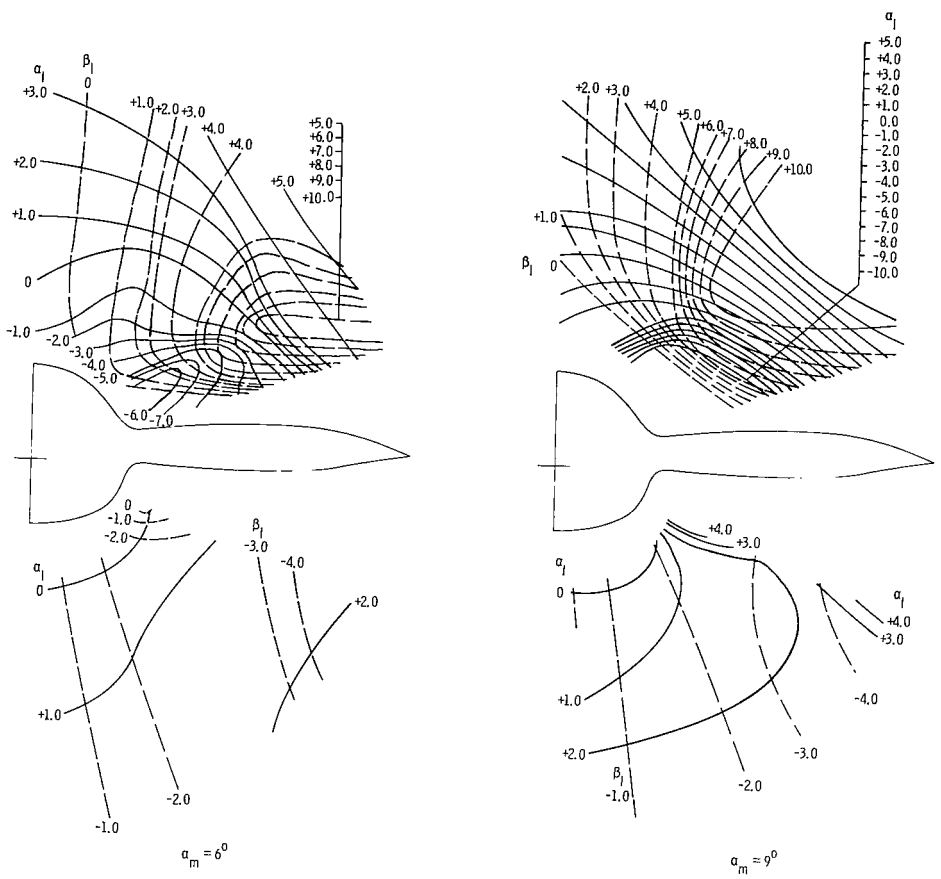

(b) Concluded.

Figure 17.- Continued.

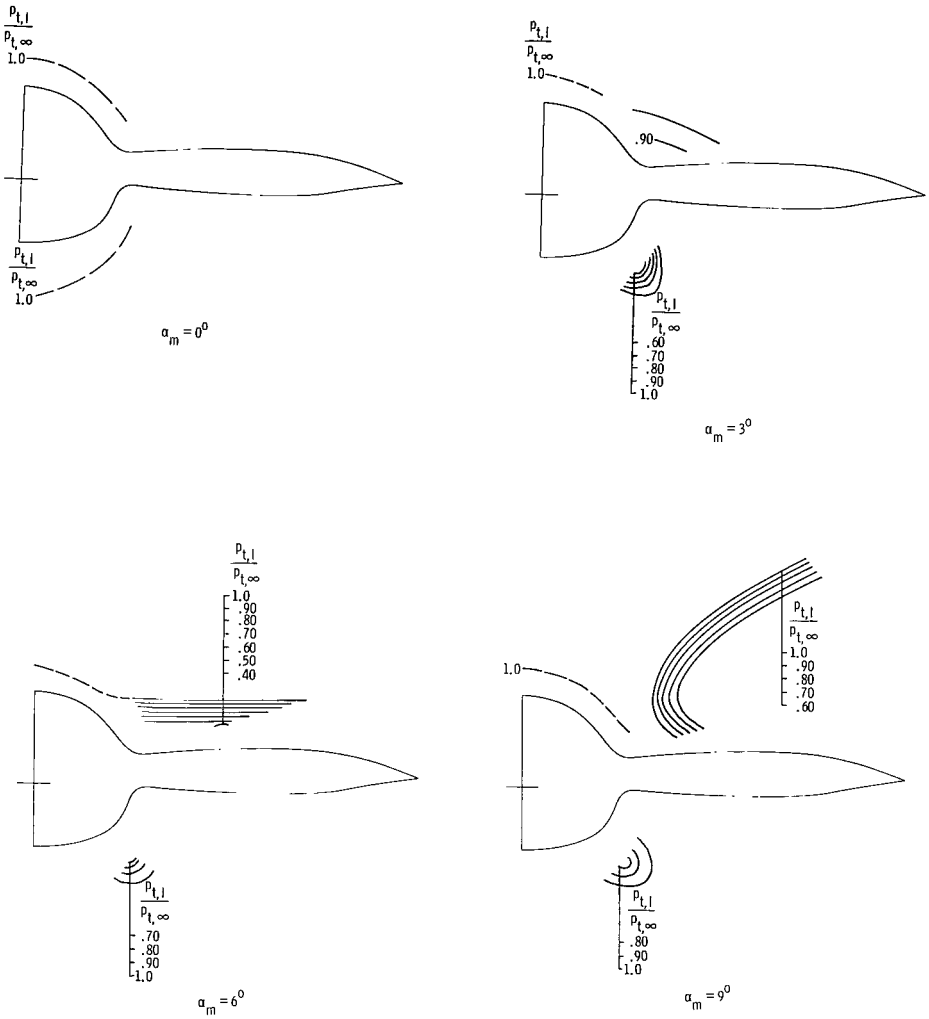

(c) Ratio of local to free-stream total pressure. x = 80.21 cm.

Figure 17.- Continued.

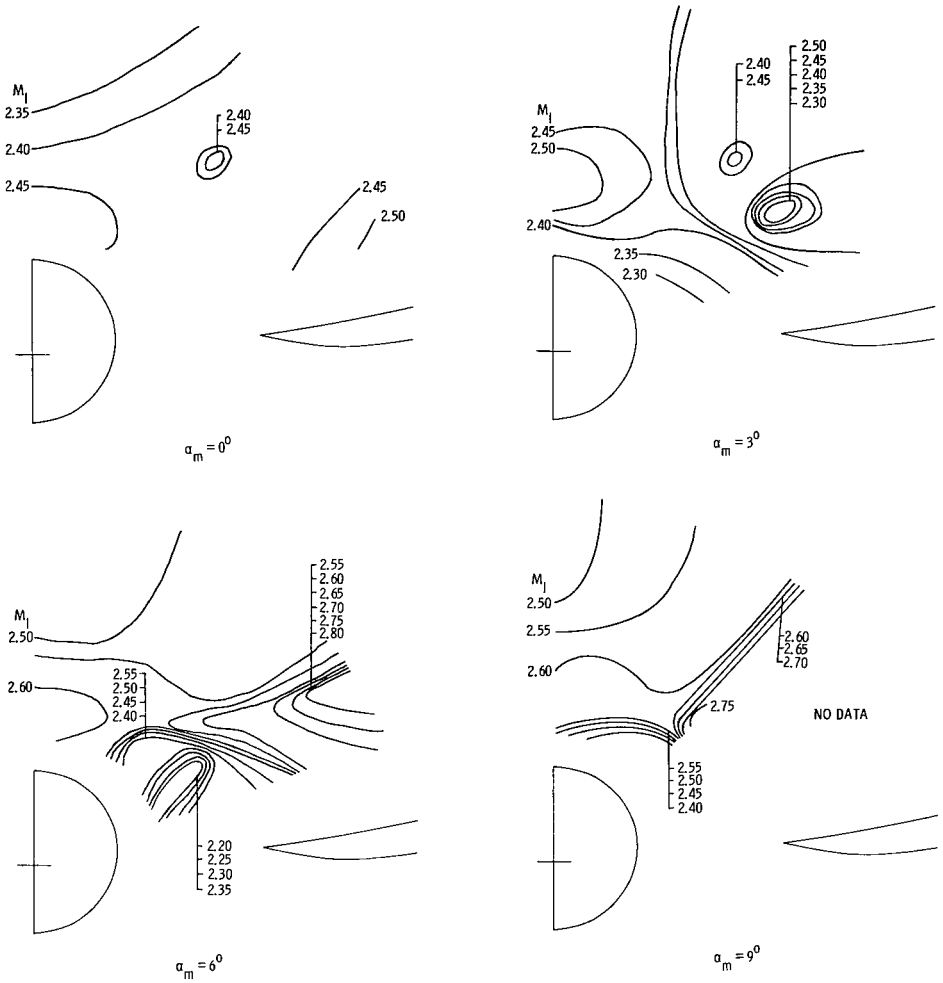

(d) Local Mach number. x = 97.49 cm.

Figure 17.- Continued.

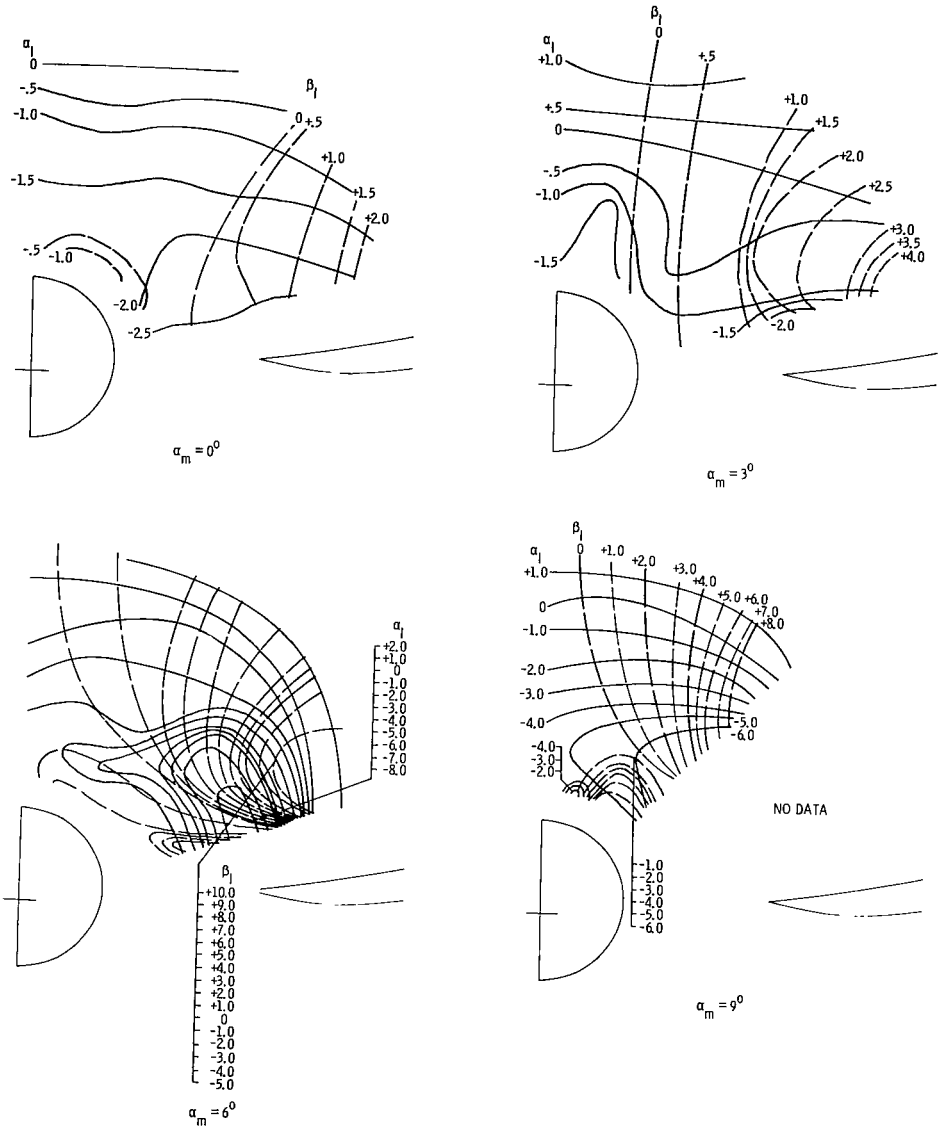

(e) Local flow angles. x = 97.49 cm.

Figure 17.- Continued.

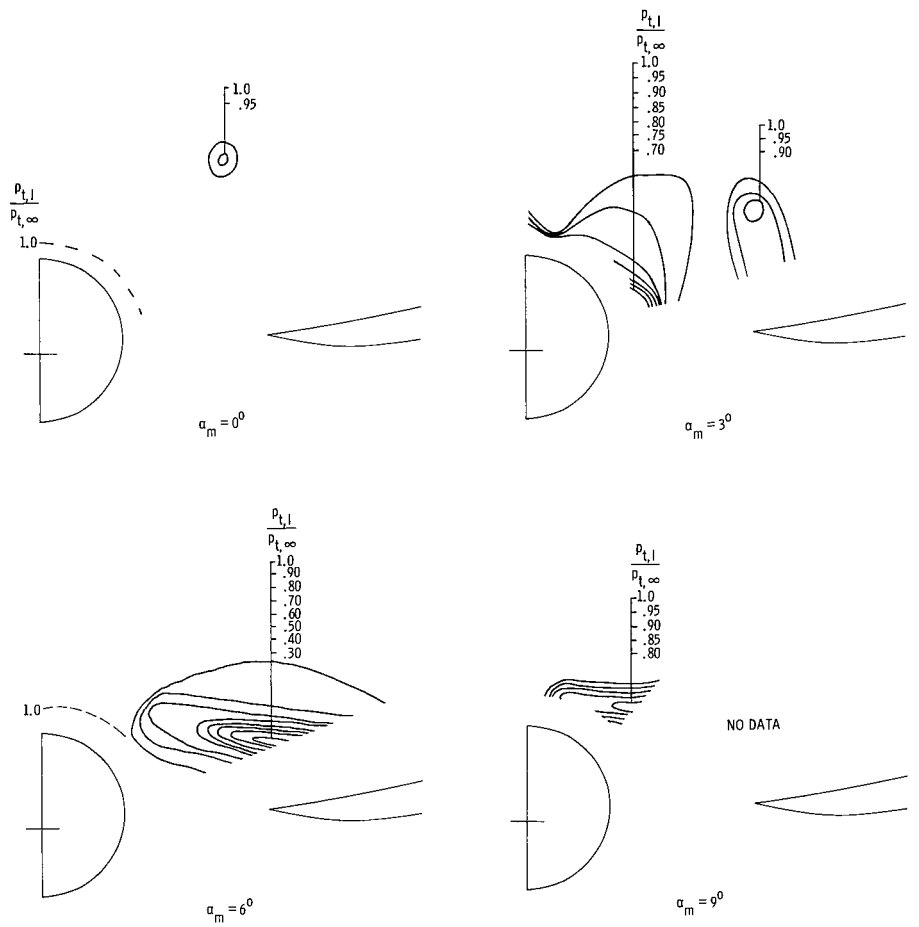

(f) Ratio of local to free-stream total pressure. x = 97.49 cm.

Figure 17.- Continued.

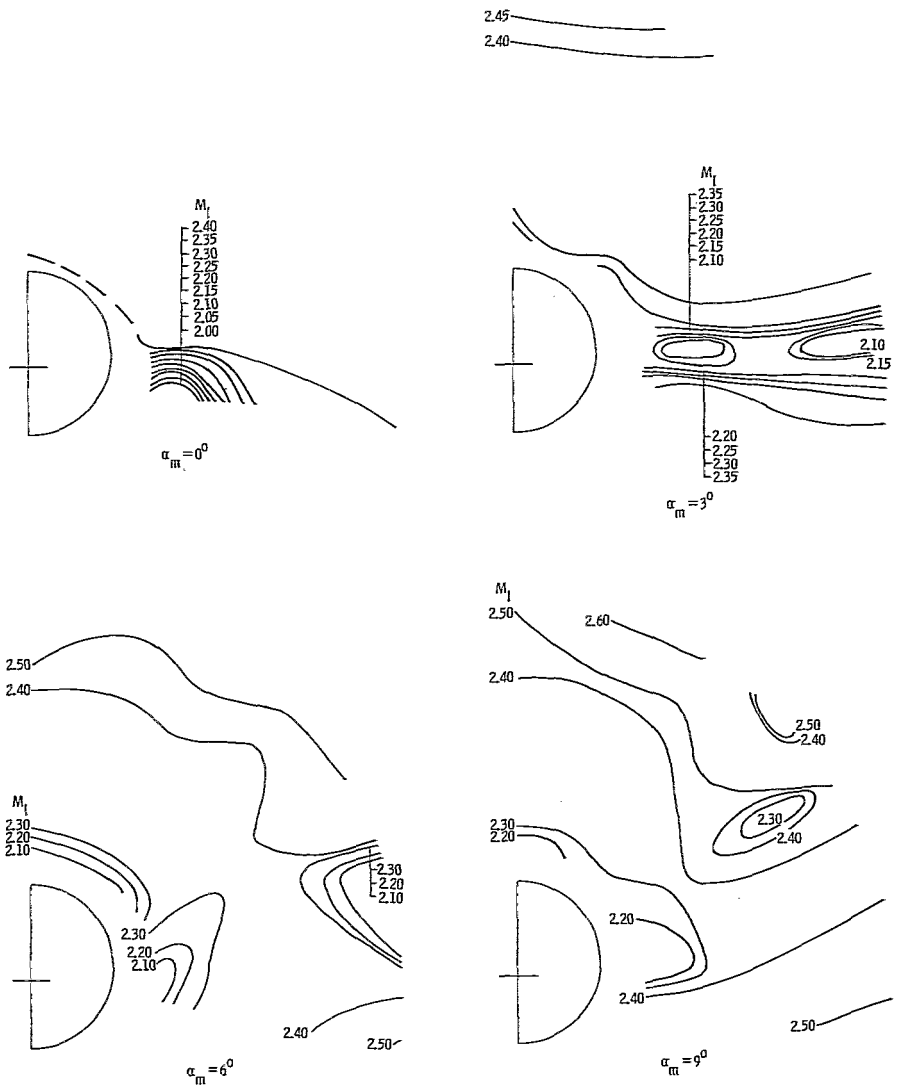

(g) Local Mach number. x = 115.14 cm.

Figure 17.- Continued.

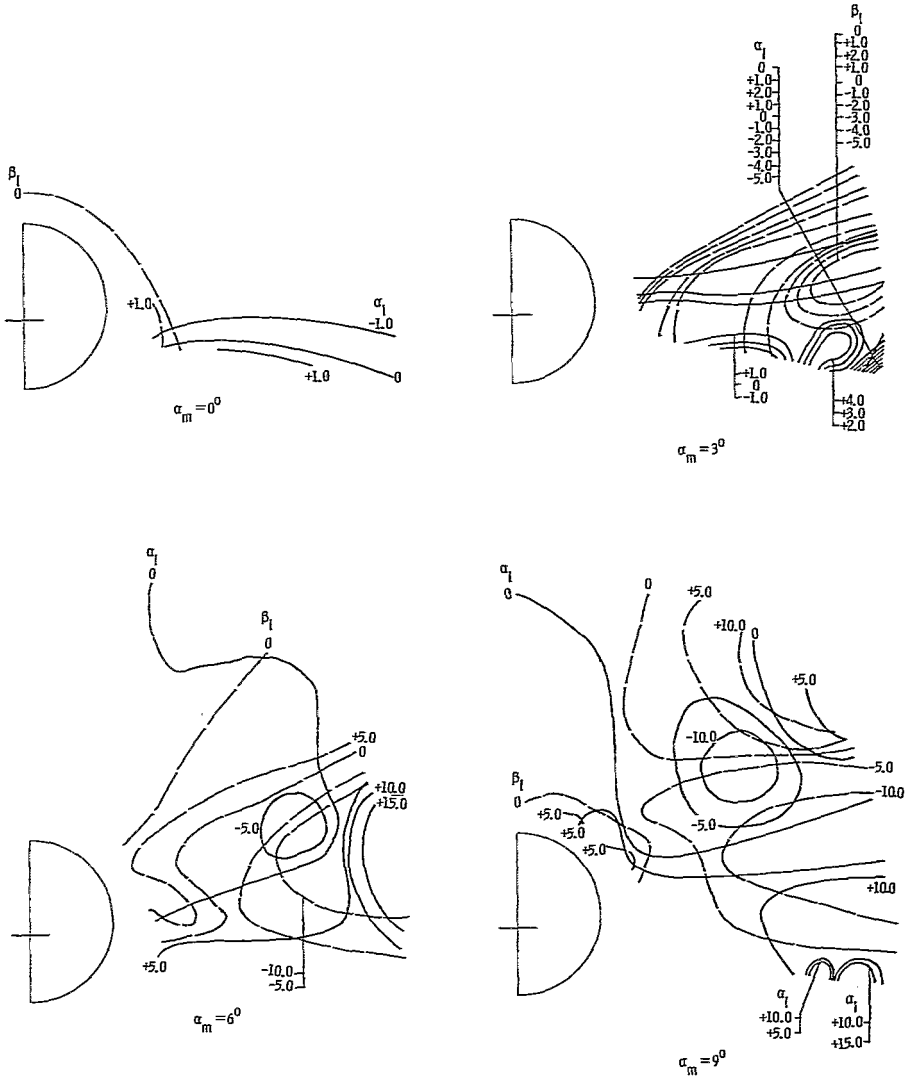

(h) Local flow angles. x = 115.14 cm.

Figure 17.- Continued.

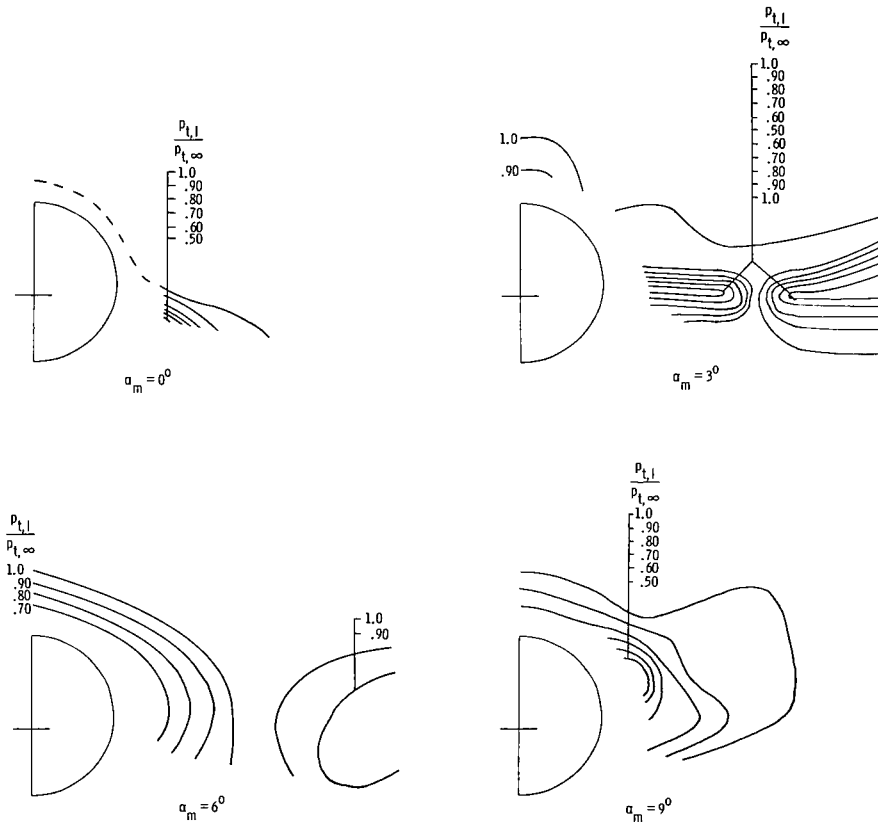

(i) Ratio of local to free-stream total pressure. x = 115.14 cm.

Figure 17.- Concluded.

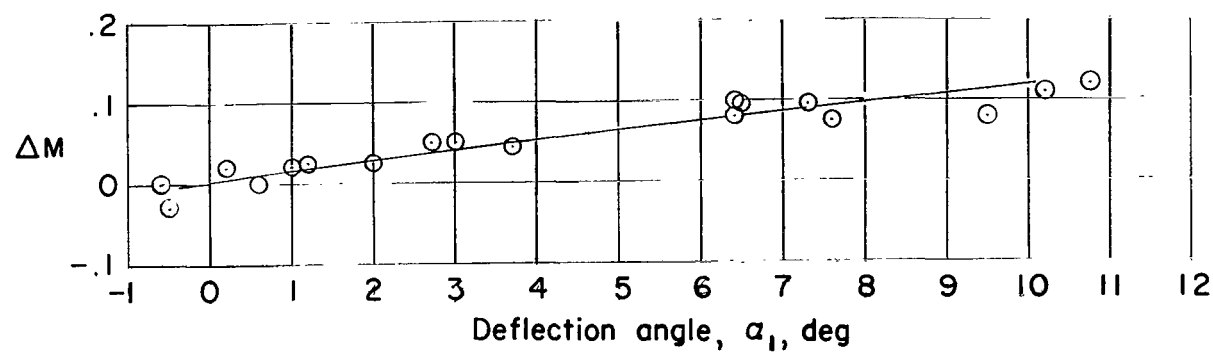

(a) x = 80.21 cm.

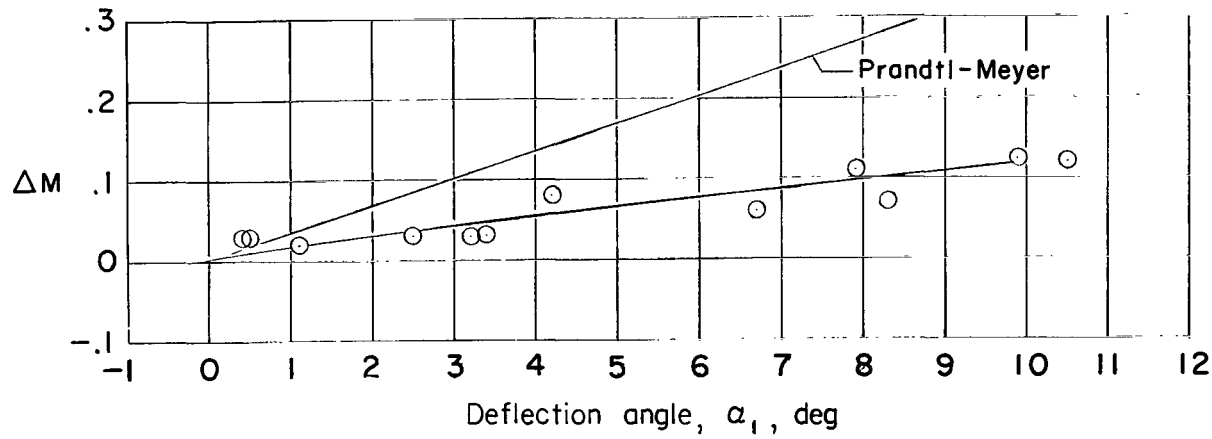

(b) x = 97.49 cm.

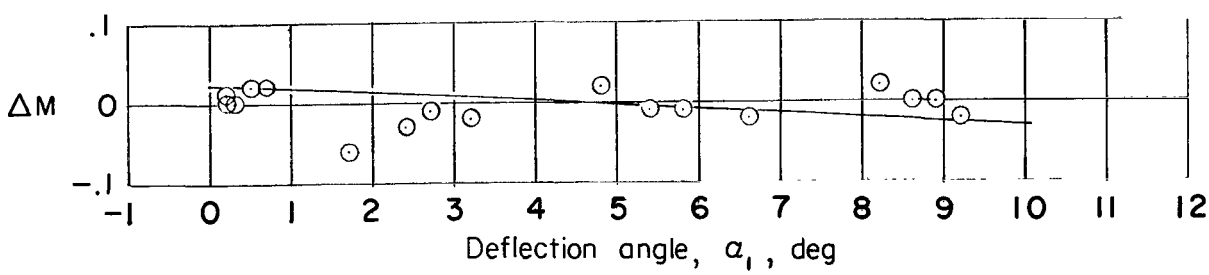

(c) x = 115.14 cm.

Figure 18.- Variation of incremental increase in local Mach number with flow deflection angle in the vertical center plane of the model. $M_\infty = 1.60$; $\beta_m = 0^0$.

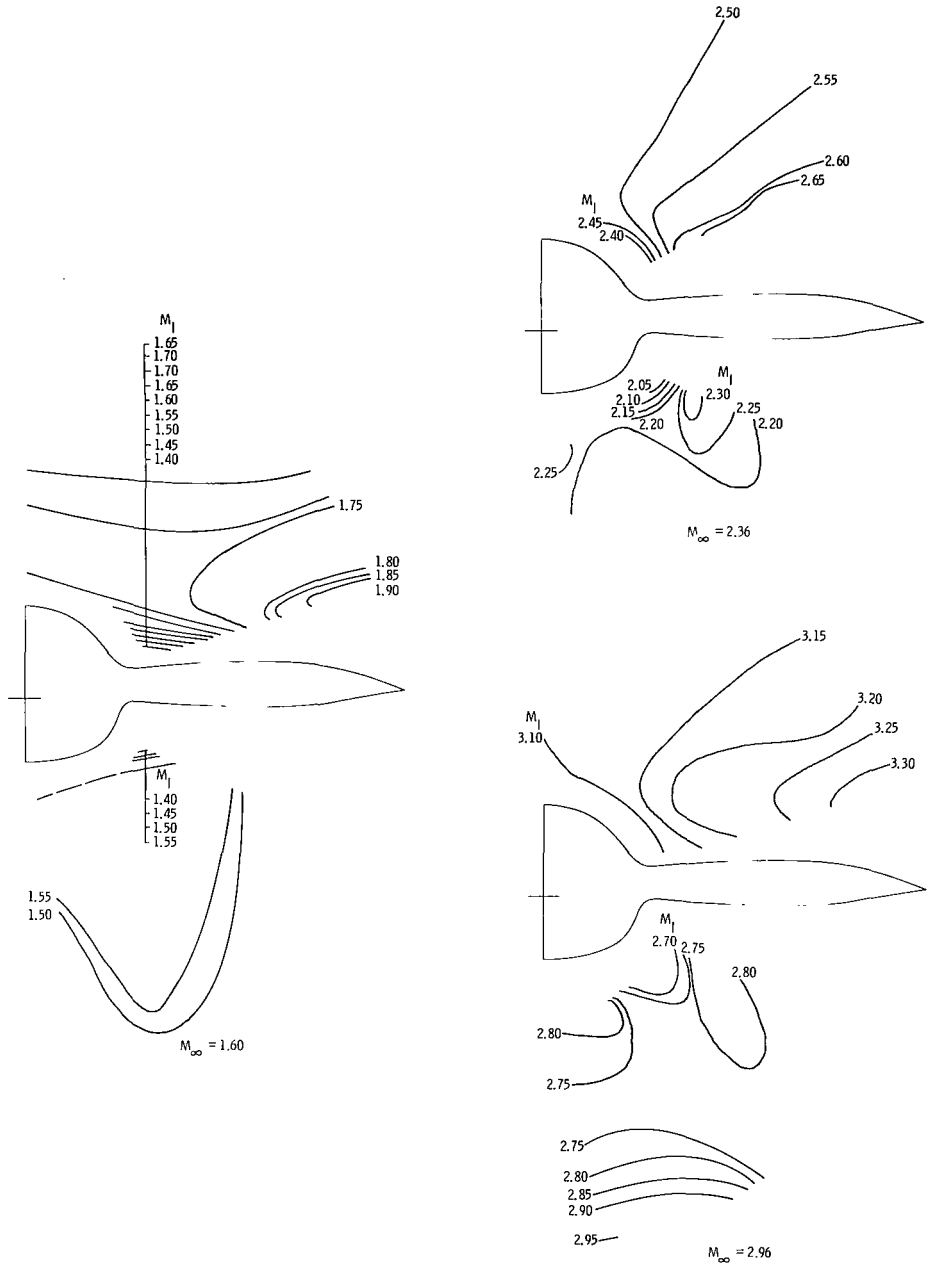

(a) Local Mach number. x = 80.21 cm.

Figure 19.- Effects of free-stream Mach number on local flow properties. $\alpha_m = 6^0$; $\beta_m = 0^0$.

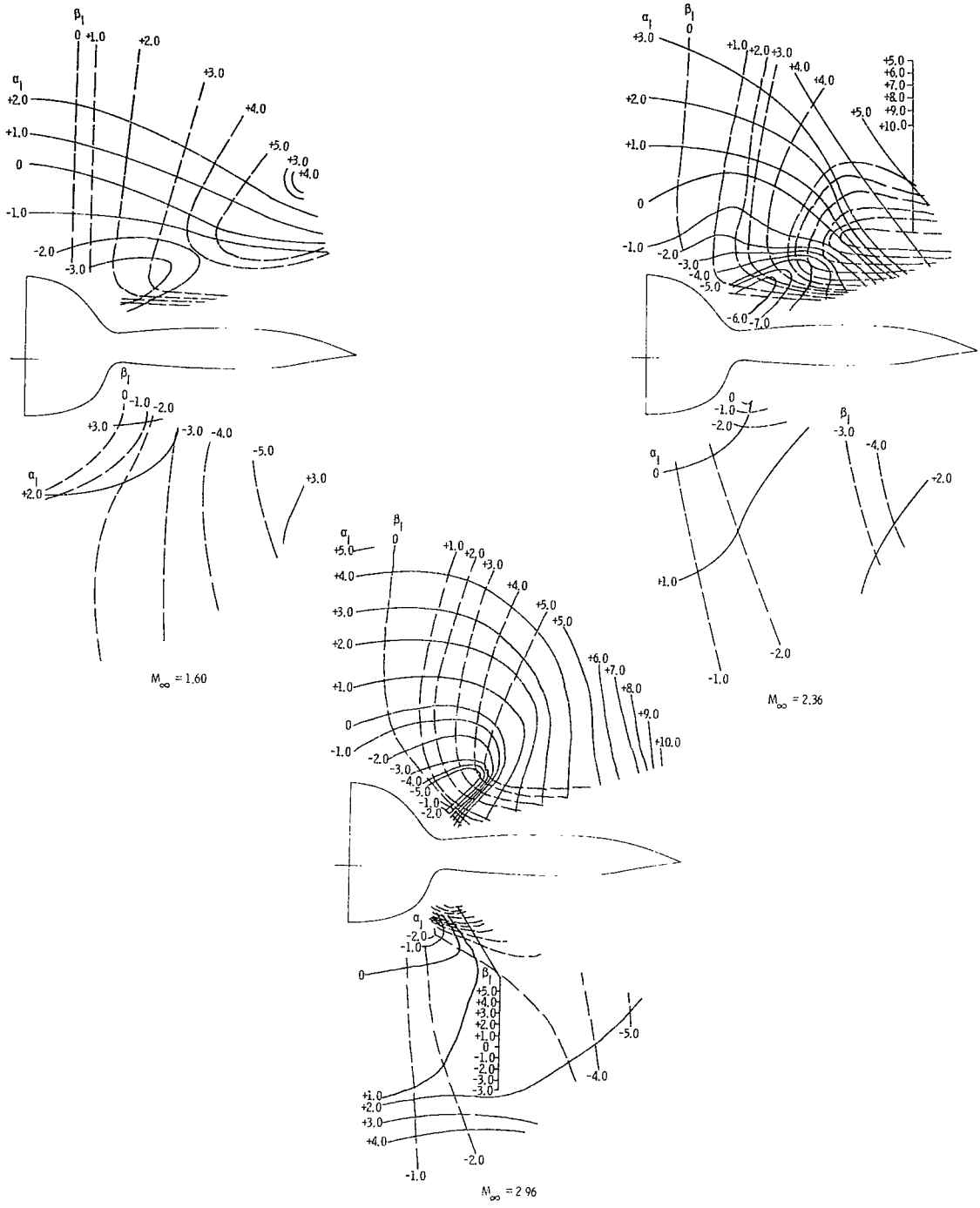

(b) Local flow angles. x = 80.21 cm.

Figure 19.- Continued.

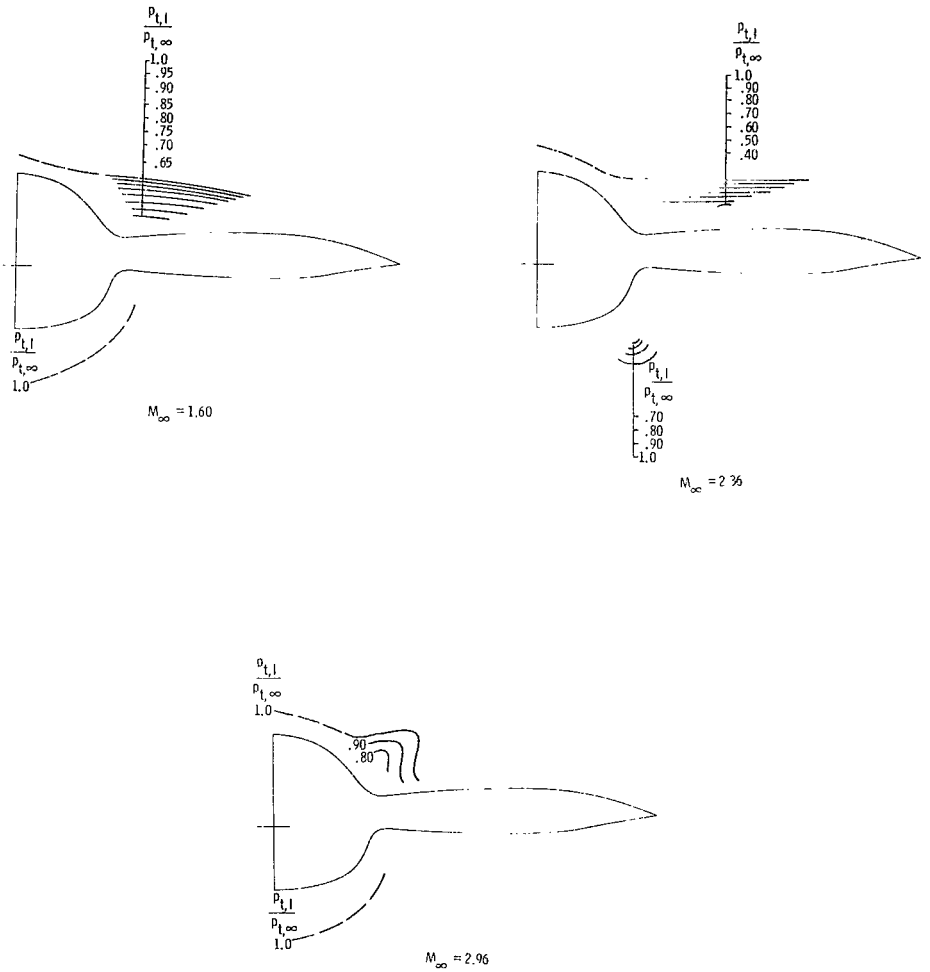

(c) Ratio of local to free-stream total pressure. x = 80.21 cm.

Figure 19.- Continued.

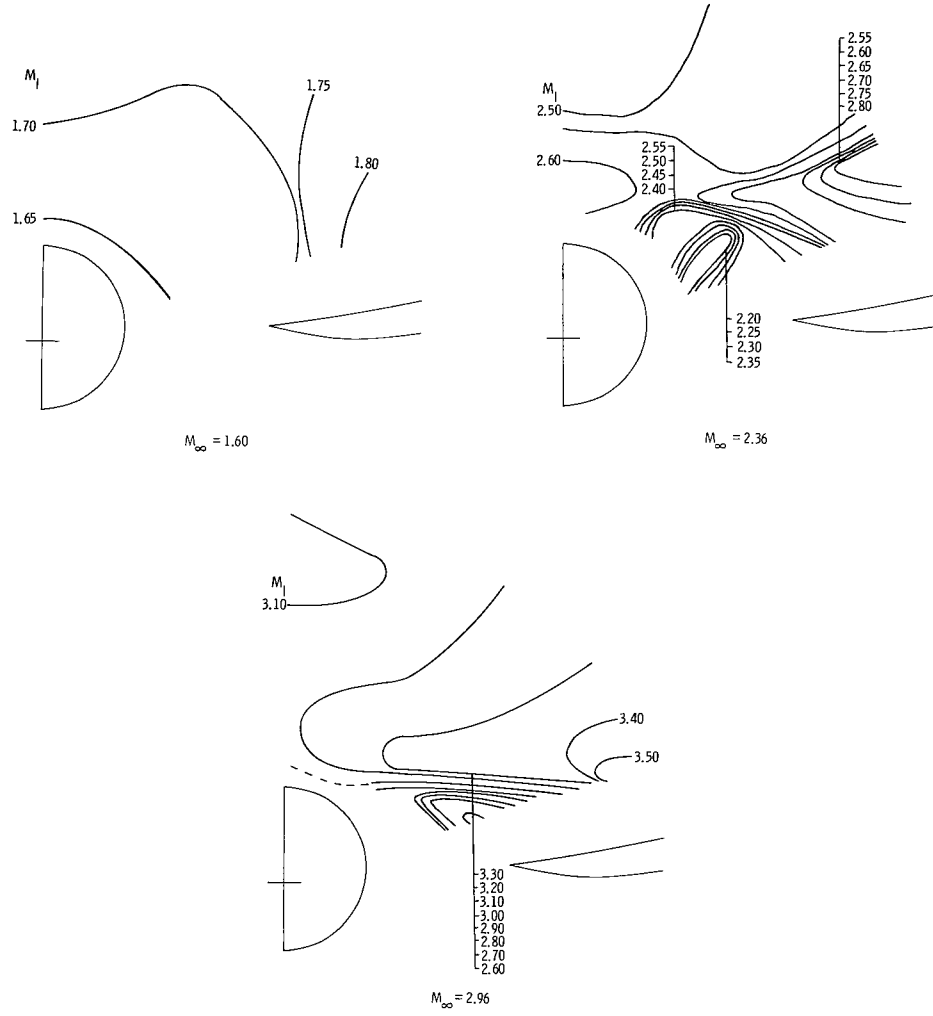

(d) Local Mach number. x = 97.49 cm.

Figure 19.- Continued.

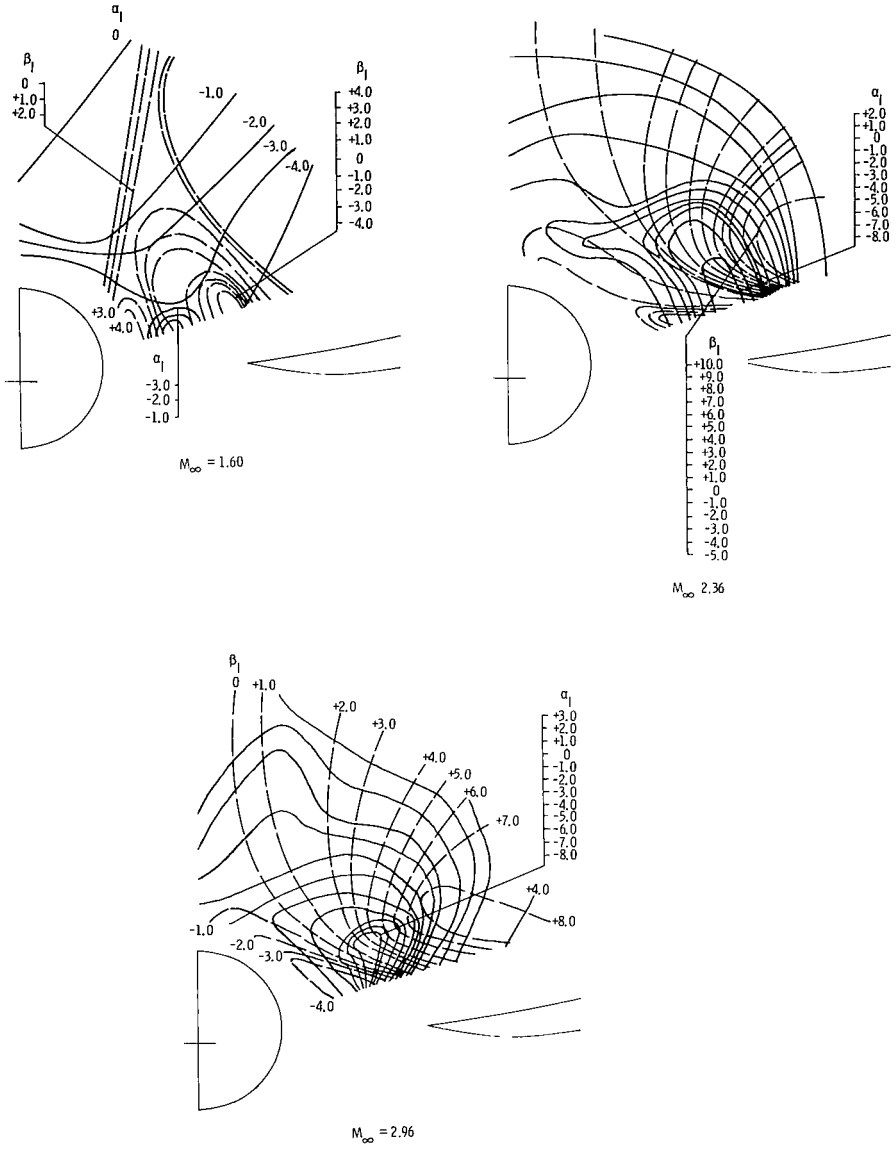

(e) Local flow angles. x = 97.49 cm.

Figure 19.- Continued.

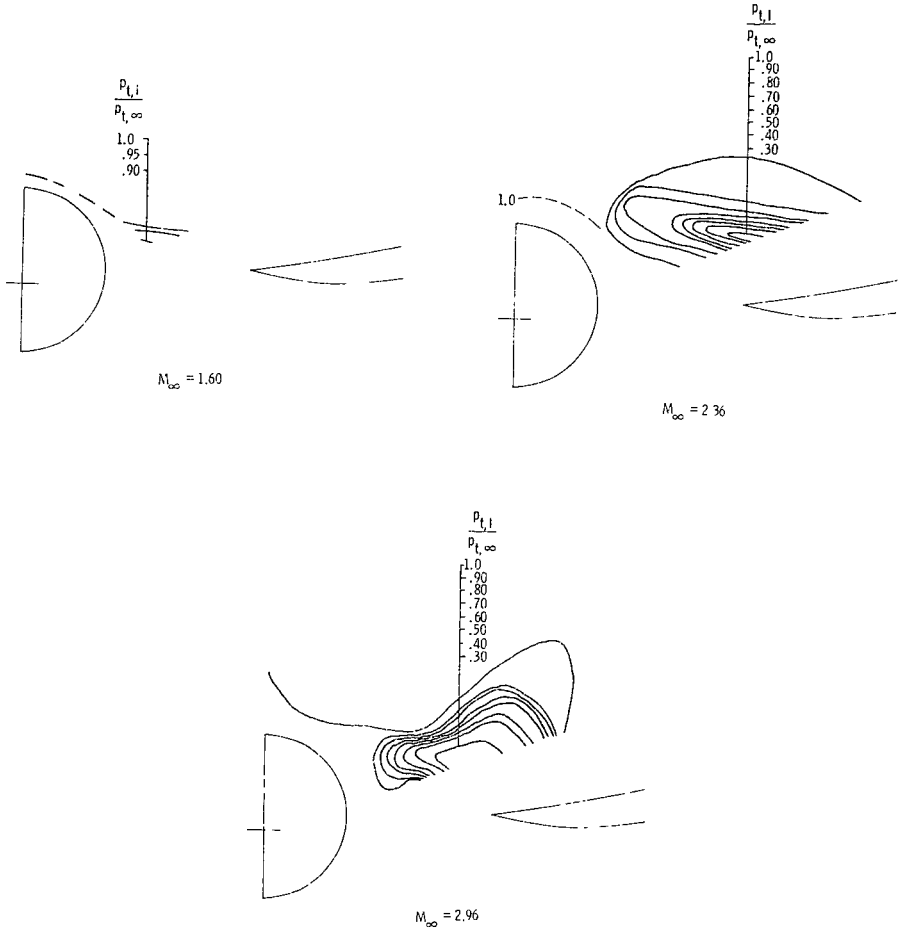

(f) Ratio of local to free-stream total pressure. x = 97.49 cm.

Figure 19.- Continued.

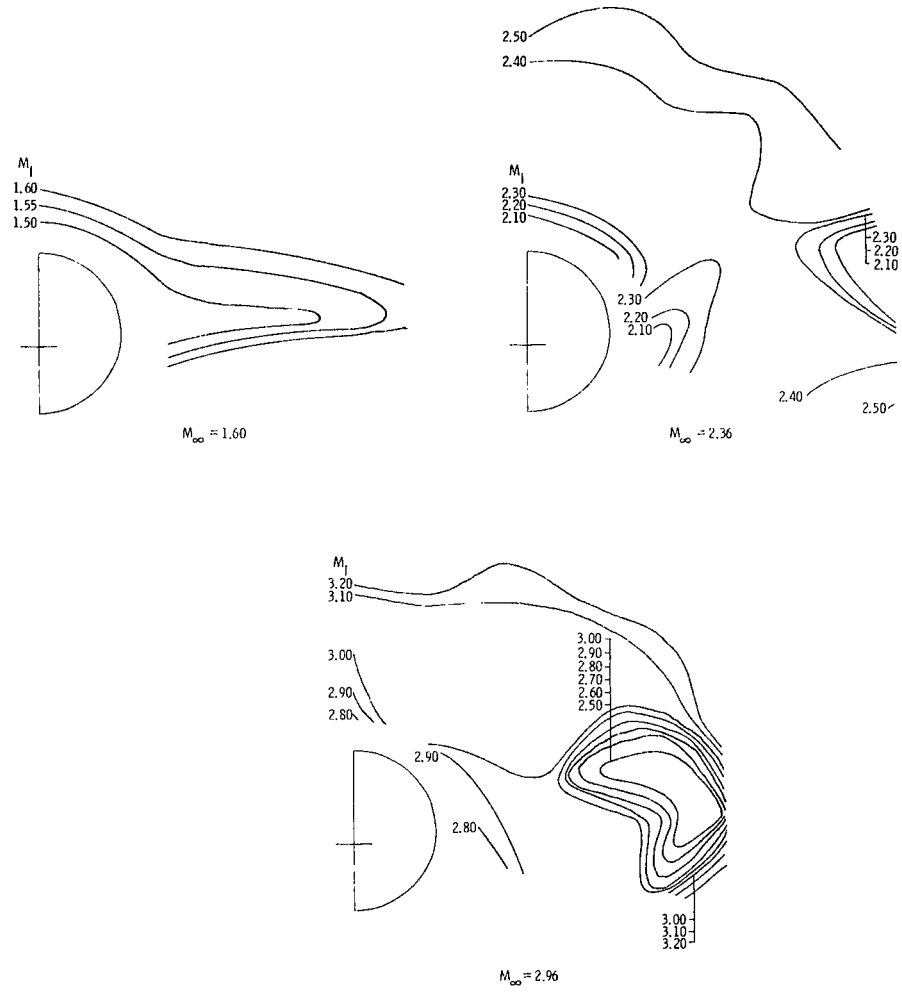

(g) Local Mach number. x = 115.14 cm.

Figure 19.- Continued.

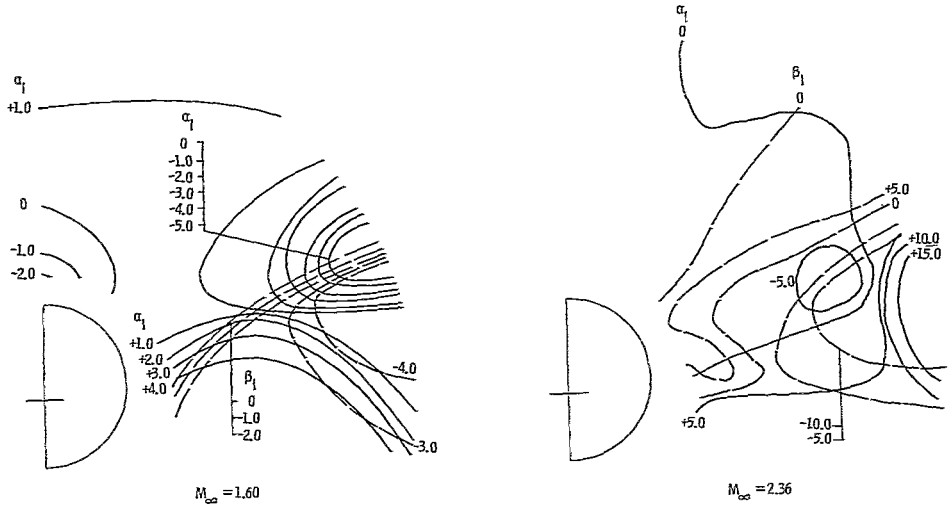

(h) Local flow angles. x = 115.14 cm.

Figure 19.- Continued.

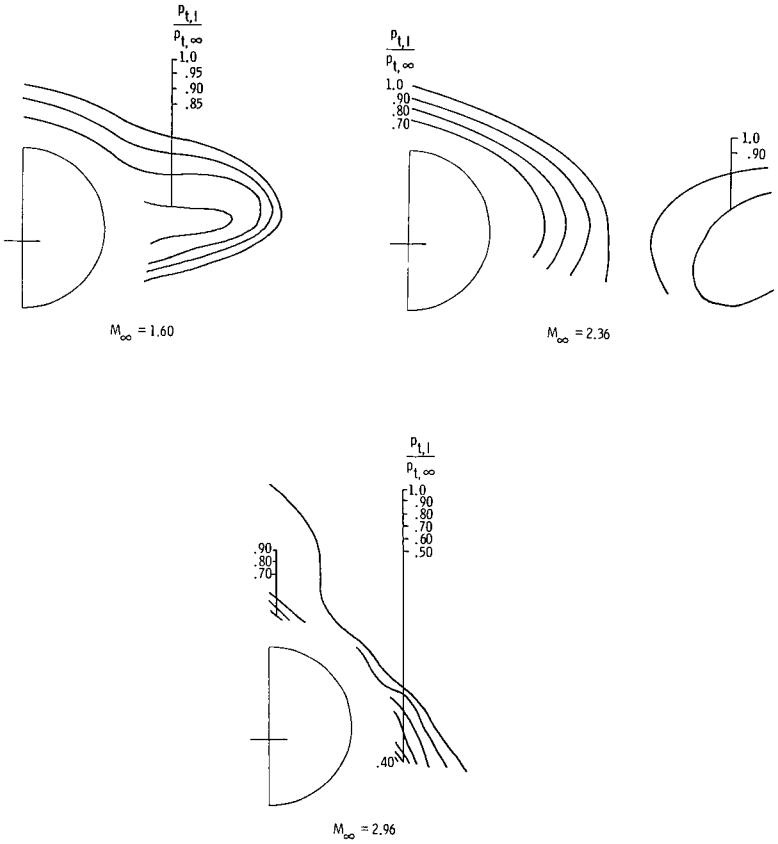

(i) Ratio of local to free-stream total pressure. x = 115.14 cm.

Figure 19.- Concluded.

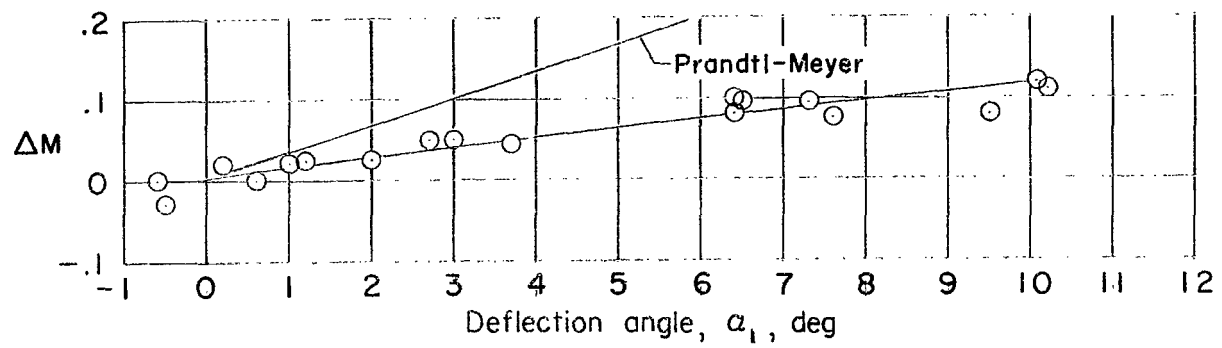

(a) M_∞ = 1.60.

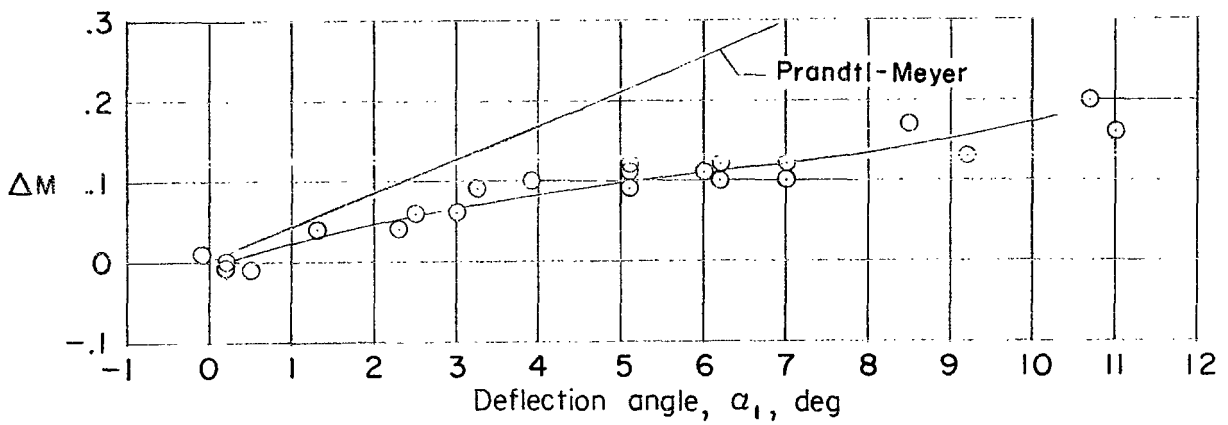

(b) M_∞ = 2.36.

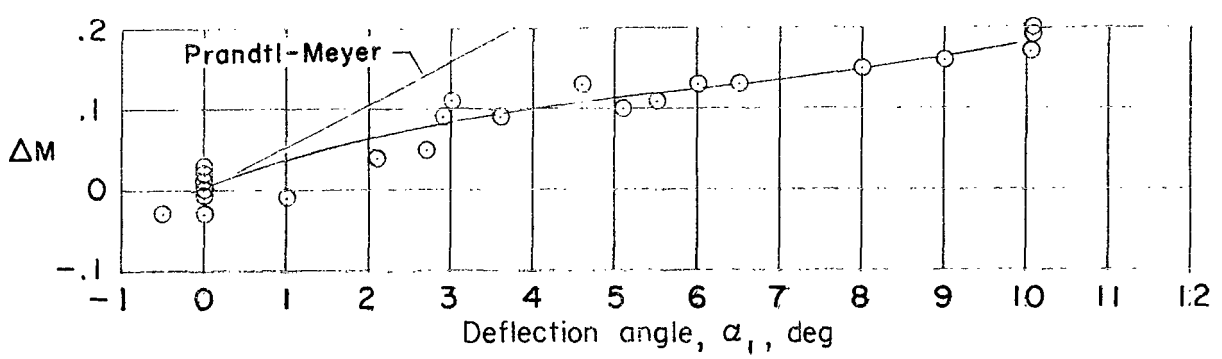

(c) M_∞ = 2.96.

Figure 20.- Effect of free-stream Mach number on the incremental increase in local Mach number with flow deflection angle in the vertical plane. x = 80.21 cm; $\beta_m = 0^0$.

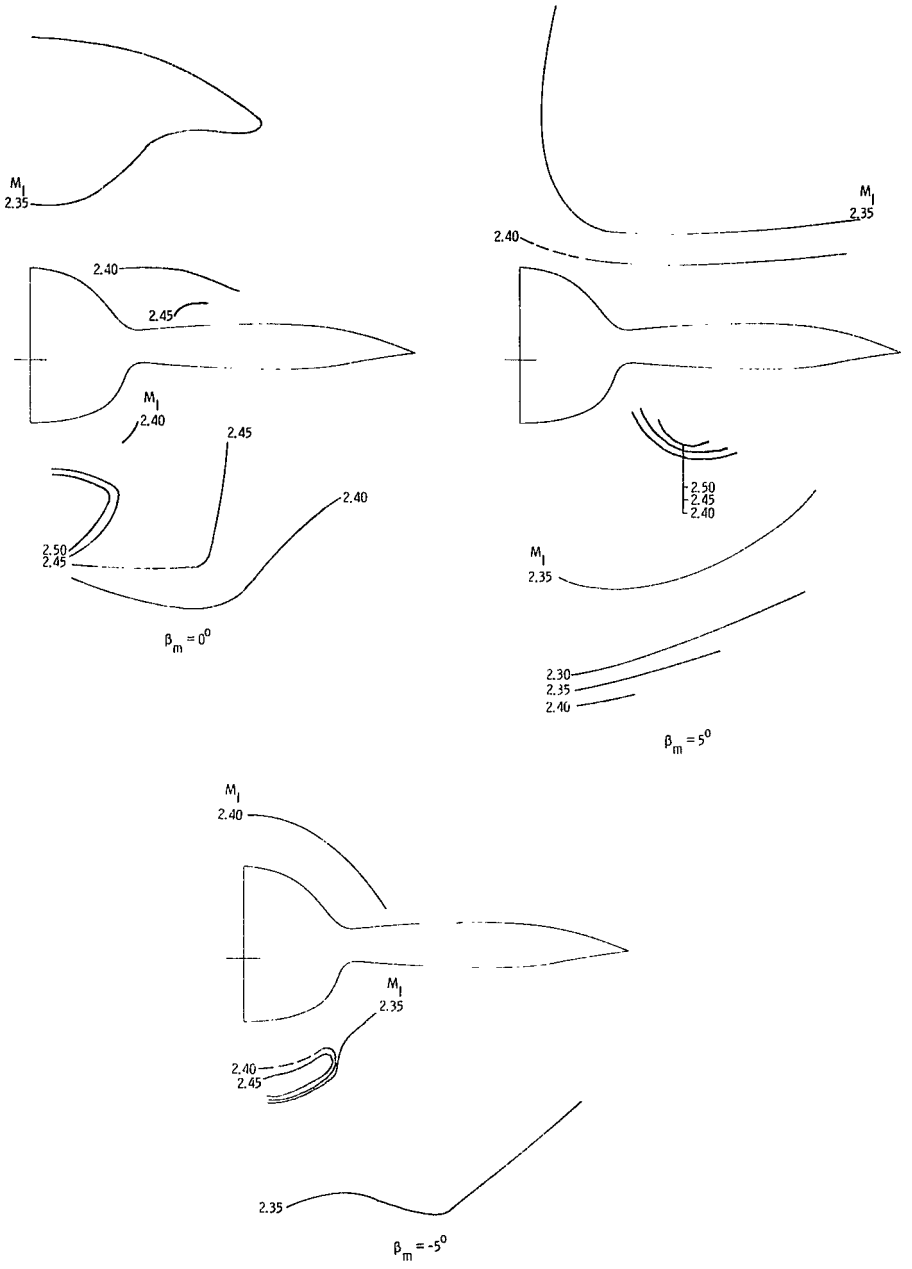

(a) Local Mach number. x = 80.21 cm.

Figure 21.- Effects of model sideslip on local flow properties. $M_\infty = 2.36$; $\alpha_m = 0^0$.

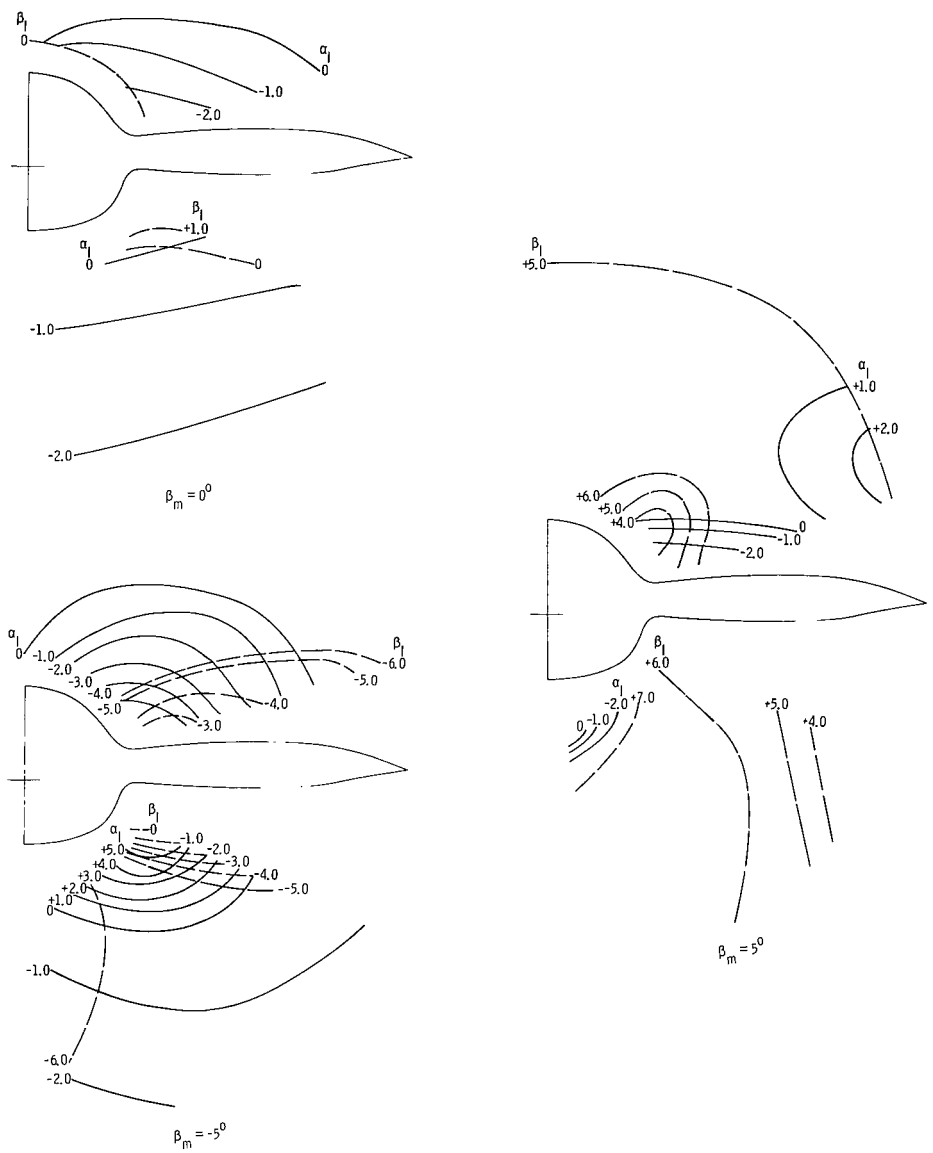

(b) Local flow angles. x = 80.21 cm.

Figure 21.- Continued.

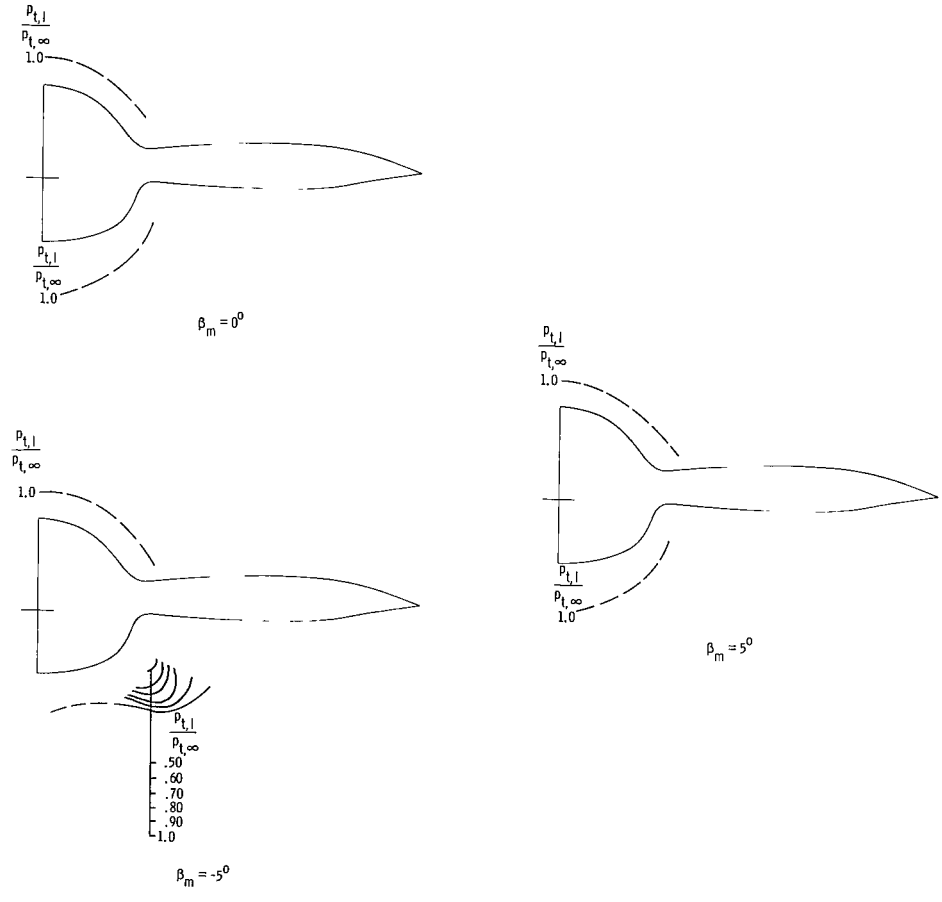

(c) Ratio of local to free-stream total pressure. x = 80.21 cm.

Figure 21.- Continued.

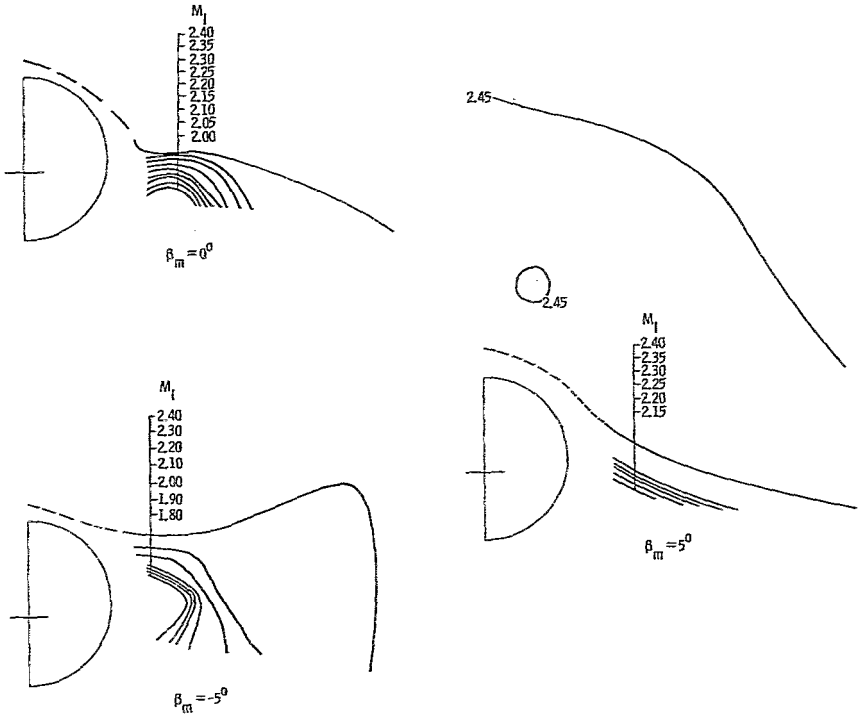

(d) Local Mach number. x = 115.14 cm.

Figure 21.- Continued.

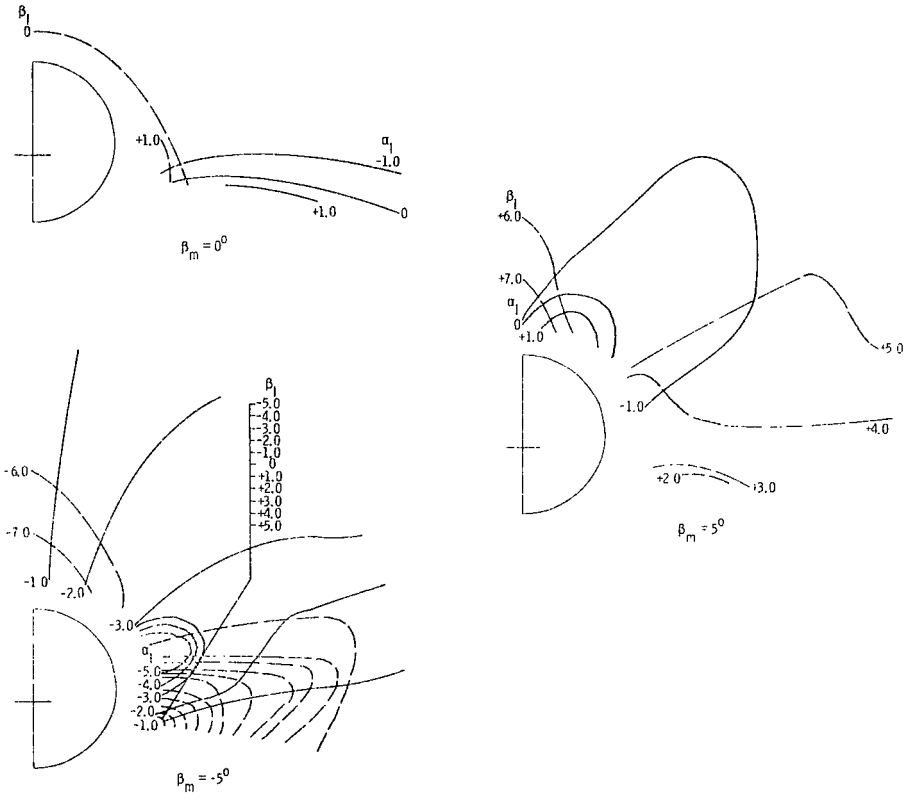

(e) Local flow angles. x = 115.14 cm.

Figure 21.- Continued.

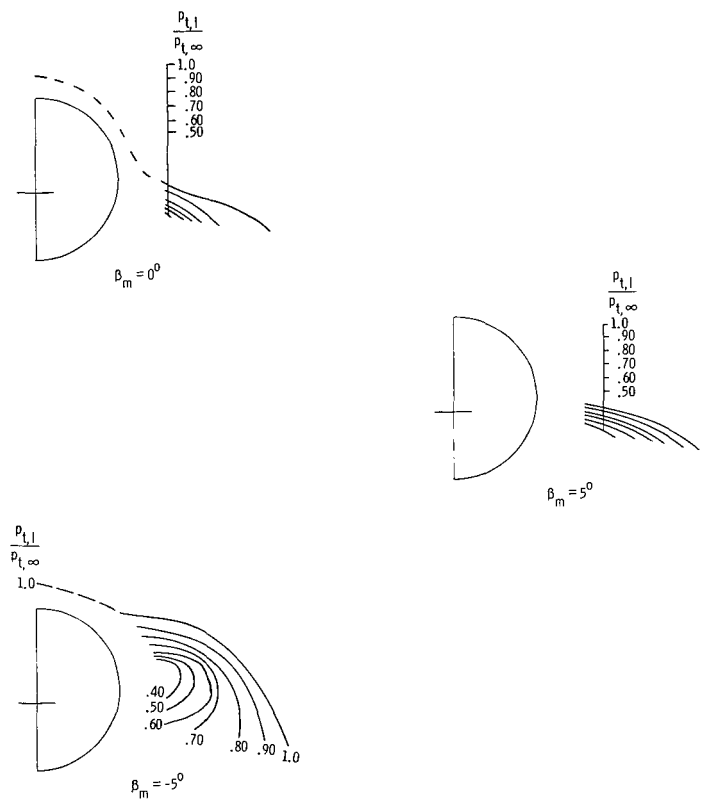

(f) Ratio of local to free-stream total pressure. x = 115.14 cm.

Figure 21.- Concluded.

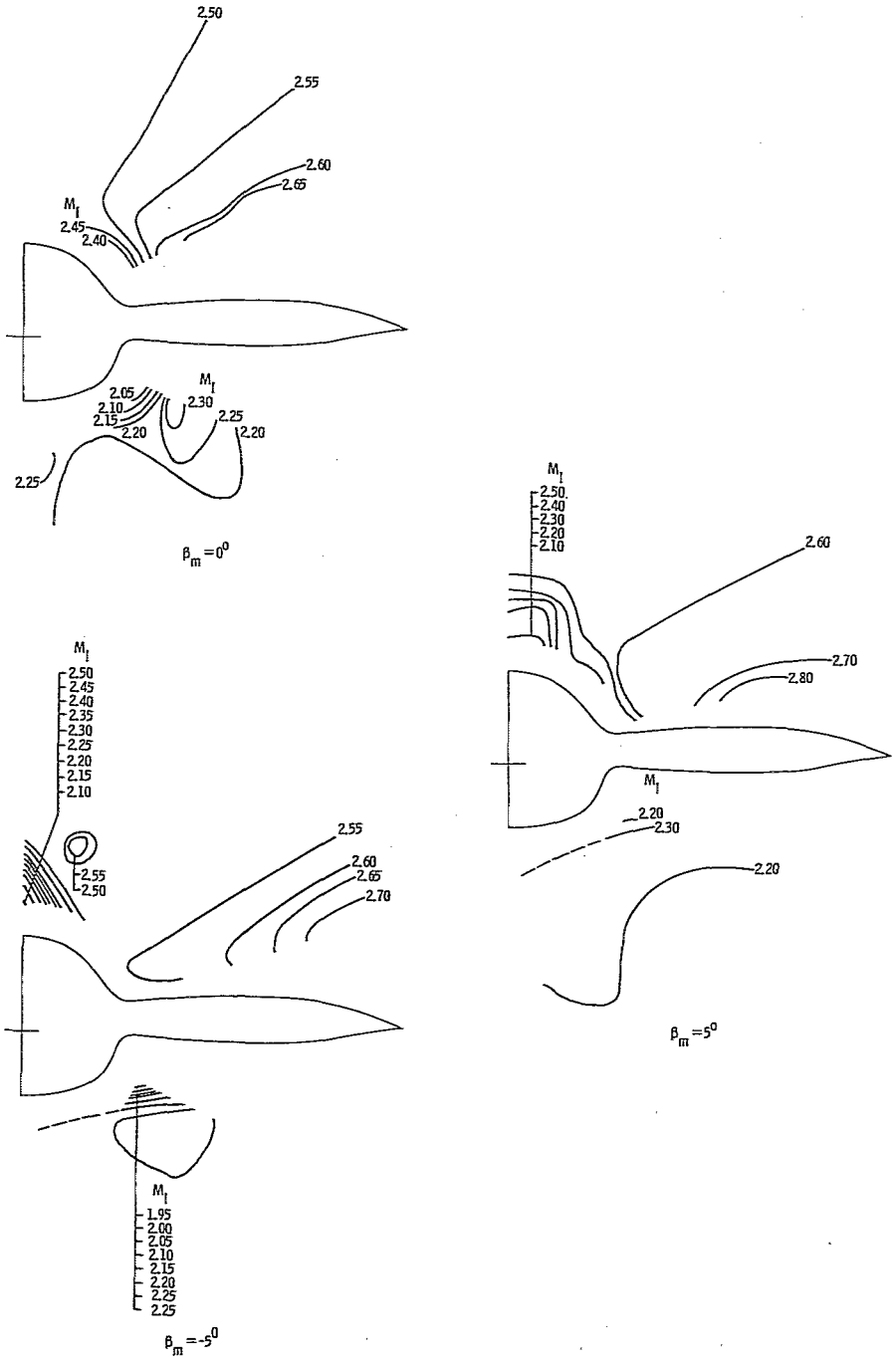

(a) Local Mach number. x = 80.21 cm.

Figure 22.- Effects of model sideslip on local flow properties. $M_\infty = 2.36$; $\alpha_m = 6^0$.

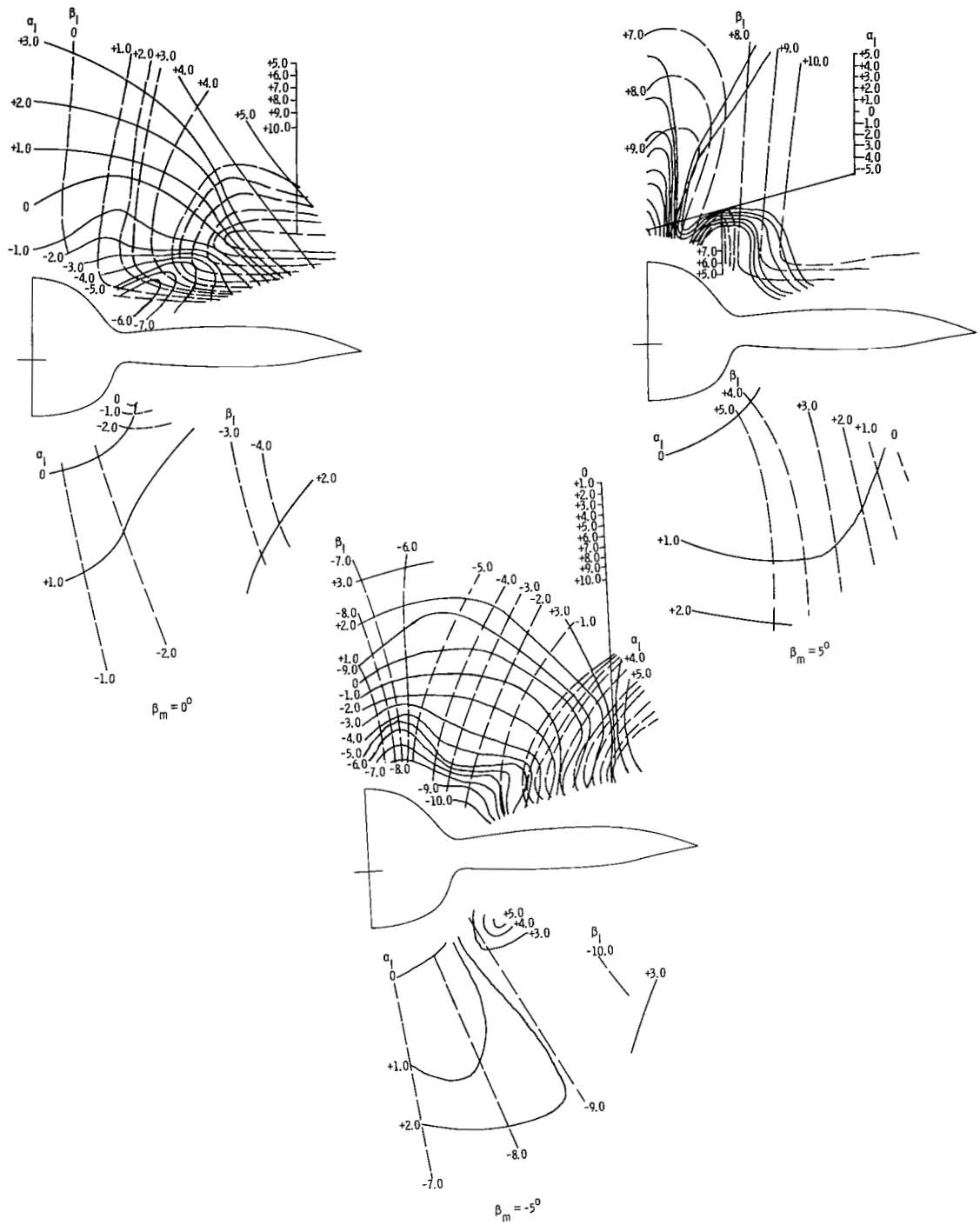

(b) Local flow angles. x = 80.21 cm.

Figure 22.- Continued.

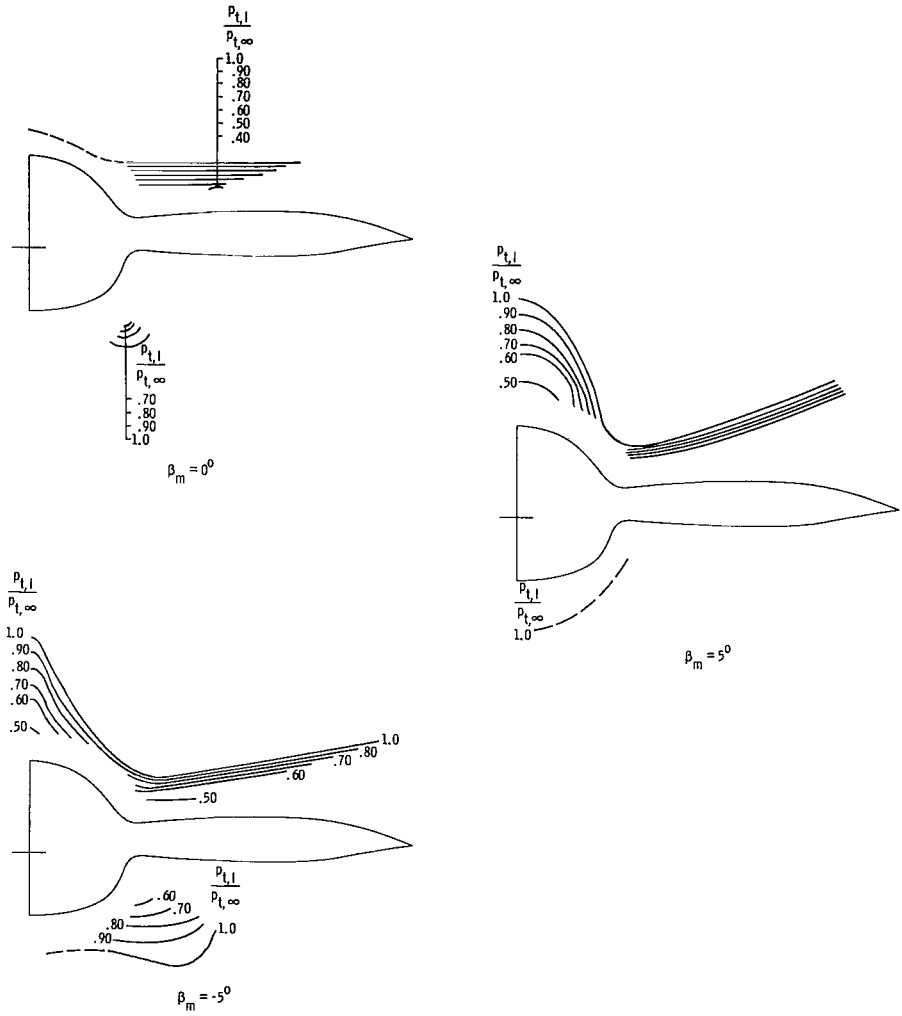

(c) Ratio of local to free-stream total pressure. x = 80.21 cm.

Figure 22.- Continued.

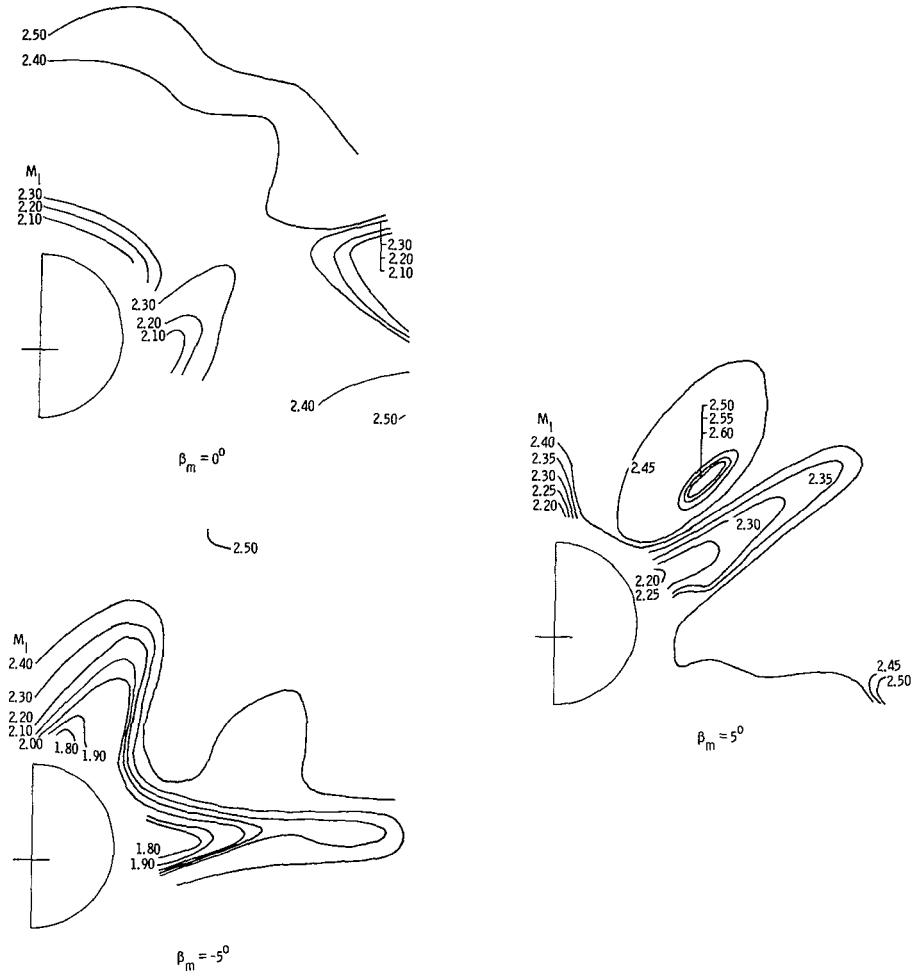

(d) Local Mach number. x = 115.14 cm.

Figure 22.- Continued.

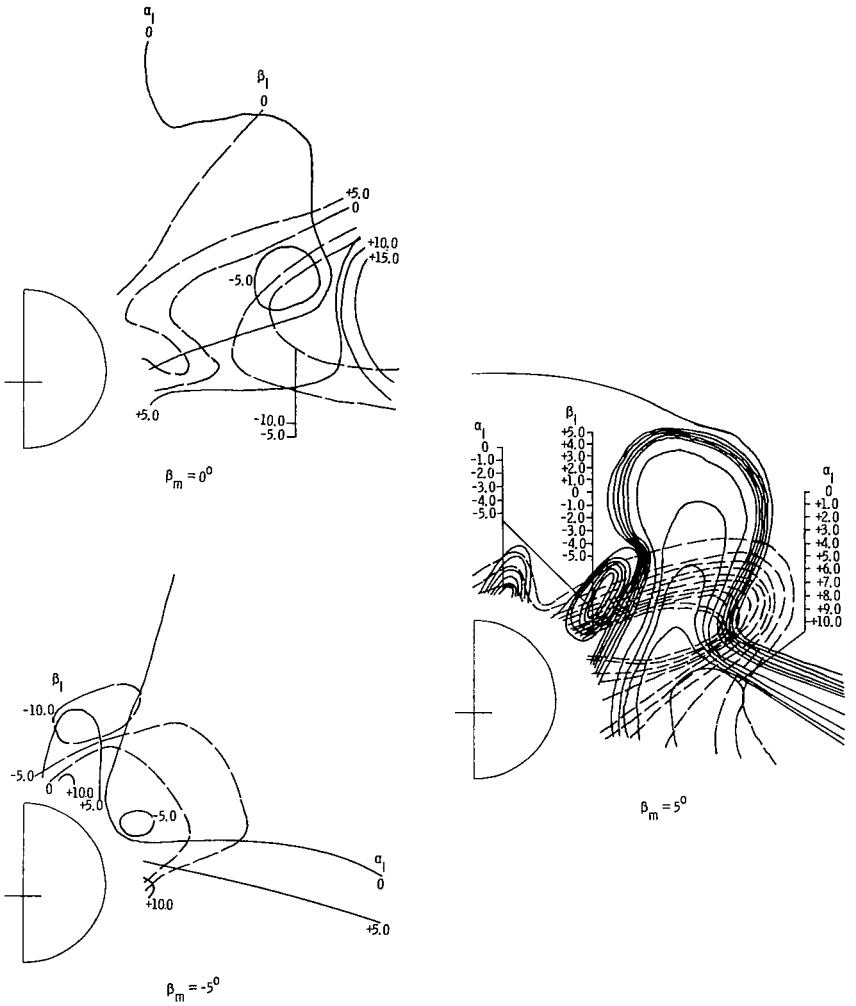

(e) Local flow angles. x = 115.14 cm.

Figure 22.- Continued.

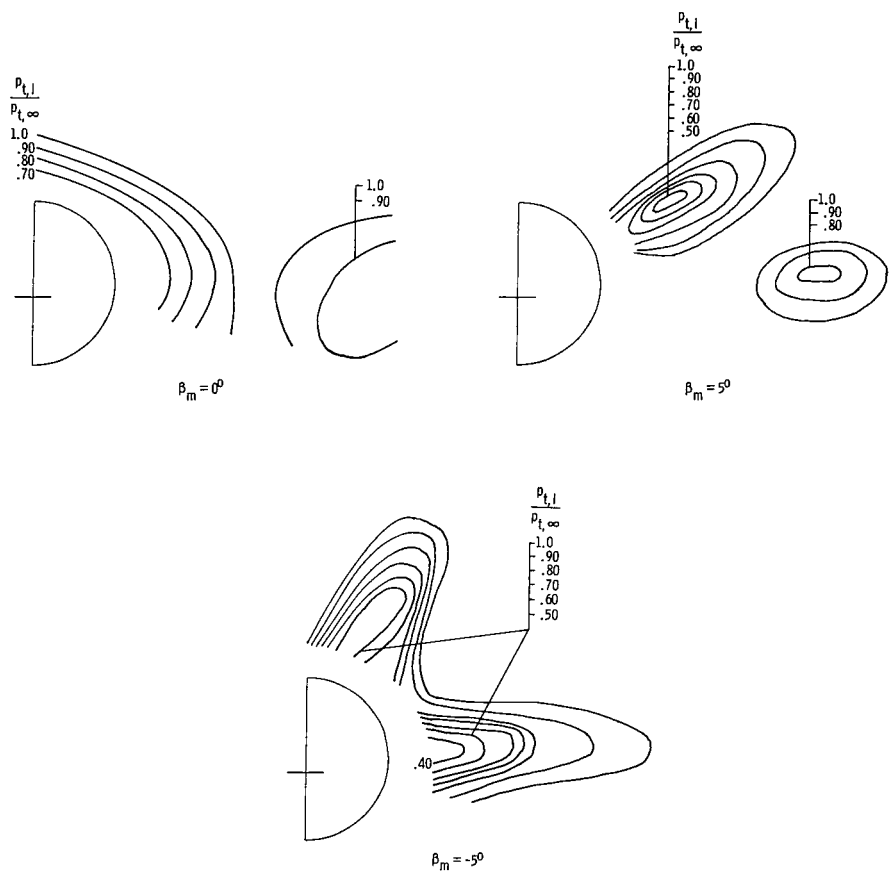

(f) Ratio of local to free-stream total pressure. x = 115.14 cm.

Figure 22.- Concluded.

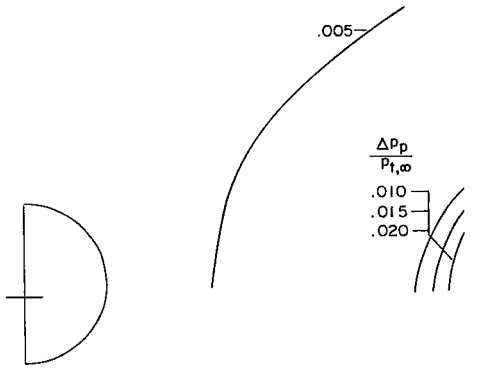

(a) $\alpha_m = 0^0$.

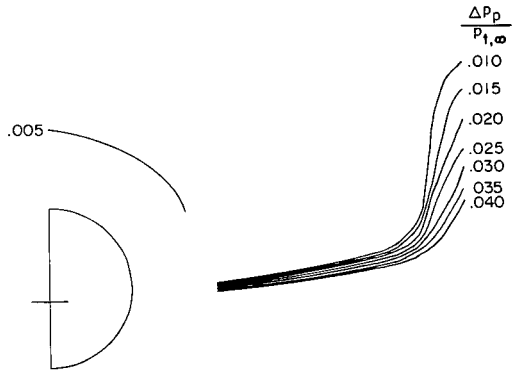

(b) $\alpha_m = 3^0$.

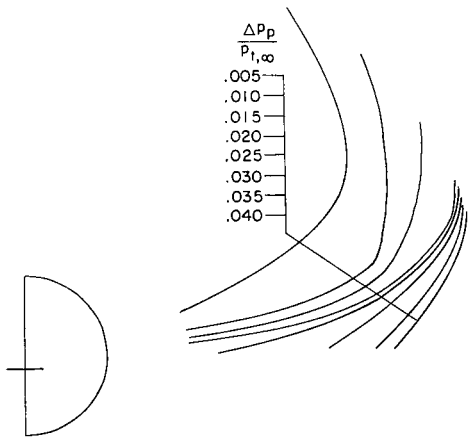

(c) $\alpha_m = 6^0$.

Figure 23.- Effect of model angle of attack on the amplitude of cyclic pitot-pressure fluctuations. $\beta_m = 0^0$; $M_\infty = 1.60$; $x = 115.14$ cm.

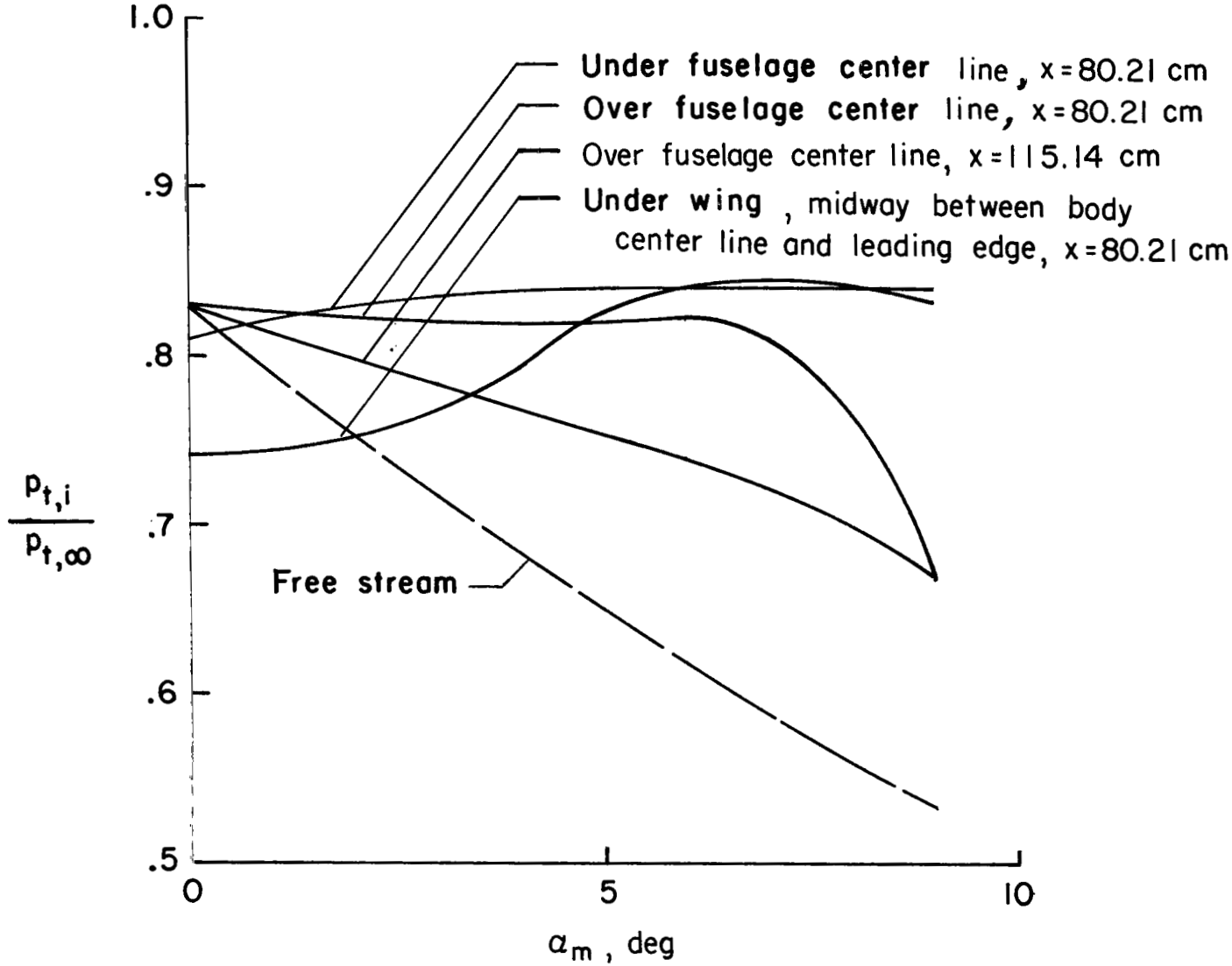

(a) $M_\infty = 2.96$.

Figure 24.- Effect of inlet placement on the variation of inlet total-pressure recovery with model angle of attack. $\beta_m = 0^o$; design $\alpha_m = 6^o$.

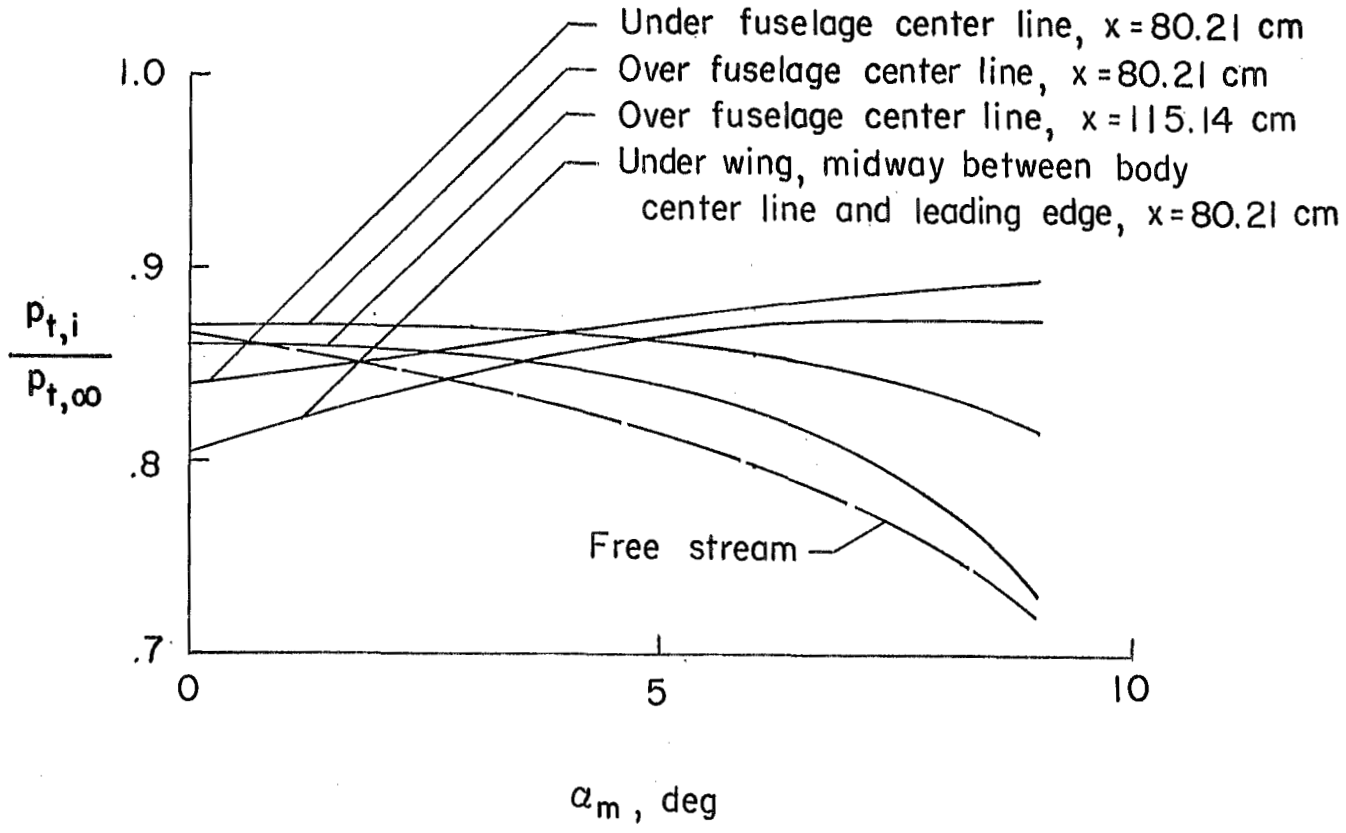

(b) $M_\infty = 2.36$.

Figure 24.- Concluded.

"The aeronautical and space activities of the United States shall be conducted so as to contribute . . . to the expansion of human knowledge of phenomena in the atmosphere and space. The Administration shall provide for the widest practicable and appropriate dissemination of information concerning its activities and the results thereof."

—NATIONAL AERONAUTICS AND SPACE ACT OF 1958

NASA SCIENTIFIC AND TECHNICAL PUBLICATIONS

TECHNICAL REPORTS: Scientific and technical information considered important, complete, and a lasting contribution to existing knowledge.

TECHNICAL NOTES: Information less broad in scope but nevertheless of importance as a contribution to existing knowledge.

TECHNICAL MEMORANDUMS: Information receiving limited distribution because of preliminary data, security classification, or other reasons.

CONTRACTOR REPORTS: Scientific and technical information generated under a NASA contract or grant and considered an important contribution to existing knowledge.

TECHNICAL TRANSLATIONS: Information published in a foreign language considered to merit NASA distribution in English.

SPECIAL PUBLICATIONS: Information derived from or of value to NASA activities. Publications include conference proceedings, monographs, data compilations, handbooks, sourcebooks, and special bibliographies.

TECHNOLOGY UTILIZATION PUBLICATIONS: Information on technology used by NASA that may be of particular interest in commercial and other non-aerospace applications. Publications include Tech Briefs, Technology Utilization Reports and Notes, and Technology Surveys.

Details on the availability of these publications may be obtained from:

SCIENTIFIC AND TECHNICAL INFORMATION DIVISION

NATIONAL AERONAUTICS AND SPACE ADMINISTRATION

Washington, D.C. 20546